

Symmetry in Multiple Self-Consistent-Field Solutions of Transition-Metal Complexes

Bang C. Huynh* and Alex J. W. Thom

University Chemical Laboratory, Lensfield Road, Cambridge CB2 1EW, United Kingdom

E-mail: cbh31@cam.ac.uk

Abstract

We use a method based on metadynamics to locate multiple low-energy Unrestricted Hartree–Fock (UHF) self-consistent-field (SCF) solutions of two model octahedral d^1 and d^2 transition-metal complexes, $[\text{MF}_6]^{3-}$ ($\text{M} = \text{Ti}, \text{V}$). By giving a group-theoretical definition of symmetry breaking, we classify these solutions in the framework of representation theory and observe that a number of them break spin or spatial symmetry, if not both. These solutions seem unphysical at first, but we show that they can be used as bases for Non-Orthogonal Configuration Interaction (NOCI) to yield multi-determinantal wavefunctions that have the right symmetry to be assigned to electronic terms. Furthermore, by examining the natural orbitals and occupation numbers of these NOCI wavefunctions, we gain insight into the amount of static correlation that they incorporate. We then investigate the behaviors of the most low-lying UHF and NOCI wavefunctions when the octahedral symmetry of the complexes is lowered and deduce that the symmetry-broken UHF solutions must first have their symmetry restored by NOCI before they can describe any vibronic stabilization effects dictated by the Jahn–Teller theorem.

1 Introduction

Strongly correlated systems such as mono- or multi-nuclear transition-metal (TM) complexes present an exciting, yet daunting, arena for

electronic structure theory and computation. The interaction between electrons in the partially filled d shells of the TM centers gives rise to many low-energy states¹ which exhibit various degrees of degeneracy when placed in a symmetric or nearly symmetric molecular geometry.^{2–4} As the spacing between these states ranges from *ca.* 200 cm^{-1} ($2.48 \times 10^{-2} \text{ eV}$, $\sim k_{\text{B}}T$ at room temperature) to *ca.* $50\,000 \text{ cm}^{-1}$ (6.20 eV , $\sim 200 \text{ nm}$, in the ultraviolet region), they play a vital role in determining the spectroscopic and magnetic behaviors of these complexes.^{1,5} Therefore, if we wish to predict or understand such properties on an *ab initio* level successfully, we must first develop methods that are capable of describing these states reliably.

Most conventional electronic structure theories and methods such as Hartree–Fock (HF) theory or Density Functional Theory (DFT) were formulated with the aim of calculating the electronic ground state of molecular systems to great precision.⁶ Both of the aforementioned methods are inherently variational: the HF equations are derived by minimizing the energy expression for a single Slater determinant,^{7–11} whereas DFT is based upon the two famous theorems first proven by Hohenberg and Kohn, the second of which asserts that the ground-state energy and density can be found by minimizing the exact energy functional of the system.¹² Unfortunately, the variational principle is not applicable to most excited states in general because its formulation only allows for an upper bound to the exact ground-state energy to be determined.^{11,13,14} As a consequence, vari-

ational techniques often struggle to ascertain if their calculations of excited states and excitation energies are sensible. Even though the above-mentioned ground-state methods can be exploited to give variationally optimized upper bounds for certain electronic excited states by imposing orthogonality to the ground state via appropriate spin or spatial irreducible representation constraints,^{6,13} their applicability can be rather limited if the irreducible representation of the exact ground state is not known or if the low-lying states span many repeated irreducible representations due to, for example, the low molecular symmetry of the system.

In the last few decades, several methods have been developed to remove the need for such *a priori* constraints in the calculation of excited states. The conceptually simplest wavefunction-based approach is Configuration Interaction Singles (CIS) in which an ansatz for excited states is written as a linear expansion in terms of single-replacement Slater determinants formed from a reference HF determinant, and the expansion coefficients can be determined using Rayleigh–Ritz variational principle.^{6,15} As CIS excited-state wavefunctions are simply linear combinations of Slater determinants, they are well defined and can be interpreted relatively easily: the expansion coefficients give an indication of the contribution of the constituting Slater determinants whose spin-orbitals provide chemical understanding. However, the construction of CIS is severely rigid: the inclusion of only single-replacement Slater determinants prevents it from describing any excited states that contain considerable double or higher excitation character, which can be abundant in strongly correlated systems. Consequently, CIS commonly produces vertical excitation energies with errors of the order of 1 eV.¹⁶

There exist more sophisticated methods still. Most notable are a host of techniques that attempt to calculate poles in the linear response of a ground-state reference to a small time-dependent external electric field perturbation: the locations of these poles and the corresponding residues in the frequency domain give vertical excitation energies and os-

cillator strengths, respectively. The single-reference wavefunction implementation of this idea is known as Time-Dependent Hartree–Fock (TDHF)¹⁷ and the density functional analogue is Time-Dependent Density Functional Theory (TDDFT).¹⁸ Whereas TDHF has only seen very limited applications in the quantum chemistry community,⁶ TDDFT has enjoyed a much more successful growth owing to its ability to produce vertical excitation energies and excited-state properties for large systems at low computational cost.¹⁹ Even though TDDFT is formally an exact theory, approximations to the time-varying exchange-correlation potential must be made since its exact functional form is not known, therefore many TDDFT results are very sensitive to the choice of exchange-correlation functional.^{6,20} Nevertheless, much effort has been put into assessing and improving the validity and quality of the large number of currently available ground-state exchange-correlation functionals used in TDDFT under the adiabatic approximation.^{20,21}

Our main concern, however, lies with the inherent dependence of these methods on the ground-state reference. For if there are errors in this reference such that it does not form a good description of the ground state, any excited-state calculation that relies on it cannot be expected to give accurate results. This property is wittily referred to by Burke et al. as *the sin of the ground state*.¹⁹ In fact, Thom and Head-Gordon demonstrate that the non-linear self-consistent-field (SCF) HF equations exhibit multiple solutions and also remark that the same behavior can be expected for the SCF Kohn–Sham (KS) equations.²² As such, choosing a suitable HF or DFT reference becomes non-trivial, especially if the SCF equations yield multiple low-energy solutions that are degenerate or nearly degenerate in strongly correlated systems. Indeed, a number of prior studies on the electronic structures of systems ranging from small radicals such as F_2^+ and O_4^+ ^{23,24} to several TM organometallic complexes such as ferrocene,²⁵ bis(η^4 -cyclobutadiene)nickel,²⁶ $Fe(CH)_2$,²⁷ a triply bridged chromium dimer,²⁸ and various iron–sulfur clusters²⁹ show that there exist several low-energy SCF HF or DFT

solutions, some of which are not exact eigenfunctions of \hat{S}^2 , or contain spin-orbitals that do not respect the molecular symmetry of the structure, or both. Therefore, it can be difficult to assign these solutions to actual electronic states or give them meaningful physical interpretations.

In this work, we look for multiple low-energy SCF HF solutions in two representative octahedral hexafluoridometallate(III) complexes, $[\text{MF}_6]^{3-}$ ($\text{M} = \text{Ti}, \text{V}$), using an approach inspired by metadynamics.²² We then carefully analyze these solutions in terms of symmetry and degeneracy so as to classify them systematically according to the irreducible representations of the underlying molecular point group. This allows for a rigorous but straightforward definition of *symmetry breaking* and *symmetry conserving* in SCF HF solutions. Afterwards, we carry out Non-Orthogonal Configuration Interaction (NOCI)³⁰ between different, possibly symmetry-broken, HF solutions to obtain multi-determinantal wavefunctions that conserve symmetry. The choice of the model octahedral complexes is thus deliberate: the group-theoretical description of their low-energy electronic terms is well known³ while their high molecular symmetry and the presence of one or two unpaired d electrons result in various symmetry-breaking effects that are illuminating yet sufficiently uncomplicated for a tractable in-depth examination. The purpose of this paper is therefore twofold: firstly, to demonstrate that symmetry-broken HF solutions are not unphysical and should not be discarded as they can be assigned definitively to actual electronic terms after their symmetry has been restored; and secondly, to show that NOCI using appropriate selections of symmetry-broken HF solutions yields wavefunction descriptions of both ground and excited electronic states that recover a decent amount of static correlation missed out by HF single determinants.³¹ Even though the use of NOCI on symmetry-broken determinants to form symmetry-conserved multi-determinantal wavefunctions describing ground and excited states has already been formalized and explored under the scope of Projected HF Theory,³²⁻³⁴ we think that the detailed analysis

presented here adds an extra layer of understanding on the nature and properties of multiple SCF solutions in TM complexes and other strongly correlated systems involving unpaired electrons, and that this understanding can better inform the choice of reference for ground- and excited-state calculations, especially when many of these states are low-lying and degenerate or nearly degenerate. We also note that, even though a comparison between NOCI and other standard multi-configurational methods such as Complete Active Space Self-Consistent Field (CASSCF) is highly desirable for a quantification of the amount of static correlation recovered by NOCI, the symmetry breaking nature of many determinants reported in this paper complicates both the CASSCF calculation and the interpretation of the results. We therefore defer this comparison to a more comprehensive study in the future.

The present paper is organized as follows. In Section 2, we formalize the notion of symmetry breaking and symmetry conserving in the language of group and representation theory and present a concrete computational method for this classification. We outline the computational details for the SCF calculations, symmetry analysis and symmetry restoration of our model systems $[\text{MF}_6]^{3-}$ ($\text{M} = \text{Ti}, \text{V}$) in Section 3. We then discuss the results of the simpler d^1 system $[\text{TiF}_6]^{3-}$ first in Section 4 to showcase some of the features of symmetry-broken SCF solutions and set the scene for what will follow. In Section 5, we aim to analyze the results of the more complicated d^2 system $[\text{VF}_6]^{3-}$. However, as these can be rather confusing, we start out in Section 5.1 with a toy system that only contains two d electrons in an octahedral electrostatic field without any core or ligand electrons. Here, we compare the expected electronic terms derived purely from a symmetry perspective with those obtained using a combination of HF and NOCI. We then use this understanding to investigate the SCF and NOCI wavefunctions in the full $[\text{VF}_6]^{3-}$ anion in Section 5.2, paying particular attention to the nature of the correlation recovered via symmetry restoration. With a decent insight into the nature of the various SCF

and NOCI wavefunctions obtained for $[\text{MF}_6]^{3-}$ ($M = \text{Ti}, \text{V}$), we study their behaviors as the molecular symmetry descends from \mathcal{O}_h to \mathcal{D}_{4h} or \mathcal{D}_{2h} in Section 6 and see how the symmetry restoration of SCF solutions is required to correctly describe the stabilization effects necessitated by the Jahn–Teller theorem.

2 Theory

We briefly review the HF formulation and revisit a fundamental theorem relating group theory to quantum mechanics to define symmetry breaking and symmetry conserving for SCF HF wavefunctions. We then give expressions for the representation matrix of a symmetry operation in the single-determinant basis and the corresponding NOCI basis.

In what follows, we define N_e and N_n as the numbers of electrons and nuclei in the system, respectively, and refer to the non-relativistic time-independent electronic Schrödinger equation as

$$\hat{\mathcal{H}}\Psi = E\Psi \quad (1)$$

where the spinless electronic Hamiltonian $\hat{\mathcal{H}}$ takes the following form in atomic units:^{1,11}

$$\hat{\mathcal{H}} = -\sum_i^{N_e} \frac{1}{2} \nabla_i^2 - \sum_i^{N_e} \sum_A^{N_n} \frac{Z_A}{|\mathbf{r}_i - \mathbf{R}_A|} + \sum_i^{N_e} \sum_{j>i}^{N_e} \frac{1}{|\mathbf{r}_i - \mathbf{r}_j|} \quad (2)$$

We also write Slater determinants as³⁵

$$\begin{aligned} \Psi_{\text{HF}} &= |\chi_1 \dots \chi_i \dots \chi_{N_e}| \\ &= \frac{1}{\sqrt{N_e!}} \sum_{\sigma} (-1)^{\sigma} \hat{\mathcal{P}}_{\sigma} \left[\prod_i^{N_e} \chi_i(\mathbf{x}_i) \right] \end{aligned} \quad (3)$$

where $\chi(\mathbf{x})$ is a one-electron spin-orbital which can be written most generally as

$$\chi(\mathbf{x}) = \omega_{\cdot\delta}(s) \varphi_{\cdot\mu}(\mathbf{r}) G^{\delta\mu}, \quad (4)$$

where ω and φ are the spin and spatial basis functions and $G^{\delta\mu}$ a contravariant component of the generalized spin-orbital coefficient vector

labeled by the double index $\delta\mu$ in the covariant direct-product basis,

$$\{\omega_{\cdot\delta}, \omega_{\cdot\epsilon}, \dots\} \otimes \{\varphi_{\cdot\mu}, \varphi_{\cdot\nu}, \dots\}$$

Any twice-occurring Greek indices are implicitly contracted over.³⁶ Furthermore, we use \mathbf{x} to denote composite spin-spatial coordinates in overall spin-orbitals, but s and \mathbf{r} to indicate separate spin and spatial coordinates in basis functions, respectively.

2.1 Symmetry Breaking in the HF Approximation

The symmetry of the Hamiltonian in Equation (1) imposes strict constraints on the symmetry and degeneracy of its eigenfunctions. This is formalized by the following theorem relating group theory to quantum mechanics:^{37–39}

Theorem 1. *If a Hamiltonian is invariant under a particular symmetry group \mathcal{G} , that is, it commutes with all symmetry operations in \mathcal{G} , then the eigenfunctions corresponding to one energy level form a basis for an irreducible representation of \mathcal{G} .*

We first consider the implications of this theorem for the spatial symmetry of SCF HF solutions. If \mathcal{B} is the largest spatial point group under which the spinless Hamiltonian $\hat{\mathcal{H}}$ defined in (1) and (2) is invariant, then Theorem 1 dictates that any exact eigenfunction Ψ of $\hat{\mathcal{H}}$ together with all of its linearly independent degenerate partners must transform according to a single irreducible representation of \mathcal{B} . However, the wavefunction Ψ_{HF} optimized under the SCF HF approximation is not guaranteed to be an exact eigenfunction of $\hat{\mathcal{H}}$ and therefore need not obey Theorem 1. In fact, this non-restriction of spatial symmetry can be traced back to the form of the Fock operator,

$$\begin{aligned} \hat{f}(\mathbf{x}_1) &= \hat{h}(\mathbf{r}_1) \\ &+ \sum_j^{N_e} \int d\mathbf{x}_2 \chi_j^*(\mathbf{x}_2) \frac{1 - \hat{\mathcal{P}}_{12}}{|\mathbf{r}_1 - \mathbf{r}_2|} \chi_j(\mathbf{x}_2) \end{aligned} \quad (5)$$

with \hat{h} being the one-electron Hamiltonian operator. Here, the explicit dependence on the bare coordinates of an electron via all the spin-orbitals χ_j in the second term implies that \hat{f} is not necessarily invariant under \mathcal{B} because there are really no *a priori* symmetry constraints placed on the χ_j .⁴⁰ Consequently, the overall SCF wavefunction Ψ_{HF} assembled from these spin-orbitals together with its linearly independent degenerate partners, if any, does not have to transform as any single irreducible representation of \mathcal{B} but may form a basis for a reducible representation instead.

Theorem 1 is also applicable to groups containing spin rotation and time reversal operations, the most general of which is the direct-product group $\mathcal{S} \otimes \mathcal{T}$ where \mathcal{S} is the full spin rotation group and \mathcal{T} the time reversal group. \mathcal{S} is identical to $\text{SU}(2)$ (the two-dimensional special unitary group) by definition⁴¹ whereas \mathcal{T} is isomorphic to \mathcal{C}_4 (the cyclic group of order 4) (Appendix A.1). The irreducible representations and characters of $\mathcal{S} \otimes \mathcal{T}$ can thus be obtained from those of $\text{SU}(2)$ and \mathcal{C}_4 , which are well known.^{42,43} The invariance of \mathcal{H} under $\mathcal{S} \otimes \mathcal{T}$ ensures that any eigenfunction Ψ and its degenerate partners must also transform as one of the irreducible representations of $\mathcal{S} \otimes \mathcal{T}$. However, once again the approximate nature of the HF method does not guarantee that the SCF wavefunctions Ψ_{HF} always satisfy this condition. Nevertheless, with suitable constraints imposed on the spin and reality of the spin-orbitals, Ψ_{HF} and its degenerate partners can be forced to transform as a single irreducible representation of one of the subgroups of $\mathcal{S} \otimes \mathcal{T}$ and thus be eigenfunctions of appropriate operators constructed from the generators of the subgroup (Appendix A.2). The hierarchy of these subgroups was originally deduced by Fukutome⁴¹ but has since been presented in connection with the various HF regimes using more modern electronic-structure nomenclatures.⁴⁴⁻⁴⁶ We will be particularly interested in $\hat{\Theta}$ (the time reversal operator), \hat{S}^2 (the operator representing the square of the magnitude of the spin angular momentum), and \hat{S}_3 (the operator representing the projection of the spin angular momentum onto the third Cartesian axis,

which is typically the z -axis). In atomic units, the eigenvalues of \hat{S}^2 are well known¹³ to be $S(S+1)$ where S can take integer or half-integer values, and the corresponding eigenvalues of \hat{S}_3 are $M_S = -S, -S+1, \dots, S$. Whenever necessary, we will use upper-case notations for overall many-electron electronic states and lower-case equivalents for individual spin-orbitals.

In light of the above discussion, we propose the following definition. If a set of degenerate wavefunctions is found to form a basis for a single irreducible representation of a group \mathcal{G} , be it a spatial point group \mathcal{B} or one of the subgroups of $\mathcal{S} \otimes \mathcal{T}$, they are *symmetry-conserved* in \mathcal{G} . On the other hand, if they span a representation that can be reduced to multiple irreducible representations of \mathcal{G} , they are *symmetry-broken* in \mathcal{G} . Theorem 1 immediately rules out symmetry-broken wavefunctions as eigenfunctions of \mathcal{H} , whereas it places no such restriction on symmetry-conserved wavefunctions.

2.2 Representation Matrices of Symmetry Operations in SCF and NOCI Bases

Consider a set of N_{det} degenerate Slater determinants that are possibly non-orthogonal and not all linearly independent,

$$\{ {}^w \Psi \mid w = 1, 2, \dots, N_{\text{det}} \} \quad (6)$$

The overlap matrix \mathbf{S} in this basis is defined as

$${}^{wx} S = (\mathbf{S})_{wx} = \langle {}^w \Psi \mid {}^x \Psi \rangle \quad (7)$$

which is a square matrix with dimensions $N_{\text{det}} \times N_{\text{det}}$ and rank $N_{\text{indept}} \leq N_{\text{det}}$. It is possible to construct an $N_{\text{det}} \times N_{\text{indept}}$ matrix \mathbf{X} that transforms the above basis into a linearly independent one (henceforth denoted by a tilde) in which the overlap matrix

$$\tilde{\mathbf{S}} = \mathbf{X}^\dagger \mathbf{S} \mathbf{X} \quad (8)$$

is of full rank. By means of the non-orthogonal projection operator defined by Soriano and Palacios,⁴⁷ we show in Appendix B that the

representation matrix of a symmetry operation \hat{R} in the linearly independent basis takes the form

$$\tilde{\mathbf{D}}(\hat{R}) = \tilde{\mathbf{S}}^{-1} \mathbf{X}^\dagger \mathbf{T}(\hat{R}) \mathbf{X} \quad (9)$$

where the elements of $\mathbf{T}(\hat{R})$ are given by

$$T_{wx}(\hat{R}) = \langle {}^w\Psi | \hat{R}^x \Psi \rangle \quad (10)$$

We now let

$$\{ {}^m\Phi \mid m = 1, 2, \dots, N_{\text{indept}} \}$$

be the set of N_{indept} linearly independent NOCI wavefunctions obtained from the above N_{det} degenerate Slater determinants as

$${}^m\Phi = \sum_w^{N_{\text{det}}} {}^w\Psi A_{wm} \quad (11)$$

where A_{wm} are elements of the $N_{\text{det}} \times N_{\text{indept}}$ matrix \mathbf{A} that solves the secular equation³⁰

$$\mathbf{H}\mathbf{A} = \mathbf{S}\mathbf{A}\mathbf{E} \quad (12)$$

with \mathbf{H} given by

$${}^{wx}H = (\mathbf{H})_{wx} = \langle {}^w\Psi | \hat{\mathcal{H}}^x \Psi \rangle \quad (13)$$

and the eigenvalues collected in $\mathbf{E} = \text{diag}(E_1, \dots, E_{N_{\text{indept}}})$ give the energies of the NOCI wavefunctions. The representation matrix of \hat{R} in the NOCI basis can be shown (Appendix B) to take the form

$$\begin{aligned} \mathbf{D}^{\text{NOCI}}(\hat{R}) &= \tilde{\mathbf{D}}^{\text{NOCI}}(\hat{R}) \\ &= (\mathbf{X}^\dagger \mathbf{S}\mathbf{A})^{-1} \mathbf{X}^\dagger \mathbf{T}(\hat{R}) \mathbf{A} \end{aligned} \quad (14)$$

The matrix elements of \mathbf{H} , \mathbf{S} , and $\mathbf{T}(\hat{R})$ involving non-orthogonal determinants can be easily calculated using Löwdin’s paired orbitals.^{30,48–50}

By solving the NOCI secular equation (12), we effectively allow the different irreducible representation components spanned by the symmetry-broken set $\{ {}^w\Psi \}$ to interact via the totally symmetric $\hat{\mathcal{H}}$ and form linear combinations that transform as single irreducible representations and hence conserve symmetry. $\mathbf{D}^{\text{NOCI}}(\hat{R})$ must therefore have a block-diagonal

structure in which each little block is an irreducible matrix representation of \hat{R} in the basis of the corresponding NOCI wavefunctions.⁵¹ Furthermore, we show in Appendix D that, from each NOCI wavefunction ${}^m\Phi$, a one-particle density matrix can be constructed which can be diagonalized to give natural orbitals and the associated occupation numbers. In addition to giving us a way to visualize the NOCI wavefunctions, these provide further insight into the correlation that they recover by restoring broken symmetry.

3 Computational Details

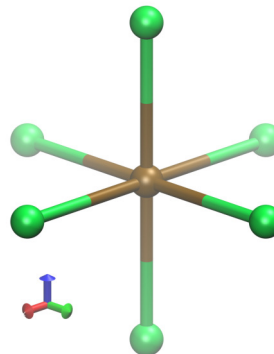


Figure 1: Generic structure of octahedral $[\text{MF}_6]^{3-}$ ($\text{M} = \text{Ti}, \text{V}$) visualized with VMD.⁵² Fluoride ligands (green) lie on the Cartesian axes equidistant to the metal center (ocher) at the origin of the coordinate system.

In both model $[\text{MF}_6]^{3-}$ ($\text{M} = \text{Ti}, \text{V}$) complexes, the fluoride ligands lie on the Cartesian axes and are equidistant to the metal center at the origin (Figure 1). The procedure for obtaining and restoring the symmetry of multiple SCF HF solutions in these complexes is sketched in Figure 2. These solutions were located within the Unrestricted Hartree–Fock (UHF) space using the Direct Inversion in the Iterative Subspace (DIIS) algorithm⁵³ in conjunction with SCF metadynamics²² in Q-CHEM 5.1.⁵⁴ Pople’s double-zeta split-valence 6-31G* basis sets were employed for all atoms with Cartesian forms for d functions and pure forms for f functions. Each solution was considered to have reached convergence when the DIIS error

fell below 1×10^{-13} (unless stated otherwise). More detailed Q-CHEM input parameters are listed in the Supporting Information.

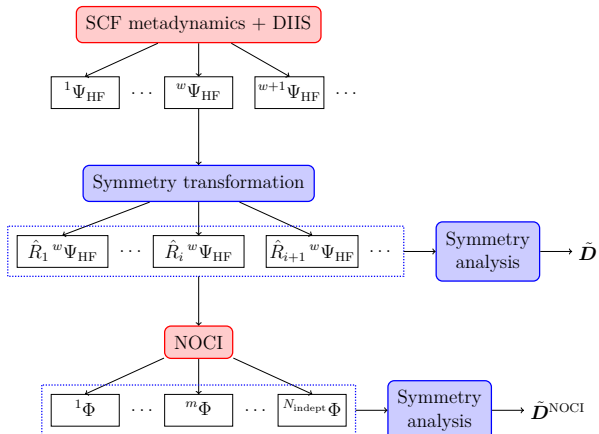


Figure 2: Computational procedure for generating and running NOCI on symmetry-equivalent SCF HF solutions. Boxes with solid red boundaries denote calculations run in Q-CHEM. Boxes with solid blue boundaries denote routines run in our Python codes. Wavefunctions enclosed in black boxes are passed between Q-CHEM and our Python codes.

Various spatial symmetry operations \hat{R} of the \mathcal{O}_h point group were then applied to the converged SCF HF solutions to generate their symmetry-equivalent partners. The effect of \hat{R} on each single-determinantal solution defined in (3) can be written as

$$\hat{R}\Psi_{\text{HF}} = \frac{1}{\sqrt{N_e!}} \sum_{\sigma} (-1)^{\sigma} \hat{\mathcal{P}}_{\sigma} \left\{ \prod_i^{N_e} [\hat{R}\chi_i(\mathbf{x}_i)] \right\} \quad (15)$$

We show in Appendix C that \hat{R} transforms the spin-orbitals $\chi_i(\mathbf{x}_i)$ into

$$\hat{R}\chi_i(\mathbf{x}_i) = \omega_{\delta}(s_i) \left\{ \hat{R}\tilde{\varphi}_{\cdot\mu} \left[\hat{R}(\mathbf{r}_i - \mathbf{R}_A) \right] \right\} G_i^{\delta\mu}, \quad (16)$$

where $\hat{R}\tilde{\varphi}_{\cdot\mu} \left[\hat{R}(\mathbf{r}_i - \mathbf{R}_A) \right]$ denotes a spatial atomic orbital that is originally centered on nucleus A but that has been moved to a possibly different nucleus, say A' , before being transformed by the same \hat{R} in its new local coor-

dinate system centered on A' . Here, A' is the nucleus onto which A is mapped by the action of \hat{R} on the nuclear framework. The calculation of $\hat{R}\tilde{\varphi}_{\cdot\mu}$ in terms of unitary transformation matrices in spherical harmonic bases is also formulated in Appendix C, which allows for a simple implementation of all symmetry transformation routines within a set of Python 2.7 codes using NumPy⁵⁵ developed in-house. Each $\hat{R}\Psi_{\text{HF}}$ determinant generated using symmetry was used as an initial guess for an SCF calculation with the same convergence criteria as described above. The converged solution was then compared with $\hat{R}\Psi_{\text{HF}}$ using the square state distance metric, d_{wx}^2 , defined by Thom and Head-Gordon²² to ensure that they were identical within numerical errors ($d_{wx}^2 \leq 1 \times 10^{-13}$ electrons), thus confirming that $\hat{R}\Psi_{\text{HF}}$ is indeed an SCF HF solution.

The volumetric data for the spatial form of all spin-orbitals was generated in Q-CHEM and are represented by isosurfaces plotted using the Tachyon ray-tracing library⁵⁶ in VMD.⁵²

The multiple SCF HF solutions generated by symmetry were reread into Q-CHEM 5.1 and a NOCI calculation was performed on them. The NOCI eigenvectors, as well as the associated SCF HF solutions, were then fed back into the Python codes so that the representation matrices in the NOCI basis, $\tilde{\mathbf{D}}^{\text{NOCI}}$, could be computed using (14) and checked for block-diagonality. The trace of each block in $\tilde{\mathbf{D}}^{\text{NOCI}}$ was obtained trivially and the irreducible representation spanned by the corresponding NOCI states deduced.

4 d^1 Metal Ground Configuration

4.1 True d^1 Octahedral System

For a single electron described by a set of spin-orbitals with d spatial symmetry in an octahedral field of point charges, group theory dictates that the only possible terms of the exact electronic wavefunctions are ${}^2T_{2g}$ and 2E_g whose forms are shown in Table 1 using the notations of Sugano et al.³ Lower-case irreducible repre-

sensation symbols (t_{2g} , e_g) are used to denote the spatial symmetry of a single spin-orbital, whereas upper-case irreducible representation symbols (T_{2g} , E_g) are reserved for the overall spatial symmetry of the wavefunction. Unsurprisingly, the two notations coincide for the one-electron d^1 system. If the spatial parts of these wavefunctions are constructed from a single set of five degenerate hydrogenic d orbitals with principal quantum number n , then first-order perturbation theory gives the following real forms for the components of t_{2g} and e_g :³

$$\begin{aligned}
 \xi(\mathbf{r}) &= d_{yz}(\theta, \phi)R_{nd}(r) \\
 \eta(\mathbf{r}) &= d_{xz}(\theta, \phi)R_{nd}(r) \\
 \zeta(\mathbf{r}) &= d_{xy}(\theta, \phi)R_{nd}(r) \\
 u(\mathbf{r}) &= d_{z^2}(\theta, \phi)R_{nd}(r) \\
 v(\mathbf{r}) &= d_{x^2-y^2}(\theta, \phi)R_{nd}(r)
 \end{aligned} \tag{17}$$

where d_{yz} , d_{xz} , d_{xy} , d_{z^2} , and $d_{x^2-y^2}$ denote the familiar (real) spherical harmonics of degree 2 and R_{nd} the hydrogenic radial wavefunction of the nd subshell. The energy difference between the ${}^2T_{2g}$ and 2E_g terms is commonly denoted as $\Delta_{\text{oct}} = 10Dq$.^{1,3,57}

4.2 $[\text{TiF}_6]^{3-}$

The octahedral $[\text{TiF}_6]^{3-}$ anion has a more complicated electronic structure, however. If all six ligands are considered to be closed-shell F^- , the metal center is then Ti^{3+} which has the configuration $[\text{Ar}]3d^1$. The unpaired $3d^1$ electron still lies in an octahedral field of point charges set up by the nuclei but now exhibits electron–electron interaction with the Ar core and the F^- ligands, and the analytic results for a true d^1 system presented above no longer rigorously applies. However, in most theoretical treatments, the fully filled shells on both the metal center and the ligands are ignored on the grounds that they only contribute a totally symmetric singlet component to the overall wavefunction which shifts the energy of every term derived for the true d^1 system by a constant amount (see Chapter 7 of Ref. 1). While this is often a reasonable assumption to simplify the analytic descriptions and provide an excellent start-

ing point for the qualitative understanding of the electronic terms present, it glosses over any electron correlations between the valence d electrons and the other electrons in the system.

Overview of UHF solutions. Figure 3 presents the energy, spatial symmetry, and labels of the lowest-energy $M_S = \frac{1}{2}$ UHF solutions located by SCF metadynamics in octahedral $[\text{TiF}_6]^{3-}$ at Ti–F bond length of 2.0274 Å. The representative Pipek–Mezey-localized^{58,59} spatial forms of the highest-occupied $m_s = \frac{1}{2}$ spin-orbitals in these solutions are shown in Table 2 and detailed solution energies and overlap matrices for the degenerate sets can be found in the Supporting Information. There are two groups of solutions approximately $0.063 E_h \approx 14\,000 \text{ cm}^{-1}$ apart, which is expected from the two possible d^1 terms in an octahedral field presented earlier and from the experimental values for Δ_{oct} in this anionic complex.⁶⁰ However, in order to assign these solutions to the expected terms, their spin and spatial symmetry properties need to be examined.

We turn first to the lower group of solutions. There are two degenerate sets within this group, namely $A_{\frac{1}{2}}$ and $A'_{\frac{1}{2}}$, whose energies differ by about $1.2 \times 10^{-5} E_h$. The $A_{\frac{1}{2}}$ set is six-fold degenerate and forms a basis for the $T_{1g} \oplus T_{2g}$ representation in \mathcal{O}_h . It is therefore symmetry-broken because it spans more than one irreducible representation. A consideration of the spatial forms of the highest-occupied spin-orbitals of the $A_{\frac{1}{2}}$ solutions (one representative shown in Table 2) suggests why this is the case: the valence $3d$ spin-orbital in each solution has the familiar $d_{xy}/d_{yz}/d_{xz}$ form but has been rotated by $\pi/4$ out of the Cartesian planes of the ligands. There are thus six equivalent orientations of the valence $3d$ spin-orbital, each of which corresponds to a linearly independent but degenerate UHF solution. On the other hand, the $A'_{\frac{1}{2}}$ set only spans T_{2g} and is therefore symmetry-conserved: the valence $3d$ spin-orbital in each $A'_{\frac{1}{2}}$ solution lies properly in one of the three Cartesian ligand planes. Consequently, the valence $3d$ electron in the $A'_{\frac{1}{2}}$ solutions experiences a stronger repulsion from the

Table 1: All possible d^1 terms in an octahedral field. ξ , η , and ζ are the components of T_{2g} while u and v are the components of E_g . Each spin-orbital is also an eigenfunction of the \hat{s}_3 operator with eigenvalue $m_s = \frac{1}{2}$ (without bar) or $-\frac{1}{2}$ (with bar).

Config.	Term	Comp.	$M_S = \frac{1}{2}$	$M_S = -\frac{1}{2}$
t_{2g}^1	${}^2T_{2g}$	ξ	$\xi(\mathbf{x})$	$\bar{\xi}(\mathbf{x})$
		η	$\eta(\mathbf{x})$	$\bar{\eta}(\mathbf{x})$
		ζ	$\zeta(\mathbf{x})$	$\bar{\zeta}(\mathbf{x})$
e_g^1	2E_g	u	$u(\mathbf{x})$	$\bar{u}(\mathbf{x})$
		v	$v(\mathbf{x})$	$\bar{v}(\mathbf{x})$

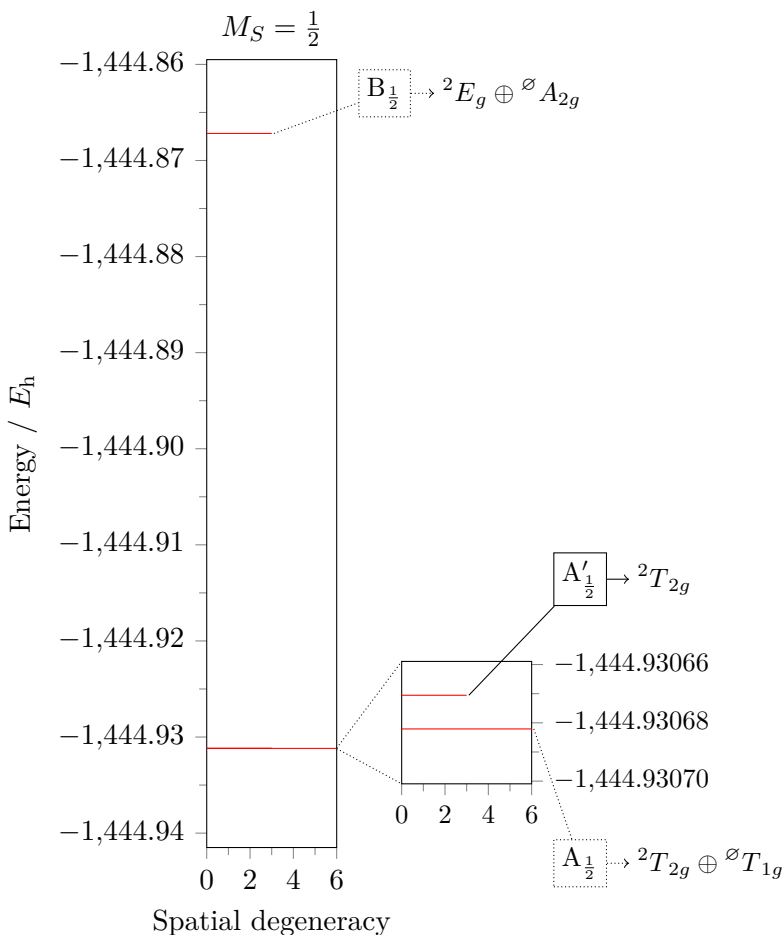
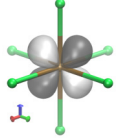
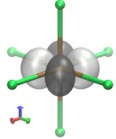
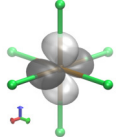


Figure 3: Energy and symmetry of low-lying UHF solutions (6-31G* basis) in octahedral $[\text{TiF}_6]^{3-}$ having $\text{Ti-F} = 2.0274 \text{ \AA}$. All solutions have DIIS errors smaller than 1×10^{-13} . All solutions have $N_\alpha - N_\beta = 1$ and are thus eigenfunctions of \hat{S}_3 with the same eigenvalue $M_S = \frac{1}{2}$ given as subscripts. Solutions are considered degenerate when their energies are at most $10^{-9} E_h$ apart and are labeled alphabetically in increasing order of their energies. Nearly degenerate solutions share the same letter but are distinguished by dashes. Solutions within one degenerate set are distinct and linearly independent. Solutions that conserve spatial symmetry are enclosed in solid boxes whereas solutions that break spatial symmetry are enclosed in dotted ones. See the main text for a discussion on spin multiplicities.

Table 2: Representative isosurface plots for the Pipek–Mezey-localized spatial parts of the highest-occupied $m_s = \frac{1}{2}$ spin-orbitals, spatial symmetry, and $\langle \hat{S}^2 \rangle$ of the $M_S = \frac{1}{2}$ UHF solutions in $[\text{TiF}_6]^{3-}$. The spin-orbitals of all solutions within one set have similar forms and are related by the symmetry operations of \mathcal{O}_h . Spatial symmetry lists the irreducible representations of \mathcal{O}_h spanned by the degenerate sets. Axis triad: red– x ; green– y ; blue– z .

Ψ_{UHF}	χ_{40}	Spatial symmetry	$\langle \hat{S}^2 \rangle$
$A_{\frac{1}{2}}$		$T_{1g} \oplus T_{2g}$	0.7522
$A'_{\frac{1}{2}}$		T_{2g}	0.7522
$B_{\frac{1}{2}}$		$A_{2g} \oplus E_g$	0.7527

ligand electrons which raises the energy of the $A'_{\frac{1}{2}}$ set slightly above that of $A_{\frac{1}{2}}$ (Figure 3).

We must now pause for a moment to consider the significance of the existence of the symmetry-broken $A_{\frac{1}{2}}$ solutions in $[\text{TiF}_6]^{3-}$. In a true d^1 system, there *cannot* exist any symmetry-broken one-electron wavefunctions comprising spin-orbitals similar to the valence $3d$ ones in the $A_{\frac{1}{2}}$ solutions. Firstly, any T_{1g} component is strictly forbidden by symmetry. Secondly, the T_{2g} space is fully spanned by the degenerate ξ , η , and ζ components shown in (17), so any linear combinations of these three functions to give the valence $3d$ spin-orbitals of $A_{\frac{1}{2}}$ necessarily live in the same space and have the same energy. However, in $[\text{TiF}_6]^{3-}$, the Ar core and the F^- electrons can relax differently in the presence of the different orientations of the valence $3d$ spin-orbitals relative to the ligand axes to give $A_{\frac{1}{2}}$ and $A'_{\frac{1}{2}}$ UHF solutions with different energies and symmetries. Both $A_{\frac{1}{2}}$ and $A'_{\frac{1}{2}}$ solutions contain a T_{2g} component and are thus approximations to an exact wavefunction with T_{2g} spatial symmetry which we assume to be the ground wavefunction,⁶¹ but the $A_{\frac{1}{2}}$ so-

lutions provide a tighter approximation in light of the variational principle because they incorporate some correlation between the valence $3d$ electron and the remaining electrons to result in symmetry-brokenness and become lower in energy.

We now shift our attention to the $B_{\frac{1}{2}}$ set. This set spans $A_{2g} \oplus E_g$ and is thus considered to be a symmetry-broken approximation of an exact wavefunction with E_g spatial symmetry, but the $d_{x^2-y^2}$ -like form of the valence $3d$ spin-orbital (Table 2) seems to suggest that this set conserves spatial symmetry, so what is going on? It turns out that, for a true d^1 system, the spatial orbital $d_{x^2-y^2}(\theta, \phi)R_{nd}(r)$ and its symmetry partners, $d_{y^2-z^2}(\theta, \phi)R_{nd}(r)$ and $d_{x^2-z^2}(\theta, \phi)R_{nd}(r)$, are clearly not all linearly independent and can be shown to indeed span the same E_g space as $u(\mathbf{r})$ and $v(\mathbf{r})$ defined in (17).³ In contrast, the presence of the core and ligand electrons in $[\text{TiF}_6]^{3-}$ removes this linear dependence such that the three $B_{\frac{1}{2}}$ solutions span a larger space that contains an additional A_{2g} component and become symmetry-broken, effectively incorporating a similar kind of correlation as discussed for the $A_{\frac{1}{2}}$ solutions.

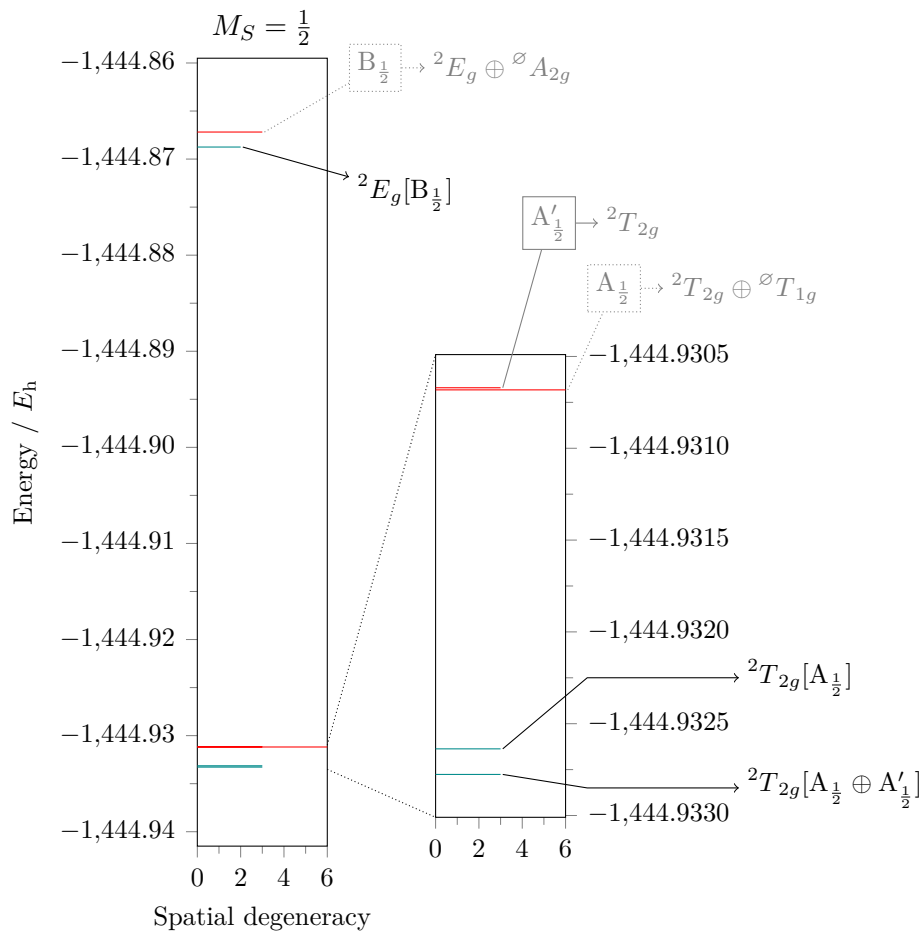
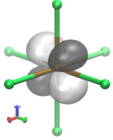
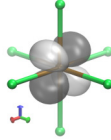
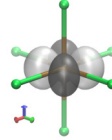
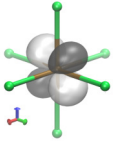
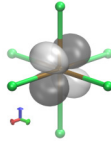
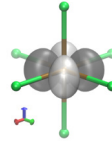
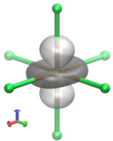
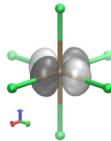


Figure 4: Low-lying NOCI wavefunctions (dark cyan) constructed from the low-lying $M_S = \frac{1}{2}$ UHF solutions in octahedral $[\text{TiF}_6]^{3-}$ (red, replotted from Figure 3 for comparison). NOCI wavefunctions are considered degenerate when their energies are at most $10^{-7} E_h$ apart. In generic notations, $\Gamma[A \oplus B]$ denotes a specific NOCI set of symmetry Γ constructed from both A and B solutions.

Table 3: Isosurface plots for the Pipek–Mezey-localized spatial parts of the $3d$ natural orbitals and $\langle \hat{S}^2 \rangle$ of the low-energy NOCI wavefunctions Φ in $[\text{TiF}_6]^{3-}$. Each $3d$ natural orbital shown in each set corresponds to one of the NOCI wavefunctions within the set that transforms as the labeled component. Shown in parentheses underneath are the occupation numbers of the natural orbitals. The occupation numbers and natural orbitals shown are solely in the $m_s = \frac{1}{2}$ space. Axis triad: red– x ; green– y ; blue– z .

Φ	$3d$ natural orbitals			$\langle \hat{S}^2 \rangle$	Term
${}^2T_{2g}[A_{\frac{1}{2}}]$				0.7512	${}^2T_{2g}(t_{2g}^1)$
	ξ (0.999)	η (0.999)	ζ (0.999)		
${}^2T_{2g}[A_{\frac{1}{2}} \oplus A'_{\frac{1}{2}}]$				0.7512	${}^2T_{2g}(t_{2g}^1)$
	ξ (1.000)	η (1.000)	ζ (1.000)		
${}^2E_g[B_{\frac{1}{2}}]$				0.7517	${}^2E_g(e_g^1)$
	u (1.000)	v (1.000)			

Symmetry restoration of individual symmetry-broken UHF sets. Even though the $A_{\frac{1}{2}}$ and $B_{\frac{1}{2}}$ solutions include additional valence–core and valence–ligand electron correlation by breaking symmetry, their symmetry-broken nature implies that they cannot be taken as good approximations of the T_{2g} and E_g wavefunctions in $[\text{TiF}_6]^{3-}$ owing to Theorem 1. This has long been known as the “symmetry dilemma” first pointed out by Löwdin.⁶² NOCI can, however, be used to form symmetry-conserved wavefunctions from multiple symmetry-broken SCF solutions. Figure 4 shows the energy and spatial symmetry of low-lying NOCI wavefunctions constructed from the UHF solutions in octahedral $[\text{TiF}_6]^{3-}$ discussed so far and Table 3 gives the forms of the corresponding $3d$ natural orbitals (see Appendix D), also localized using the Pipek–Mezey algorithm. Detailed NOCI results can be found in the Supporting Information. Arising from the six symmetry-broken $A_{\frac{1}{2}}$ solutions are a set of triply degenerate multi-determinantal wavefunctions that transform as T_{2g} with the expected $3d_{xy}/3d_{yz}/3d_{xz}$ natural orbitals and another set that transform as T_{1g} . These two sets are denoted ${}^2T_{2g}[A_{\frac{1}{2}}]$ and ${}^{\circ}T_{1g}[A_{\frac{1}{2}}]$, respectively. The spatial irreducible representation designation in these notations is obvious, but we will come back to the designation of spin multiplicity at the end of this section. The ${}^2T_{2g}[A_{\frac{1}{2}}]$ set is $1.96 \times 10^{-3} E_h$ lower in energy than the $A_{\frac{1}{2}}$ solutions whereas the ${}^{\circ}T_{1g}[A_{\frac{1}{2}}]$ set is more than $2 E_h$ higher and is thus discarded on the basis that it is too high in energy to be of any physical interest. Likewise, from the symmetry-broken $B_{\frac{1}{2}}$ solutions, we obtain a ${}^2E_g[B_{\frac{1}{2}}]$ set $1.56 \times 10^{-3} E_h$ lower in energy with $3d_{x^2-y^2}$ and $3d_{z^2}$ natural orbitals and an unphysical ${}^{\circ}A_{2g}[B_{\frac{1}{2}}]$ set approximately $2 E_h$ higher in energy. These results are very encouraging as they illustrate that NOCI has the capability to purify the symmetry component that a set of symmetry-broken SCF wavefunctions are trying to approximate while definitively picking out symmetry components that have been mixed in only as a consequence of symmetry breaking to incorporate electron

correlation.

NOCI between multiple degenerate UHF sets. We can, however, take a step further. Observing that the $A_{\frac{1}{2}}$ and $A'_{\frac{1}{2}}$ sets both contain a spatial T_{2g} component, we expect them to interact with each other via the common T_{2g} space. Indeed, when taking both the $A_{\frac{1}{2}}$ and $A'_{\frac{1}{2}}$ solutions as bases for NOCI, we obtain a set denoted by ${}^2T_{2g}[A_{\frac{1}{2}} \oplus A'_{\frac{1}{2}}]$ that transforms as T_{2g} and two other high-energy sets denoted by ${}^{\circ}T_{2g}[A_{\frac{1}{2}} \oplus A'_{\frac{1}{2}}]$ and ${}^{\circ}T_{1g}[A_{\frac{1}{2}} \oplus A'_{\frac{1}{2}}]$. The ${}^2T_{2g}[A_{\frac{1}{2}} \oplus A'_{\frac{1}{2}}]$ set has similar $3d$ natural orbitals to ${}^2T_{2g}[A_{\frac{1}{2}}]$ but is $1.4 \times 10^{-4} E_h$ lower in energy and must therefore be a better approximation of the true ${}^2T_{2g}$ ground-state wavefunctions by the variational principle.

Spin multiplicity assignments. We conclude this section with a few comments on the spin properties of the UHF and NOCI wavefunctions of $[\text{TiF}_6]^{3-}$. All UHF solutions discussed so far have $N_{\alpha} - N_{\beta} = 1$ and are thus eigenfunctions of \hat{S}_z with eigenvalue $M_S = \frac{1}{2}$, as expected from Fukutome’s classification for UHF.⁴¹ The NOCI wavefunctions obtained as linear combinations of these UHF solutions must also be eigenfunctions of \hat{S}_z with the same eigenvalue $M_S = \frac{1}{2}$. However, the $\langle \hat{S}^2 \rangle$ values in Tables 2 and 3 show that none of these wavefunctions is a strict eigenfunction of \hat{S}^2 because a true doublet must have $\langle \hat{S}^2 \rangle$ equal to $\frac{3}{4}$ exactly, and the observed deviations on the order of 1×10^{-3} must be an indication of spin contamination from the $M_S = \frac{1}{2}$ components of higher spin states. Slight but consistent reduction of $\langle \hat{S}^2 \rangle$ in the NOCI wavefunctions compared to the basis UHF solutions shows that, even by restoring spatial symmetry, NOCI can improve spin purity as well, although not by much. Nevertheless, we can still regard the NOCI wavefunctions ${}^2T_{2g}[A_{\frac{1}{2}}]$, ${}^2T_{2g}[A_{\frac{1}{2}} \oplus A'_{\frac{1}{2}}]$, and ${}^2E_g[B_{\frac{1}{2}}]$ as reasonable approximations of true spin doublets and assign them a spin multiplicity of two as denoted by their pre-superscripts. On the other hand, the high-lying NOCI sets that we discarded,

${}^{\circ}T_{1g}[A_{\frac{1}{2}}]$, ${}^{\circ}T_{2g}[A_{\frac{1}{2}} \oplus A'_{\frac{1}{2}}]$, ${}^{\circ}T_{1g}[A_{\frac{1}{2}} \oplus A'_{\frac{1}{2}}]$, and ${}^{\circ}A_{2g}[B_{\frac{1}{2}}]$, have $\langle \hat{S}^2 \rangle$ values that do not correspond to any integral spin multiplicities (more than 1×10^{-2} away from any expected \hat{S}^2 eigenvalues, see Supporting Information). The symbol “ \circ ” is therefore used to denote these undefined spin multiplicities.

5 d^2 Metal Ground Configuration

5.1 True d^2 Octahedral System

The main aim of this Section is to discuss the low-energy UHF and NOCI wavefunctions of the octahedral $[\text{VF}_6]^{3-}$ anion. However, the interaction between the two d electrons in the presence of the core and ligand electrons complicates the results significantly, so we will first study a toy system where all core and ligand electrons are stripped away. We will then see that the results in this system help clarify the correlation nature of the UHF and NOCI wavefunctions in $[\text{VF}_6]^{3-}$.

5.1.1 Symmetry-Conserved Wavefunctions in the Strong-Field Coupling Scheme

For a true d^2 system in an octahedral field of point charges, the strong-field coupling scheme¹ describes each electron by an independent set of $m_s = \pm\frac{1}{2}$ spin-orbitals with spatial symmetry of either t_{2g} or e_g and then couples them together using Clebsch–Gordan coefficients for the spatial part and Wigner coefficients for the spin part³ such that the resulted wavefunctions satisfy Pauli’s antisymmetry, transform as single irreducible representations in \mathcal{O}_h , and are eigenfunctions of \hat{S}^2 . There are thus three possible configurations split into 11 allowed terms whose components are summarized in Table 4 from Sugano et al.³ Once again, only if each electron is described by a single set of five degenerate hydrogenic nd orbitals are the t_{2g} and e_g components given by (17). In addition, unlike the d^1 case, there is now a clear distinction between the lower-case irreducible representation

symbols denoting the spatial symmetry of a single electron in the strong-field coupling scheme and the upper-case irreducible representation symbols describing the overall spatial symmetry of the wavefunction. Inspection of Table 4 reveals that each allowed $M_S = \pm 1$ wavefunction only needs a single determinant to satisfy spin and spatial symmetry, whereas every $M_S = 0$ wavefunction requires at least two determinants to fulfill the same conditions and thus exhibits strong correlation between the d electrons that is due solely to spin and spatial symmetry demands.

To further complicate matters, there are pairs of terms arising from different strong-field configurations which have identical spin and spatial symmetry and can therefore interact with each other in what is known as *configuration mixing*.³ One example would be the interaction between ${}^3T_{1g}(t_{2g}^2)$ and ${}^3T_{1g}(t_{2g}^1 e_g^1)$ to give rise to two new terms labeled a^3T_{1g} and b^3T_{1g} with the former having a lower energy than the latter (also defined in the caption of Table 4). When this happens, the number of determinants required to describe the mixed-configuration wavefunctions must increase, thereby signifying even more correlation effects. As a consequence, the true ${}^3T_{1g}$ ground term cannot be described by any single determinants, even within the $M_S = \pm 1$ spaces. This behavior turns out to have important implications for the nature of the UHF solutions in both the d^2 octahedral toy system and the full $[\text{VF}_6]^{3-}$ anion.

5.1.2 UHF and NOCI Wavefunctions in a d^2 Octahedral Toy System

The strong-field coupling scheme enables wavefunctions that respect all symmetry requirements to be constructed from spin-orbitals. However, this scheme quickly becomes tedious when more interacting electrons are introduced (see, for example, Chapters 3 and 4 of Ref. 3). Furthermore, as the scheme relies on symmetry alone, it cannot provide any functional descriptions of the constituting spin-orbitals *ab initio*. Fortunately, the HF method combined with NOCI for symmetry restoration gives us

Table 4: All possible d^2 terms in an octahedral field. $|\chi_1\chi_2|$ denotes a normalized Slater determinant constructed from spin-orbitals χ_1 and χ_2 . e_1 is the only component of A_{1g} ; e_2 the only component of A_{2g} ; α , β , and γ the components of T_{1g} ; ξ , η , and ζ the components of T_{2g} ; and u and v the components of E_g , with $u_x = -\frac{1}{2}u + \frac{\sqrt{3}}{2}v$, $u_y = -\frac{1}{2}u - \frac{\sqrt{3}}{2}v$, $u_z = u$, $v_x = -\frac{\sqrt{3}}{2}u - \frac{1}{2}v$, $v_y = \frac{\sqrt{3}}{2}u - \frac{1}{2}v$, and $v_z = v$. Each spin-orbital is also an eigenfunction of the \hat{s}_3 operator with eigenvalue $m_s = \frac{1}{2}$ (without bar) or $-\frac{1}{2}$ (with bar). Two terms of the same symmetry Γ but belonging to two different configurations can interact further to give rise to two new terms $a\Gamma$ and $b\Gamma$ (not shown here) where $E(a\Gamma) < E(b\Gamma)$.³

Config.	Term	Comp.	$M_S = 1$	$M_S = 0$	$M_S = -1$
t_{2g}^2	${}^3T_{1g}$	α	$ \eta\zeta $	$\frac{1}{\sqrt{2}}(\eta\bar{\zeta} - \zeta\bar{\eta})$	$ \bar{\eta}\bar{\zeta} $
		β	$ \zeta\xi $	$\frac{1}{\sqrt{2}}(\zeta\bar{\xi} - \xi\bar{\zeta})$	$ \bar{\zeta}\bar{\xi} $
		γ	$ \xi\eta $	$\frac{1}{\sqrt{2}}(\xi\bar{\eta} - \eta\bar{\xi})$	$ \bar{\xi}\bar{\eta} $
	${}^1T_{2g}$	ξ	–	$\frac{1}{\sqrt{2}}(\eta\bar{\zeta} + \zeta\bar{\eta})$	–
		η	–	$\frac{1}{\sqrt{2}}(\zeta\bar{\xi} + \xi\bar{\zeta})$	–
		ζ	–	$\frac{1}{\sqrt{2}}(\xi\bar{\eta} + \eta\bar{\xi})$	–
	1E_g	u	–	$\frac{1}{\sqrt{6}}(- \xi\bar{\xi} - \eta\bar{\eta} + 2 \zeta\bar{\zeta})$	–
		v	–	$\frac{1}{\sqrt{2}}(\xi\bar{\xi} - \eta\bar{\eta})$	–
	${}^1A_{1g}$	e_1	–	$\frac{1}{\sqrt{3}}(\xi\bar{\xi} + \eta\bar{\eta} + \zeta\bar{\zeta})$	–
	$t_{2g}^1e_g^1$	${}^3T_{1g}$	α	$ \xi v_x $	$\frac{1}{\sqrt{2}}(\xi\bar{v}_x - v_x\bar{\xi})$
β			$ \eta v_y $	$\frac{1}{\sqrt{2}}(\eta\bar{v}_y - v_y\bar{\eta})$	$ \bar{\eta}\bar{v}_y $
γ			$ \zeta v_z $	$\frac{1}{\sqrt{2}}(\zeta\bar{v}_z - v_z\bar{\zeta})$	$ \bar{\zeta}\bar{v}_z $
${}^3T_{2g}$		ξ	$ \xi u_x $	$\frac{1}{\sqrt{2}}(\xi\bar{u}_x - u_x\bar{\xi})$	$ \bar{\xi}\bar{u}_x $
		η	$ \eta u_y $	$\frac{1}{\sqrt{2}}(\eta\bar{u}_y - u_y\bar{\eta})$	$ \bar{\eta}\bar{u}_y $
		ζ	$ \zeta u_z $	$\frac{1}{\sqrt{2}}(\zeta\bar{u}_z - u_z\bar{\zeta})$	$ \bar{\zeta}\bar{u}_z $
${}^1T_{1g}$		α	–	$\frac{1}{\sqrt{2}}(\xi\bar{v}_x + v_x\bar{\xi})$	–
		β	–	$\frac{1}{\sqrt{2}}(\eta\bar{v}_y + v_y\bar{\eta})$	–
		γ	–	$\frac{1}{\sqrt{2}}(\zeta\bar{v}_z + v_z\bar{\zeta})$	–
${}^1T_{2g}$		ξ	–	$\frac{1}{\sqrt{2}}(\xi\bar{u}_x + u_x\bar{\xi})$	–
		η	–	$\frac{1}{\sqrt{2}}(\eta\bar{u}_y + u_y\bar{\eta})$	–
		ζ	–	$\frac{1}{\sqrt{2}}(\zeta\bar{u}_z + u_z\bar{\zeta})$	–
e_g^2		${}^3A_{2g}$	e_2	$ uv $	$\frac{1}{\sqrt{2}}(u\bar{v} - v\bar{u})$
	1E_g	u	–	$\frac{1}{\sqrt{2}}(- u\bar{u} + v\bar{v})$	–
		v	–	$\frac{1}{\sqrt{2}}(u\bar{v} + v\bar{u})$	–
	${}^1A_{1g}$	e_1	–	$\frac{1}{\sqrt{2}}(u\bar{u} + v\bar{v})$	–

a plausible way around this. To investigate how this works for a true d^2 octahedral system, we carried out SCF metadynamics calculations on a toy complex consisting of a B^{3+} center at the origin surrounded by six -1 point charges placed along the Cartesian axes at a distance of 1.9896 Å from the origin. We denote this system as $[(B^{3+})(q^-)_6]$. There are only two electrons in this system, each of which is described by a basis set composed only of five pure d functions contracted from the three primitive Gaussian functions in the first D shell of vanadium’s 6-31G*.⁶³ The boron nucleus is chosen so that the two electrons experience a nuclear charge of $+5$, which is also the effective nuclear charge experienced by the $3d^2$ electrons in $[VF_6]^{3-}$ if we assume that the [Ar] core shields the vanadium nucleus perfectly and that the F^- ligands do not shield the vanadium nucleus at all. As the sole purpose of the toy system is to help us understand the symmetry of the UHF solutions, we are not too concerned with the accuracy of the above assumptions, nor with the fact that all solutions found have positive energy (Table 5).

$M_S = 1$. Table 5a gives the energy and symmetry of the low-lying $M_S = 1$ UHF solutions in $[(B^{3+})(q^-)_6]$, all having DIIS errors smaller than 1×10^{-13} . As we will point out in Section 5.2.1, they can all be correlated to the $M_S = 1$ solutions in $[VF_6]^{3-}$ by the forms of their spin-orbitals (shown in the Supporting Information) and overall symmetry. We therefore pre-emptively denote these solutions with lower-case letters that match the upper-case labels of those in $[VF_6]^{3-}$. Expectedly, the symmetry-conserved solutions b_1 , c_1 , e_1 , and f_1 correspond exactly to the $M_S = 1$ two-electron single determinants of ${}^3T_{1g}(t_{2g}^2)$, ${}^3T_{2g}(t_{2g}^1e_g^1)$, ${}^3T_{1g}(t_{2g}^1e_g^1)$, and ${}^3A_{2g}(e_g^2)$, respectively. Since there are no core or ligand electrons in this toy system, the symmetry breaking observed in a_1 , a'_1 , and d_1 must come from the correlation between the two d electrons. To determine how much of this correlation is already accounted for by the strong-field coupling scheme in Table 4, we first restored their spatial symmetry by NOCI, the results of which are also shown in Table 5a. The NOCI wavefunctions ${}^3A_{2g}[a_1]$,

${}^3T_{2g}[a'_1]$, ${}^3T_{2g}[d_1]$, and ${}^3T_{1g}[d_1]$ have the same energy as the UHF solutions f_1 , c_1 , c_1 , and e_1 , respectively, and therefore do not recover any more correlation energy than the corresponding symmetry-conserved single determinants already do. On the other hand, the NOCI wavefunctions ${}^3T_{1g}[a_1]$ and ${}^3T_{1g}[a'_1]$ are significantly lower in energy than b_1 and not degenerate to any other symmetry-conserved single determinants we have found. Hence, they must incorporate some additional correlation missed out by the strong-field coupling scheme of independent particles occupying pure d orbitals prior to configuration mixing. In fact, it turns out that ${}^3T_{1g}[a_1]$ and ${}^3T_{1g}[a'_1]$ are both very close in energy to a ${}^3T_{1g}[b_1 \oplus e_1]$ which is the NOCI description of the lower ${}^3T_{1g}$ term arising from the configuration mixing between ${}^3T_{1g}(t_{2g}^2)$ and ${}^3T_{1g}(t_{2g}^1e_g^1)$. We can thus reasonably deduce that the symmetry breaking in a_1 and a'_1 is the consequence of an attempt within the $M_S = 1$ single-determinantal space to incorporate this inherently multi-determinantal correlation effect between the two d electrons.

$M_S = 0$. Table 5b gives the energy and symmetry of the low-lying $M_S = 0$ UHF solutions in $[(B^{3+})(q^-)_6]$, all having DIIS errors smaller than 1×10^{-13} . These solutions are also denoted with lower-case letters matching the upper-case labels of the $M_S = 0$ solutions in $[VF_6]^{3-}$, their spin-orbitals are shown in the Supporting Information, and the reason for the asterisk in the a_0^* solutions will be explained in Section 5.2.2. We note that the $S = 1$ NOCI wavefunctions ${}^3T_{1g}[a_0'']$, ${}^3T_{2g}[b_0]$, ${}^3T_{2g}[c_0]$, and ${}^3T_{1g}[e_0]$ are exactly degenerate with the spatial-symmetry-conserved $M_S = 1$ single determinants b_1 , c_1 , c_1 , and e_1 , respectively. This is not surprising at all: even though the a_0'' , c_0 , and e_0 solutions are symmetry-broken overall, within the $S = 1$ spin space they conserve spatial symmetry, so that when NOCI restores time-reversal symmetry and subsequently spin symmetry (exactly in this case as $S = 0$ and $S = 1$ are the only possible spin states for two electrons; further explanations will be detailed in Section 5.2.2), it gives the spatial-symmetry-conserved $M_S = 0$ components in

Table 5: UHF and NOCI wavefunctions in the toy system $[(B^{3+})(q^-)_6]$. All UHF wavefunctions have DIIS errors smaller than 1×10^{-13} . The symmetry of each set of symmebry-broken solutions lists terms in increasing order of NOCI energy. Each term symbol is immediately followed by the predominant associated strong-field configuration in parentheses. If configuration mixing is found to be present following an analysis of NOCI natural orbitals and occupation numbers, a second pair of parentheses denotes the minor configuration introduced to the term by this interaction. Repeated terms due to configuration mixing are distinguished based on their energy ordering using the prefixes a and b where the a term is lower in energy than the b term. If the energy ordering is not known or cannot be ascertained, a hollow diamond (\diamond) is used instead.

(a) $M_S = 1$

Ψ_{UHF}	Symmetry	Energy/ E_h	Term	$\Phi(S=1)$	Energy/ E_h	Term
a_1	${}^3T_{1g} \oplus {}^3A_{2g}$	0.948 898 2	–	${}^3T_{1g}[a_1]$	0.948 834 6	$a {}^3T_{1g}(t_{2g}^2)(t_{2g}^1 e_g^1)$
				${}^3A_{2g}[a_1]$	0.954 797 0	${}^3A_{2g}(e_g^2)$
a'_1	${}^3T_{1g} \oplus {}^3T_{2g}$	0.948 990 8	–	${}^3T_{1g}[a'_1]$	0.948 834 8	$a {}^3T_{1g}(t_{2g}^2)(t_{2g}^1 e_g^1)$
				${}^3T_{2g}[a'_1]$	0.951 493 8	${}^3T_{2g}(t_{2g}^1 e_g^1)$
b_1	${}^3T_{1g}$	0.967 763 7	${}^3T_{1g}(t_{2g}^2)$			
c_1	${}^3T_{2g}$	0.951 493 8	${}^3T_{2g}(t_{2g}^1 e_g^1)$			
d_1	${}^3T_{1g} \oplus {}^3T_{2g}$	0.971 066 9	–	${}^3T_{2g}[d_1]$	0.951 493 8	${}^3T_{2g}(t_{2g}^1 e_g^1)$
				${}^3T_{1g}[d_1]$	1.029 786 3	${}^3T_{1g}(t_{2g}^1 e_g^1)$
e_1	${}^3T_{1g}$	1.029 786 3	${}^3T_{1g}(t_{2g}^1 e_g^1)$			
f_1	${}^3A_{2g}$	0.954 797 0	${}^3A_{2g}(e_g^2)$			
				$a {}^3T_{1g}[b_1 \oplus e_1]$	0.948 833 7	$a {}^3T_{1g}(t_{2g}^2)(t_{2g}^1 e_g^1)$
				$b {}^3T_{1g}[b_1 \oplus e_1]$	1.048 716 3	$b {}^3T_{1g}(t_{2g}^1 e_g^1)(t_{2g}^2)$

(b) $M_S = 0$

$$\Gamma_{a'_0} = {}^3T_{1g} \oplus {}^3A_{2g} \oplus {}^1T_{2g} \oplus {}^1E_g \oplus {}^1T_{1g}; \quad \Gamma_{a_0} = {}^3T_{1g} \oplus {}^3T_{2g} \oplus {}^1T_{2g} \oplus {}^1T_{1g}; \quad \Gamma_{b_0} = {}^3T_{2g} \oplus {}^1E_g \oplus {}^1A_{1g}.$$

Ψ_{UHF}	Symmetry	Energy/ E_h	$\Phi(S=1)$	Energy/ E_h	Term	$\Phi(S=0)$	Energy/ E_h	Term	
a_0^*	$\Gamma_{a_0^*}$	1.000 420 2	${}^3T_{1g}[a_0^*]$	0.948 844 9	$a {}^3T_{1g}(t_{2g}^2)(t_{2g}^1 e_g^1)$	${}^1T_{2g}[a_0^*]$	1.041 527 3	$b {}^1T_{2g}(t_{2g}^2)(t_{2g}^1 e_g^1)$	
			${}^3A_{2g}[a_0^*]$	0.954 797 0	${}^3A_{2g}(e_g^2)$	${}^1E_g[a_0^*]$	1.066 148 3	$\diamond {}^1E_g(t_{2g}^2)(e_g^2)$	
						${}^1T_{1g}[a_0^*]$	1.080 660 3	${}^1T_{1g}(t_{2g}^1 e_g^1)$	
a'_0	$\Gamma_{a'_0}$	1.000 512 9	${}^3T_{1g}[a'_0]$	0.948 846 2	$a {}^3T_{1g}(t_{2g}^2)(t_{2g}^1 e_g^1)$	${}^1T_{2g}[a'_0]$	1.046 142 6	$b {}^1T_{2g}(t_{2g}^2)(t_{2g}^1 e_g^1)$	
			${}^3T_{2g}[a'_0]$	0.951 493 8	${}^3T_{2g}(t_{2g}^1 e_g^1)$	${}^1T_{1g}[a'_0]$	1.080 660 4	${}^1T_{1g}(t_{2g}^1 e_g^1)$	
a''_0	${}^3T_{1g} \oplus {}^1T_{2g}$	1.012 773 8	${}^3T_{1g}[a''_0]$	0.967 763 7	${}^3T_{1g}(t_{2g}^2)$	${}^1T_{2g}[a''_0]$	1.057 784 0	${}^1T_{2g}(t_{2g}^2)$	
b_0	Γ_{b_0}	1.003 001 8	${}^3T_{2g}[b_0]$	0.951 493 8	${}^3T_{2g}(t_{2g}^1 e_g^1)$	${}^1E_g[b_0]$	1.035 561 9	$\diamond {}^1E_g(t_{2g}^2)(e_g^2)$	
						${}^1A_{1g}[b_0]$	1.081 266 5	$\diamond {}^1A_{1g}(e_g^2)(t_{2g}^2)$	
c_0	${}^3T_{2g} \oplus {}^1T_{2g}$	1.003 028 3	${}^3T_{2g}[c_0]$	0.951 493 8	${}^3T_{2g}(t_{2g}^1 e_g^1)$	${}^1T_{2g}[c_0]$	1.054 562 8	${}^1T_{2g}(t_{2g}^1 e_g^1)$	
d_0	${}^1E_g \oplus {}^1A_{1g}$	1.102 794 1				${}^1E_g[d_0]$	1.057 784 0	${}^1E_g(t_{2g}^2)$	
						${}^1A_{1g}[d_0]$	1.192 814 4	${}^1A_{1g}(t_{2g}^2)$	
e_0	${}^3T_{1g} \oplus {}^1T_{1g}$	1.055 223 3	${}^3T_{1g}[e_0]$	1.029 786 3	${}^3T_{1g}(t_{2g}^1 e_g^1)$	${}^1T_{1g}[e_0]$	1.080 660 3	${}^1T_{1g}(t_{2g}^1 e_g^1)$	
				$a {}^3T_{1g}[a'_0 \oplus e_0]$	0.948 833 7	$a {}^3T_{1g}(t_{2g}^2)(t_{2g}^1 e_g^1)$	$a {}^1T_{2g}[a'_0 \oplus c_0]$	1.033 515 0	$a {}^1T_{2g}(t_{2g}^1 e_g^1)(t_{2g}^2)$
				$b {}^3T_{1g}[a'_0 \oplus e_0]$	1.048 716 3	$b {}^3T_{1g}(t_{2g}^1 e_g^1)(t_{2g}^2)$	$b {}^1T_{2g}[a'_0 \oplus c_0]$	1.078 831 8	$b {}^1T_{2g}(t_{2g}^2)(t_{2g}^1 e_g^1)$

the triplets whose $M_S = 1$ components are described by the b_1 , c_1 , and e_1 solutions. This tells us that the symmetry breaking in a_0'' , b_0 , c_0 , and e_0 indeed comes entirely from the correlation between the two d electrons but does not introduce any more correlation within the $S = 1$ space beyond that already described by the strong-field coupling scheme in Table 4. A similar observation can also be made for the ${}^3A_{2g}[a_0^*]$ and ${}^3T_{2g}[a_0']$ NOCI wavefunctions, despite the fact that the a_0^* and a_0' solutions break spatial symmetry within the $S = 1$ space. Unfortunately, such comparisons are not possible for the $S = 0$ space because none of the singlets has any single-determinantal components, as shown in Table 4.

5.2 $[\text{VF}_6]^{3-}$

We can now turn to the octahedral $[\text{VF}_6]^{3-}$ anion. The $3d^2$ electrons on the V^{3+} center are expected to be strongly correlated on grounds of symmetry as discussed in the previous Section. However, similar to $[\text{TiF}_6]^{3-}$, the Ar core and the F^- ligands in $[\text{VF}_6]^{3-}$ also introduce additional correlation which further complicates the electronic structure. Figure 5 presents the energy, spatial symmetry, and labels of the lowest-energy UHF solutions located by SCF metadynamics in octahedral $[\text{VF}_6]^{3-}$ at V–F bond length of 1.9896 Å for both $M_S = 1$ and $M_S = 0$. Table 6 plots the representative spatial forms of the highest-occupied $3d$ spin-orbitals and shows the $\langle \hat{S}^2 \rangle$ values of these solutions. Detailed solution energies and overlap matrices for the degenerate sets can be found in the Supporting Information. Comparing to Figure 3, we immediately see that there are significantly more low-lying UHF solutions in $[\text{VF}_6]^{3-}$ than in $[\text{TiF}_6]^{3-}$ as a consequence of the increase in the number of possible terms due to the strong correlation between the two valence d electrons. Considering both $M_S = 1$ and $M_S = 0$, these solutions do not appear to segregate into three distinct groups as one would naively expect from the three possible strong-field configurations (Table 4). It is therefore important that we first understand the symmetry of the UHF solutions, restoring any broken

symmetry whenever necessary, before we can assign them to the expected d^2 terms.

5.2.1 $M_S = 1$

Overview of UHF solutions. We focus first on the $M_S = 1$ solutions (Figure 5a) because they are simpler to understand. Since the true d^2 wavefunctions with $M_S = 1$ are all single-determinantal (Table 4), it is without surprise that we have located the spatial-symmetry-conserved $M_S = 1$ solutions B_1 , C_1 , E_1 , and F_1 that have the correct spatial symmetry and reasonable $\langle \hat{S}^2 \rangle$ values to describe the $M_S = 1$ components of ${}^3T_{1g}(t_{2g}^2)$, ${}^3T_{2g}(t_{2g}^1e_g^1)$, ${}^3T_{1g}(t_{2g}^1e_g^1)$, and ${}^3A_{2g}(e_g^2)$, respectively. The distinction between B_1 and E_1 , both of which transform as T_{1g} , is made by referring to the Pipek–Mezey-localized forms of their χ_{40} and χ_{41} (Table 6a). However, more interesting are the spatial-symmetry-broken solutions A_1 , A_1' , and D_1 . The forms of χ_{40} and χ_{41} in these solutions do not let them be assigned to any of the terms listed in Table 4 immediately: although χ_{40} and χ_{41} individually resemble a d orbital, they have been distorted away from the canonical shapes and orientations given in (17) such that they can no longer be associated with the components of t_{2g} or e_g .

Symmetry restoration of individual symmetry-broken UHF sets. The results of the toy system discussed in Section 5.1.2 make it clear that symmetry breaking is an indication of electron correlation being incorporated into UHF single determinants and NOCI allows for some of it to be recovered via symmetry restoration. Figure 6a shows the energy of the NOCI wavefunctions constructed from single sets of symmetry-broken $M_S = 1$ UHF solutions, and Table 7a gives some of their Pipek–Mezey-localized $3d$ natural orbitals which provide a very satisfying visual demonstration of the capability of NOCI to restore spatial symmetry. Comparing, for example, the $3d$ orbitals of the A_1 UHF solutions in Table 6a with some of the $3d$ natural orbitals of the ${}^3T_{1g}[A_1]$ NOCI wavefunctions in Table 7a, we see that, unlike the former, the latter are

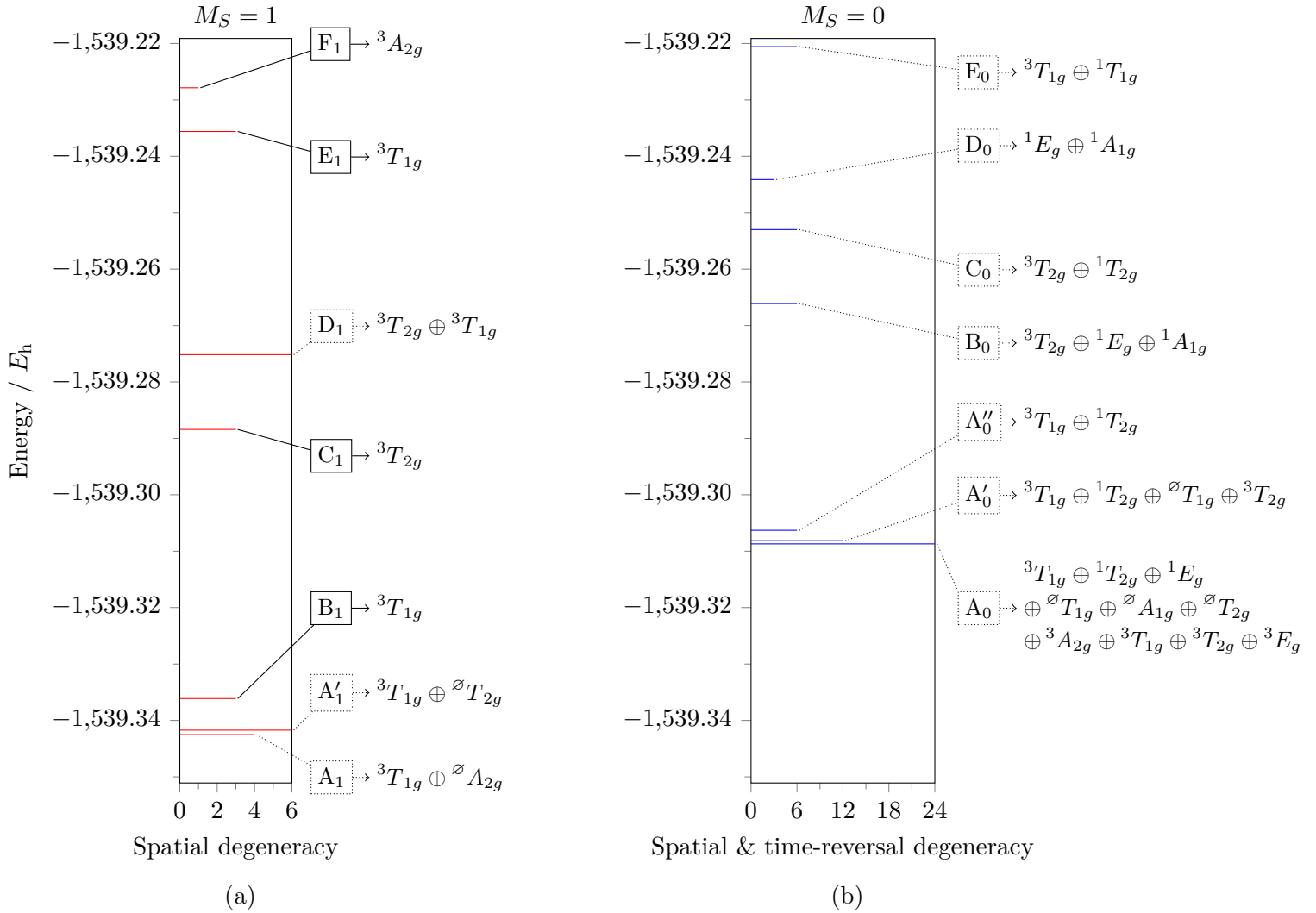
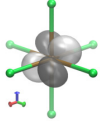
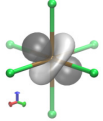
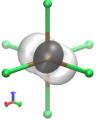
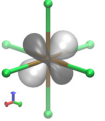
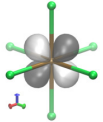
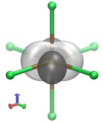
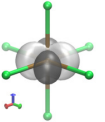
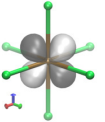
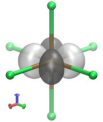
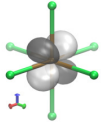
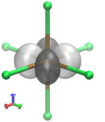
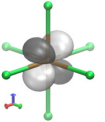
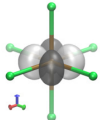
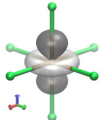
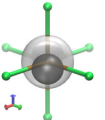
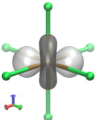
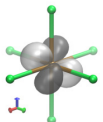
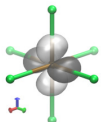
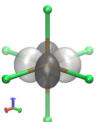
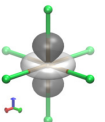
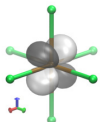
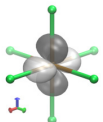
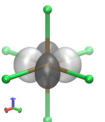
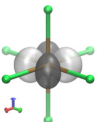
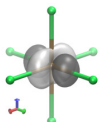
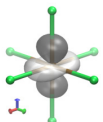
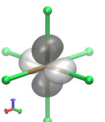
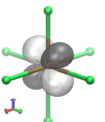


Figure 5: Energy and symmetry of low-lying UHF solutions (6-31G* basis) in octahedral $[VF_6]^{3-}$ having V-F = 1.9896 Å. (a) Solutions with $N_\alpha - N_\beta = 2$ (red). (b) Solutions with $N_\alpha = N_\beta$ (blue). All solutions have DIIS errors smaller than 1×10^{-13} and are eigenfunctions of \hat{S}_3 whose M_S eigenvalues are given as subscripts. Solutions are considered degenerate when there energies are at most $10^{-9} E_h$ apart and are labeled alphabetically in increasing order of their energies. Nearly degenerate solutions share the same letter but are distinguished by dashes. Solutions within one degenerate set are distinct and linearly independent. Solutions that conserve spatial symmetry are enclosed in solid boxes whereas solutions that break spatial symmetry are enclosed in dotted ones. The time-reversal partners of the $M_S = 0$ solutions are also eigenfunctions of \hat{S}_3 with $M_S = 0$ and are thus included in (b). See the main text for a discussion on spin multiplicities.

Table 6: Representative isosurface plots for the Pipek–Mezey-localized spatial parts of the highest-occupied spin-orbitals, spatial symmetry, and $\langle \hat{S}^2 \rangle$ of the UHF solutions in $[\text{VF}_6]^{3-}$. In (a), both spin-orbitals χ_{40} and χ_{41} have $m_s = \frac{1}{2}$. In (b), χ_{40} has $m_s = \frac{1}{2}$ whereas $\bar{\chi}_{80}$ has $m_s = -\frac{1}{2}$ as indicated by the bar. The spin-orbitals of all solutions within one set have similar forms and are related by the symmetry operations of \mathcal{O}_h . Spatial symmetry lists the irreducible representations of \mathcal{O}_h spanned by the degenerate sets. Axis triad: red– x ; green– y ; blue– z .

(a) $M_S = 1$					(b) $M_S = 0$				
Ψ_{UHF}	χ_{40}	χ_{41}	Spatial symmetry	$\langle \hat{S}^2 \rangle$	Ψ_{UHF}	χ_{40}	$\bar{\chi}_{80}$	Spatial symmetry	$\langle \hat{S}^2 \rangle$
A ₁			$T_{1g} \oplus A_{2g}$	2.0040	A ₀			$A_{1g} \oplus A_{2g} \oplus 2E_g \oplus 3T_{1g} \oplus 3T_{2g}$	1.0025
A' ₁			$T_{1g} \oplus T_{2g}$	2.0040	A' ₀			$2T_{1g} \oplus 2T_{2g}$	1.0029
B ₁			T_{1g}	2.0045	A' ₀			$T_{1g} \oplus T_{2g}$	1.0037
C ₁			T_{2g}	2.0035	B ₀			$A_{1g} \oplus E_g \oplus T_{2g}$	0.8090
D ₁			$T_{1g} \oplus T_{2g}$	2.0039	C ₀			$2T_{2g}$	1.0034
E ₁			T_{1g}	2.0049	D ₀			$A_{1g} \oplus E_g$	0.0000
F ₁			A_{2g}	2.0044	E ₀			$2T_{1g}$	1.0046

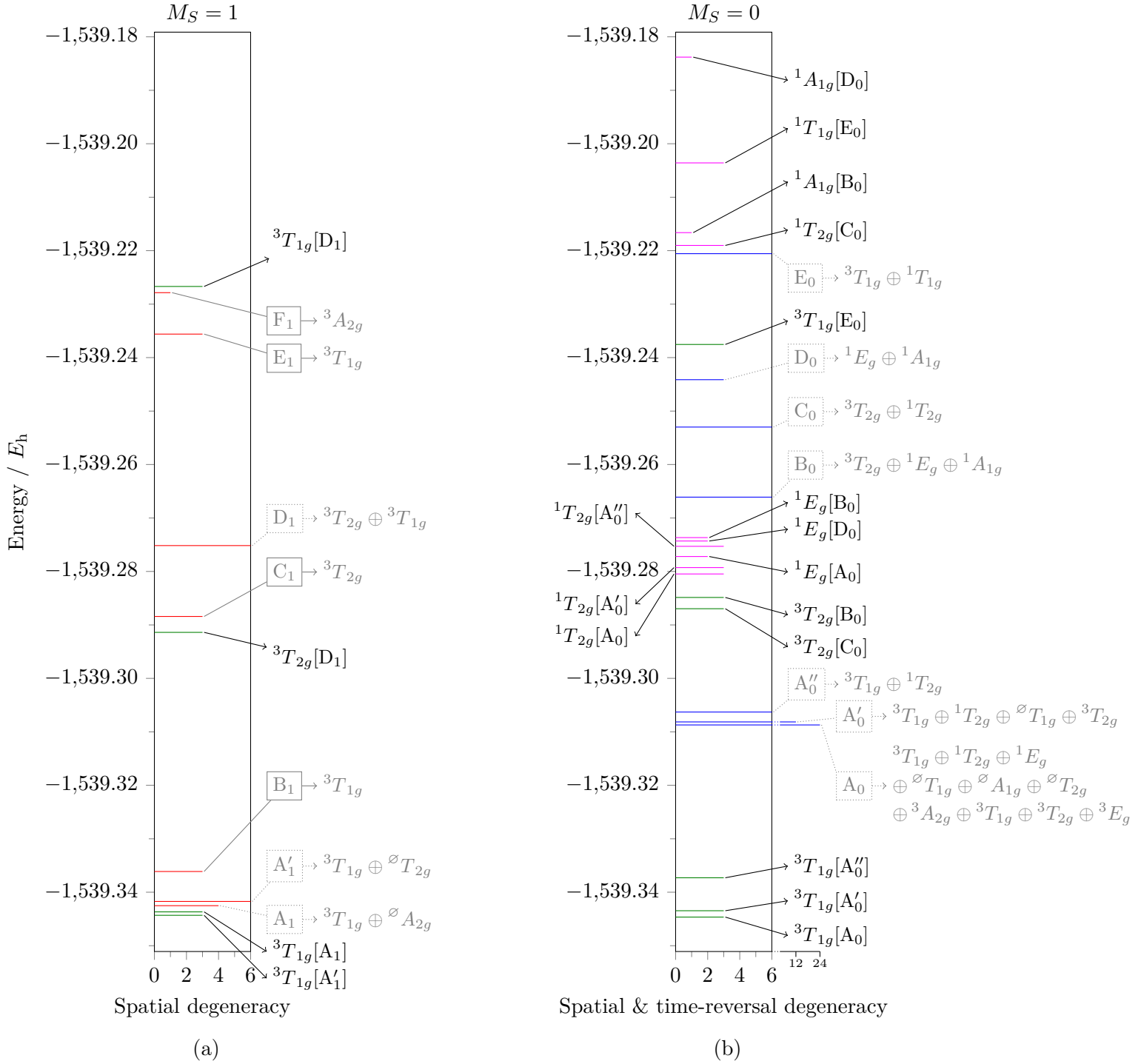


Figure 6: Low-lying NOCI wavefunctions constructed from single sets of degenerate UHF solutions in octahedral $[VF_6]^{3-}$ (replotted from Figure 5 for comparison). The horizontal axis in (b) has been broken at 6 and a more compact scale is used between 6 and 24 so that the degeneracy of most states can be shown clearly. Green indicates NOCI wavefunctions with $\langle \hat{S}^2 \rangle \approx 2$ while magenta indicates those with $\langle \hat{S}^2 \rangle \approx 0$. NOCI wavefunctions are considered degenerate when their energies are at most $10^{-7} E_h$ apart.

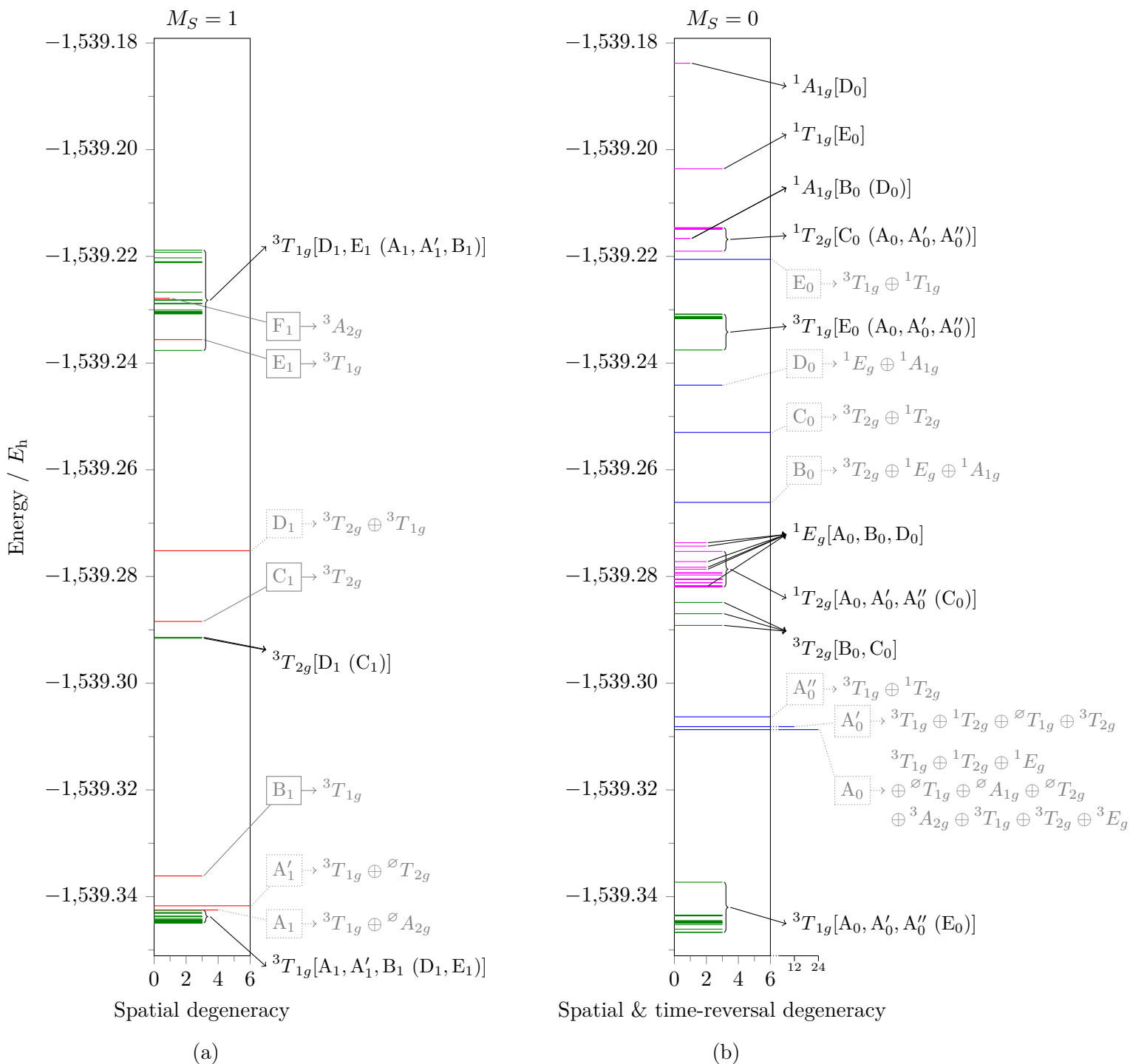


Figure 7: Low-lying NOCI wavefunctions constructed from all interacting low-lying UHF solutions in octahedral $[\text{VF}_6]^{3-}$ (replotted from Figure 5 for comparison). The horizontal axis in (b) has been broken at 6 and a more compact scale is used between 6 and 24 so that the degeneracy of most states can be shown clearly. Green indicates NOCI wavefunctions with $\langle \hat{S}^2 \rangle \approx 2$ while magenta indicates those with $\langle \hat{S}^2 \rangle \approx 0$. NOCI wavefunctions are considered degenerate when their energies are at most $10^{-7} E_h$ apart. In generic notations, $\Gamma[A, B (C, D)]$ denotes multiple NOCI sets of symmetry Γ constructed from all non-trivial combinations of *at least one* of A and B, but of none, some, or all of C and D.

properly symmetrized such that each of them can be attributed to one of the ξ , η , and ζ components of t_{2g} .

However, to assign these NOCI wavefunctions to terms, we need a careful understanding of the correlation they recover. By drawing analogies to the $M_S = 1$ UHF and NOCI wavefunctions of the toy model $[(B^{3+})(q^-)_6]$ analyzed in Section 5.1.2, we can infer the correlation nature of the symmetry-broken solutions A_1 , A'_1 , and D_1 from the corresponding a_1 , a'_1 , and d_1 . Firstly, their symmetry breaking is indeed a consequence of the correlation between the two $3d$ electrons, but the symmetry-conserved single determinants C_1 , E_1 , and F_1 already capture most of this for the corresponding electronic terms. However, when the $3d$ electrons break symmetry, they cause the now-present core and ligand electrons to relax accordingly and incorporate correlation to these electrons as a result. This is evident by the fact that the NOCI wavefunctions ${}^3T_{2g}[D_1]$ and ${}^3T_{1g}[D_1]$ no longer coincide with the symmetry-conserved UHF solutions C_1 and E_1 (Figure 6a), and that ${}^\infty A_{2g}[A_1]$ and ${}^\infty T_{2g}[A'_1]$ do not have well defined spin multiplicities and are so high in energy (well outside the range of Figure 6a) that they no longer match with F_1 and C_1 . On the other hand, the symmetry breaking in A_1 and A'_1 arises from the additional configuration-mixing correlation between the $3d$ electrons that is missed out by the symmetry-conserved B_1 solutions. This symmetry breaking incidentally also results in the inclusion of some correlation with the core and ligand electrons as previously mentioned.

Based on the above understanding together with the forms and occupation numbers of the natural orbitals (Table 7a), we can assign the NOCI wavefunctions as follows. The predominantly occupied $3d$ natural orbitals of ${}^3T_{1g}[A_1]$ (all having occupation numbers of 0.945) suggest that they mainly describe the $M_S = 1$ components of the ${}^3T_{1g}(t_{2g}^2)$ term, and the minorly occupied $3d$ natural orbitals (all having occupation numbers of 0.055) indicate that they have some ${}^3T_{1g}(t_{2g}^1 e_g^1)$ character mixed in. We thus assign ${}^3T_{1g}[A_1]$ to the mixed-configuration term $a {}^3T_{1g}(t_{2g}^2)(t_{2g}^1 e_g^1)$ (see the caption of Table 5 for the explanation of this notation).

In a similar manner, we assign ${}^3T_{1g}[A'_1]$ to $a {}^3T_{1g}(t_{2g}^2)(t_{2g}^1 e_g^1)$, ${}^3T_{2g}[D_1]$ to ${}^3T_{2g}(t_{2g}^1 e_g^1)$, and ${}^3T_{1g}[D_1]$ to ${}^3T_{1g}(t_{2g}^1 e_g^1)$, as also listed in Table 7a. It cannot be emphasized enough that, as the symmetry breaking in A_1 and A'_1 is a consequence of configuration mixing, restoring symmetry in these solutions automatically gives symmetry-conserved wavefunctions that also incorporate this effect *without having to explicitly construct or obtain determinants belonging to the various interacting configurations*.

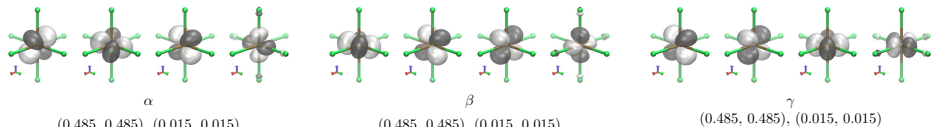
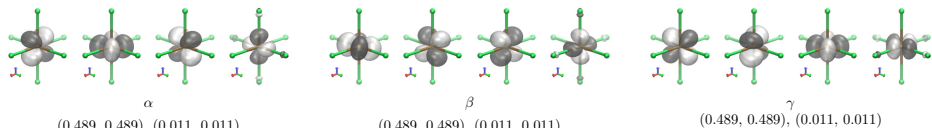
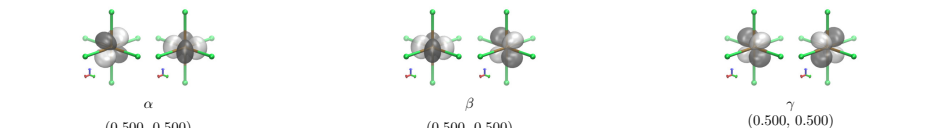
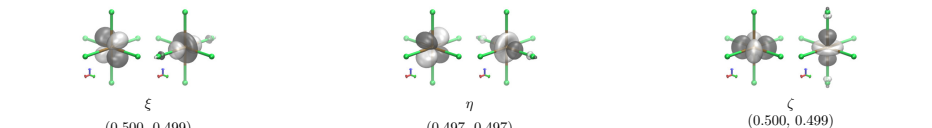
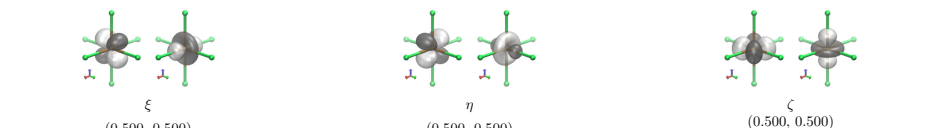
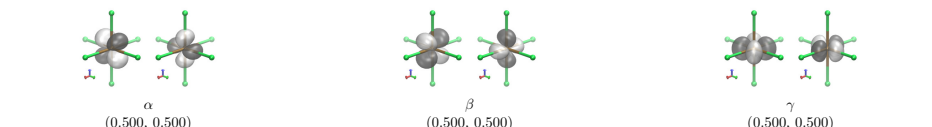
NOCI between multiple degenerate UHF sets. The NOCI wavefunctions obtained above can be improved if multiple degenerate UHF sets that span one or more common spaces are to be included in the basis. For instance, A_1 , A'_1 , B_1 , D_1 , and E_1 all span a common ${}^3T_{1g}$ space with $M_S = 1$ and we therefore expect them to interact with one another to give rise to various ${}^3T_{1g}$ NOCI wavefunctions. However, while the ${}^3T_{1g}$ space of A_1 and A'_1 has both t_{2g}^2 and $t_{2g}^1 e_g^1$ characters, the ${}^3T_{1g}$ space of B_1 only has t_{2g}^2 character and that of D_1 and E_1 only has $t_{2g}^1 e_g^1$ character. Thus, by allowing some or all of A_1 , A'_1 , and B_1 to interact with none, some, or all of D_1 and E_1 , we obtain ${}^3T_{1g}$ NOCI wavefunctions that have mainly t_{2g}^2 character but with some $t_{2g}^1 e_g^1$ mixed in. Their energies are labeled collectively as ${}^3T_{1g}[A_1, A'_1, B_1 (D_1, E_1)]$ in Figure 7a. This collection can be considered to consist principally of NOCI wavefunctions constructed from all possible non-trivial combinations of A_1 , A'_1 , and B_1 and thus incorporating whatever correlation responsible for any symmetry breaking in these UHF solutions. These wavefunctions are then further improved by interactions with D_1 and E_1 . There are 27 non-trivial combinations in this collection: $(2^3 - 1) \times 2^2$ minus the trivial one that includes only the symmetry-conserved B_1 set. It is precisely because this trivial combination is excluded that the NOCI wavefunctions in this collection are all of $a {}^3T_{1g}(t_{2g}^2)(t_{2g}^1 e_g^1)$ character and spread over a rather small range of $2.36 \times 10^{-3} E_h$, or approximately 517 cm^{-1} (see Supporting Information for the detailed energies). By the variational principle, the best

Table 7: Isosurface plots for the Pipek–Mezey-localized spatial parts of some $3d$ natural orbitals, $\langle \hat{S}^2 \rangle$, and term assignment of selected NOCI wavefunctions Φ in $[\text{VF}_6]^{3-}$. Each group of $3d$ natural orbitals shown in each set corresponds to one of the NOCI wavefunctions within the set that transforms as the labeled component. From left to right within each group of natural orbitals, shown in the first pair of parentheses are the occupation numbers of the natural orbitals corresponding to the dominant configuration, and whenever applicable, shown in the second pair of parentheses are the occupation numbers of the natural orbitals corresponding to the minor configuration. These configurations are also indicated next to the term symbol in the same order. Axis triad: red– x ; green– y ; blue– z .

(a) $M_S = 1$. The occupation numbers and natural orbitals are solely in the $m_s = \frac{1}{2}$ space.

Φ	3d natural orbitals			$\langle \hat{S}^2 \rangle$	Term
${}^3T_{1g}[A_1]$	 α (0.945, 0.945), (0.055, 0.055)	 β (0.945, 0.945), (0.055, 0.055)	 γ (0.945, 0.945), (0.055, 0.055)	2.0035	$a^3T_{1g}(t_{2g}^2)(t_{2g}^1 e_g^1)$
${}^3T_{1g}[A_1]$	 α (0.957, 0.957), (0.043, 0.043)	 β (0.957, 0.957), (0.043, 0.043)	 γ (0.957, 0.957), (0.044, 0.043)	2.0033	$a^3T_{1g}(t_{2g}^2)(t_{2g}^1 e_g^1)$
${}^3T_{2g}[D_1]$	 ξ (0.999, 0.999)	 η (0.999, 0.999)	 ζ (0.999, 0.999)	2.0025	${}^3T_{2g}(t_{2g}^1 e_g^1)$
${}^3T_{1g}[D_1]$	 α (0.983, 0.981)	 β (0.990, 0.988)	 γ (0.998, 0.995)	2.0079	${}^3T_{1g}(t_{2g}^1 e_g^1)$

(b) $M_S = 0, S \approx 1$. The occupation numbers and natural orbitals are identical for both $m_s = \pm \frac{1}{2}$.

Φ	3d natural orbitals			$\langle \hat{S}^2 \rangle$	Term
${}^3T_{1g}[A_0]$		2.0000	$a^3T_{1g}(t_{2g}^2)(t_{2g}^1e_g^1)$		
${}^3T_{1g}[A'_0]$		2.0000	$a^3T_{1g}(t_{2g}^2)(t_{2g}^1e_g^1)$		
${}^3T_{1g}[A''_0]$		2.0000	${}^3T_{1g}(t_{2g}^2)$		
${}^3T_{2g}[B_0]$		2.0000	${}^3T_{2g}(t_{2g}^1e_g^1)$		
${}^3T_{2g}[C_0]$		2.0000	${}^3T_{2g}(t_{2g}^1e_g^1)$		
${}^3T_{1g}[E_0]$		2.0000	${}^3T_{1g}(t_{2g}^1e_g^1)$		

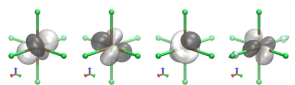
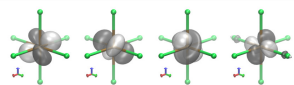
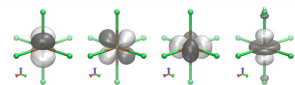
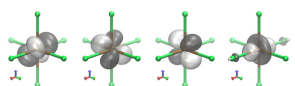
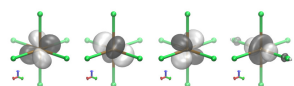
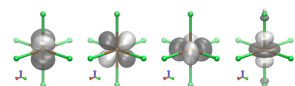
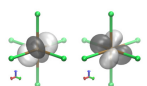
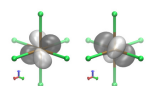
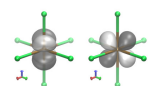
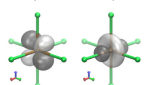
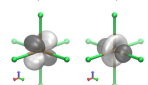
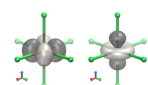
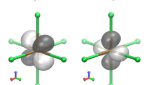
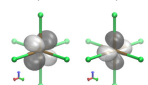
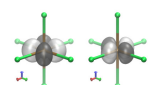
approximation to $a^3T_{1g}(t_{2g}^2)(t_{2g}^1e_g^1)$ must be as low in energy as possible and turns out to be $a^3T_{1g}[A_1 \oplus A'_1 \oplus B_1 \oplus D_1 \oplus E_1]$. However, from a physical perspective, $a^3T_{1g}[A_1 \oplus A'_1 \oplus B_1 \oplus D_1 \oplus E_1]$ does not really recover much more configuration-mixing correlation than ${}^3T_{1g}[A_1]$ and ${}^3T_{1g}[A'_1]$ already do, so that even if one were not able to locate the higher D_1 and E_1 UHF solutions, one could still get a reasonable description of the ground mixed-configuration $a^3T_{1g}(t_{2g}^2)(t_{2g}^1e_g^1)$ term from either A_1 or A'_1 , as suggested by the small energy range of the ${}^3T_{1g}[A_1, A'_1, B_1 (D_1, E_1)]$ collection.

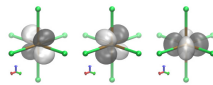
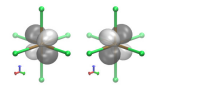
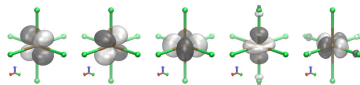
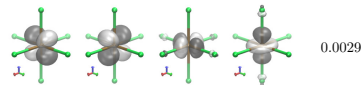
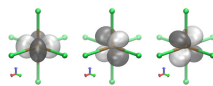
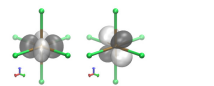
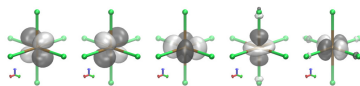
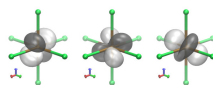
Similarly, there are 23 non-trivial NOCI wavefunctions in ${}^3T_{1g}[D_1, E_1 (A_1, A'_1, B_1)]$ that all contain a major $t_{2g}^1e_g^1$ character, and those that include at least one of A_1, A'_1 , or B_1 also have some t_{2g}^2 character mixed in. However, since all of these NOCI wavefunctions have the same symmetry as the ground term, and since the exact ground term is unknown, we cannot be sure if any of them is indeed orthogonal to the exact ground term in order for the variational principle to apply.¹³ This is rather unfortunate

as the collection ${}^3T_{1g}[D_1, E_1 (A_1, A'_1, B_1)]$ spans a rather large range in energy (about $0.0188 E_h$ or 4130 cm^{-1}) which makes it difficult to give a reasonable estimate for $b^3T_{1g}(t_{2g}^1e_g^1)(t_{2g}^2)$.

Spin multiplicity assignments. Before moving on, we briefly discuss the spin symmetry of the $M_S = 1$ solutions. In a very similar manner to the $[\text{TiF}_6]^{3-}$ case discussed earlier, none of these solutions is an exact eigenfunction of \hat{S}^2 due to the slight deviation of their $\langle \hat{S}^2 \rangle$ from the exact value of 2 expected for a triplet. Nevertheless, we still assign them to triplet states on grounds that a discrepancy smaller than 1×10^{-2} is negligible for our purposes while acknowledging that there is still some spin symmetry breaking due to contamination from the $M_S = 1$ components of higher spin states. Spin purification can be achieved somewhat by spatial symmetry restoration just as noted for $[\text{TiF}_6]^{3-}$, but ultimately, to fully restore spin symmetry, one needs to include in the NOCI basis all spin symmetry partners generated by the spin rotation operations in

(c) $M_S = 0, S \approx 0$. The occupation numbers and natural orbitals are identical for both $m_s = \pm \frac{1}{2}$.

Φ	3d natural orbitals			$\langle \hat{S}^2 \rangle$	Term
${}^1T_{2g}[A_0]$				0.0038	$a^1T_{2g}(t_{2g}^2)(t_{2g}^1e_g^1)$
	ξ (0.491, 0.491), (0.009, 0.009)	η (0.496, 0.486), (0.010, 0.009)	ζ (0.492, 0.490), (0.009, 0.009)		
${}^1T_{2g}[A_0']$				0.0042	$a^1T_{2g}(t_{2g}^2)(t_{2g}^1e_g^1)$
	ξ (0.496, 0.496), (0.004, 0.004)	η (0.496, 0.496), (0.004, 0.004)	ζ (0.496, 0.496), (0.004, 0.004)		
${}^1T_{2g}[A_0'']$				0.0073	${}^1T_{2g}(t_{2g}^2)$
	ξ (0.500, 0.500)	η (0.500, 0.500)	ζ (0.500, 0.500)		
${}^1T_{2g}[C_0]$				0.0067	${}^1T_{2g}(t_{2g}^1e_g^1)$
	ξ (0.498, 0.498)	η (0.497, 0.497)	ζ (0.499, 0.499)		
${}^1T_{1g}[E_0]$				0.0092	${}^1T_{1g}(t_{2g}^1e_g^1)$
	α (0.500, 0.500)	β (0.499, 0.499)	γ (0.500, 0.500)		

Φ	3d natural orbitals		$\langle \hat{S}^2 \rangle$	Term
${}^1E_g[A_0]$			0.0032	${}^1E_g(t_{2g}^2)$
	u (0.216, 0.122, 0.661)	v (0.433, 0.558)		
${}^1E_g[B_0]$			0.0029	$\diamond^1E_g(t_{2g}^2)(e_g^2)$
	u (0.188, 0.115, 0.595), (0.052, 0.051)	v (0.400, 0.493), (0.052, 0.051)		
${}^1E_g[D_0]$			0.0000	${}^1E_g(t_{2g}^2)$
	u (0.221, 0.118, 0.661)	v (0.446, 0.549)		
${}^1A_{1g}[B_0]$			0.0027	$\diamond^1A_{1g}(t_{2g}^2)(e_g^2)$
	e_1 (0.272, 0.272, 0.272), (0.093, 0.093)			
${}^1A_{1g}[D_0]$			0.0000	${}^1A_{1g}(t_{2g}^2)$
	e_1 (0.333, 0.333, 0.334)			

SU(2).

5.2.2 $M_S = 0$

Unlike the $M_S = \pm 1$ wavefunctions, the $M_S = 0$ wavefunctions in a true d^2 system are all required by symmetry to be multi-determinantal (Table 4). It therefore comes as no surprise that the $M_S = 0$ single-determinantal UHF solutions in $[\text{VF}_6]^{3-}$ are all symmetry-broken, be it in \mathcal{O}_h , $\mathcal{S} \otimes \mathcal{T}$, or both (Figure 5b and Table 6b). In particular, apart from the D_0 solutions which are effectively RHF, have $\langle \hat{S}^2 \rangle = 0.0000$ and can be considered true singlets, these $M_S = 0$ solutions all have $\langle \hat{S}^2 \rangle$ in the vicinity of unity which indicates heavy spin mixing. The symmetry breaking in D_0 is therefore purely spatial, whereas the symmetry breaking in the other solutions is much less straightforward to classify without symmetry restoration. This is because in the presence of significant spin contamination, the different spin components can break or conserve spatial symmetry independently such that the overall spatial representation obtained from the analysis of symmetry in \mathcal{O}_h (Table 6b) only gives a direct sum of all spatial irreducible representations but does not segregate them into the different spin components. Therefore, NOCI must first be carried out so that the $\langle \hat{S}^2 \rangle$ values of the spatial-symmetry-conserved NOCI wavefunctions can be worked out and that the spatial irreducible representations can be assigned to definite spin states. The symmetry labels of the UHF solutions in Figure 5b reflect the outcomes of this, and the energy of the resulted low-lying NOCI wavefunctions constructed from single sets of symmetry-broken solutions are plotted in Figure 6b with some representative Pipek–Mezey-localized natural orbitals shown in Tables 7b and 7c.

Time-reversal symmetry. The $M_S = 0$ space is rather interesting. We show in Appendix A.3 that the time-reversal operator $\hat{\Theta}$ and the \hat{S}_3 operator, which have the following

effects on a spin-pure state $|S, M_S\rangle$,⁶⁴

$$\hat{\Theta} |S, M_S\rangle = (-1)^{S-M_S} |S, -M_S\rangle \quad (18)$$

$$\hat{S}_3 |S, M_S\rangle = M_S |S, M_S\rangle \quad (19)$$

only commute when acting on wavefunctions with $M_S = 0$. As such, $M_S = 0$ wavefunctions can be made to be simultaneous eigenfunctions of both $\hat{\Theta}$ and \hat{S}_3 . A given $M_S = 0$ UHF determinant, say Ψ_0 , is obviously an eigenfunction of \hat{S}_3 by construction, but there is no *a priori* restriction that it must also be an eigenfunction of $\hat{\Theta}$. However, the commutativity between $\hat{\Theta}$ and \hat{S}_3 and the finite cyclic structure of the time-reversal group \mathcal{T} (Section 2.1, also Appendix A.1) ensure that Ψ_0 and all possible linearly independent UHF determinants $(\hat{\Theta}^n)\Psi_0$ where $n = 1, 2, 3$ can be arranged into linear combinations that have $M_S = 0$ and are also eigenfunctions of $\hat{\Theta}$. Since \mathcal{T} is abelian, if the set $\{(\hat{\Theta}^n)\Psi_0 \mid n = 0, \dots, 3\}$ contains more than one linearly independent member, it is necessarily symmetry-broken in \mathcal{T} . But as $\hat{\Theta}$ also commutes with the spinless electronic Hamiltonian defined in (2) and is antiunitary,⁴² all members of the above set have the same energy which the degeneracy depicted in Figures 5b, 6b, and 7b must take into account.

The above discussion brings to attention the fact that $\hat{\Theta}$ is also a symmetry operator that needs to be considered on top of the spatial symmetry operations \hat{R} in \mathcal{O}_h in order to obtain enough UHF determinants and complete any symmetry-broken set within the $M_S = 0$ space prior to running NOCI. However, there is a fortuitous exception to this as demonstrated by the A_0 , A_0'' , B_0 , and D_0 solutions. Consider the set of all linearly independent spatial-symmetry-equivalent UHF determinants, $\{\hat{R}\Psi_0 \mid \hat{R} \in \mathcal{O}_h\}$, where Ψ_0 is a determinant in any one of A_0 , A_0'' , B_0 , or D_0 . A character analysis shows that this set spans multiple but *complete* irreducible representations in \mathcal{T} , and that augmenting this set to $\{(\hat{\Theta}^n\hat{R})\Psi_0 \mid n = 0, \dots, 3; \hat{R} \in \mathcal{O}_h\}$ and retaining only the linearly independent elements does not change the representations spanned in \mathcal{O}_h or \mathcal{T} . There thus exists a subset T in \mathcal{O}_h

such that

$$\hat{\Theta}\Psi_0 = \sum_{\hat{R} \in T} c_{\hat{R}} \hat{R}\Psi_0$$

Typically, T consists of only one element \hat{R}' with $c_{\hat{R}'} = \pm 1$. Consequently, A_0 , A_0'' , B_0 , and D_0 are said to exhibit *time-reversal coincidence* and the origin of this effect can be somewhat understood by noting from Table 6b that the spatial forms of χ_{40} and $\bar{\chi}_{80}$ in these solutions can be interconverted (up to a phase factor of ± 1) by a symmetry operation in \mathcal{O}_h . The remaining solutions, however, do not benefit from this coincidence as the set $\{\hat{R}\Psi_0 \mid \hat{R} \in \mathcal{O}_h\}$ for these solutions does not span complete irreducible representations in \mathcal{T} and therefore $\hat{\Theta}$ must be involved to complete the set. This is also obvious from Table 6b that their χ_{40} and $\bar{\chi}_{80}$ are not related by any symmetry operations in \mathcal{O}_h at all.

The use of NOCI on time-reversal symmetry partners to restore spin symmetry of the heavily spin-contaminated $M_S = 0$ UHF solutions needs a more careful explanation. The effect of $\hat{\Theta}$ on the spin-pure state $|S, 0\rangle$ can be deduced from (18) as

$$\hat{\Theta}|S, 0\rangle = (-1)^S |S, 0\rangle$$

It is then obvious that an $|S, 0\rangle$ state with even S is totally symmetric in \mathcal{T} whereas an $|S, 0\rangle$ state with odd S spans the B irreducible representation of \mathcal{T} (Table 9). Thus, by allowing all spin-contaminated $M_S = 0$ determinants and their time-reversal partners to interact via the totally symmetric Hamiltonian, we restore time-reversal symmetry and decouple states with even and odd S as a consequence. The $M_S = 0$ NOCI wavefunctions in Figure 6b, Figure 7b, Table 7b, and Table 7c are therefore all symmetry-conserved in \mathcal{T} and contain either odd or even S components, but not both: those with $\langle \hat{S}^2 \rangle \approx 2$ are mainly $|1, 0\rangle$ in character but are contaminated by higher $|S, 0\rangle$ states with odd S , while those with $\langle \hat{S}^2 \rangle \approx 0$ contain a main $|0, 0\rangle$ component together with smaller contributions from higher $|S, 0\rangle$ with even S . As such, by restoring time-reversal symmetry, NOCI also restores spin-rotation symmetry but not completely, unless $S = 0$ and $S = 1$ are

the only possible spin states as in the toy system $[(B^{3+})(q^-)_6]$. The multiplicity labels for these NOCI states therefore only reflect the most dominant $|S, 0\rangle$ component, but this is sufficiently accurate as deviations smaller than 1×10^{-2} of $\langle \hat{S}^2 \rangle$ from the exact values are negligible for our purposes, as stated before.

Correlation from symmetry restoration.

To understand the kind of correlation recovered by NOCI, we once again make reference to the $M_S = 0$ UHF and NOCI wavefunctions of the toy system $[(B^{3+})(q^-)_6]$ (Section 5.1.2). We were unfortunately not able to find any solutions in $[\text{VF}_6]^{3-}$ that can be correlated exactly to the symmetry-broken a_0^* in $[(B^{3+})(q^-)_6]$ based on their symmetry and degeneracy. However, we located a set of symmetry-broken solutions labeled A_0 whose spin-orbitals are similar to those of a_0^* but that span more irreducible representations than a_0^* . This is the reason for the asterisk in the label of a_0^* . We posit that the implication of this result is twofold. Firstly, the symmetry breaking in a_0^* must be due to the correlation between the two d electrons, so the space that is common to both a_0^* and A_0 must contain descriptions of this strong correlation.⁶⁵ Secondly, the additional symmetry breaking in A_0 , which gives rise to the observed increase in size of the linearly independent space spanned by these solutions compared to that spanned by a_0^* , must be a consequence of the correlation between the two d electrons with the core and ligand electrons which are only present in the full $[\text{VF}_6]^{3-}$ system. The severe symmetry breaking in A_0 is therefore the result of both types of correlation.

The symmetry breaking in A_0 , A'_0 , and B_0 contains configuration mixing information for various electronic terms. In fact, an inspection of the $3d$ natural orbitals and occupation numbers of the NOCI wavefunctions constructed from A_0 , A'_0 , and B_0 (Tables 7b and 7c) reveals that the symmetry breaking of A_0 and A'_0 accounts for some configuration mixing in $a^3T_{1g}(t_{2g}^2)(t_{2g}^1e_g^1)$ and $a^1T_{2g}(t_{2g}^2)(t_{2g}^1e_g^1)$, and that the symmetry breaking of B_0 accounts for some configuration mixing in $\diamond^1E_g(t_{2g}^2)(e_g^2)$ and $\diamond^1A_{1g}(t_{2g}^2)(e_g^2)$. This is further supported by the

NOCI results of the corresponding solutions a_0^* , a'_0 , and b_0 in the toy system $[(B^{3+})(q^-)_6]$ as shown in Table 5b where similar configuration mixing effects are also observed.

For the remaining solutions A''_0 , C_0 , and E_0 that can be corresponded to a''_0 , c_0 , and e_0 of the toy system $[(B^{3+})(q^-)_6]$, we expect from the analysis in Section 5.1.2 that the most of the correlation in their $S \approx 1$ components is already captured by the symmetry-conserved $M_S = 1$ solutions B_1 , C_1 , and E_1 . However, the energies of ${}^3T_{1g}[A''_0]$, ${}^3T_{2g}[C_0]$, and ${}^3T_{1g}[E_0]$ all deviate from those of B_1 , C_1 , and E_1 by slight amounts (Figure 6, see also the Supporting Information for precise energy values), which must be the result of some correlation with the core and ligand electrons. Unfortunately, the NOCI $3d$ natural orbitals and occupation numbers in Tables 7b and 7c show that ${}^3T_{1g}[A''_0]$, ${}^1T_{2g}[A''_0]$, ${}^1T_{2g}[C_0]$ and ${}^3T_{1g}[E_0]$ miss out large amounts of configuration mixing correlation between the two d electrons. Fortunately, this problem can be overcome by including multiple degenerate sets of UHF solutions describing different configurations of the same term in the NOCI basis, the results of which are shown in Figure 7b. Drastic improvements to the NOCI wavefunctions can be most easily seen through the energy distribution of the collections ${}^3T_{1g}[A_0, A'_0, A''_0 (E_0)]$, ${}^3T_{1g}[E_0 (A_0, A'_0, A''_0)]$, and ${}^1T_{2g}[C_0 (A_0, A'_0, A''_0)]$. Take the collection ${}^3T_{1g}[A_0, A'_0, A''_0 (E_0)]$ for example: there is a very distinctive gap between the energy of ${}^3T_{1g}[A''_0]$ that have no configuration mixing and the energy of the remaining NOCI wavefunctions in the collection that all include configuration mixing to some extent.

6 UHF and NOCI Wavefunctions upon Symmetry Descent

The understanding of the symmetry of the various low-lying UHF solutions in octahedral $[\text{TiF}_6]^{3-}$ and $[\text{VF}_6]^{3-}$ obtained so far sheds light on their behaviors when the molecular symmetry of the system descends from the highly sym-

metric \mathcal{O}_h . The ground terms for $[\text{TiF}_6]^{3-}$ and $[\text{VF}_6]^{3-}$ are ${}^2T_{2g}$ and ${}^3T_{1g}$, respectively. With spin-orbit coupling ignored for the current purposes, the Jahn-Teller theorem predicts that both octahedral anions undergo stabilizing and symmetry-lowering distortions via the e_g or t_{2g} vibrational modes since both E_g and T_{2g} are contained in the symmetrized squares of both T_{1g} and T_{2g} .^{3,66} We will distinguish between the symmetry of vibrational modes and the symmetry of electronic terms by the use of lower-case and upper-case symbols, respectively. In this work, we consider the $e_g u$ and $e_g v$ normal vibrational coordinates (Figure 8): the \mathcal{O}_h symmetry of $[\text{TiF}_6]^{3-}$ and $[\text{VF}_6]^{3-}$ is lowered to \mathcal{D}_{4h} along $Q_{e_g u}$ and to \mathcal{D}_{2h} along $Q_{e_g v}$. We thus expect the octahedral ${}^2T_{2g}$ and ${}^3T_{1g}$ ground terms to split as shown in Table 8.

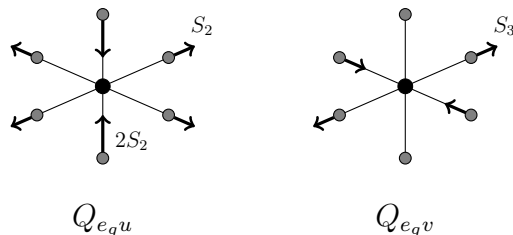


Figure 8: Displacement components of the normal coordinates $Q_{e_g u}$ and $Q_{e_g v}$ of an octahedral MF_6 ($M = \text{Ti}, \text{V}$) nuclear framework. S_2 and S_3 are magnitudes of displacement vectors as derived by Sugano et al.³

In Figures 9 and 10, we show the behaviors of the lowest-lying SCF solutions that we have found for $[\text{VF}_6]^{3-}$ and $[\text{TiF}_6]^{3-}$. Immediately obvious is that the symmetry-broken solutions A_1 , A'_1 , and $A_{\frac{1}{2}}$ remain symmetry-broken to various degrees upon symmetry descent. Specifically, Figure 10 reveals that the $A_{\frac{1}{2}}$ solutions which span $T_{1g} \oplus T_{2g}$ in \mathcal{O}_h split² into a symmetry-conserved set E_g and a symmetry-broken set $A_{2g} \oplus B_{2g} \oplus E_g$ in \mathcal{D}_{4h} , and into three symmetry-broken sets $B_{1g} \oplus B_{2g}$, $B_{1g} \oplus B_{3g}$, and $B_{2g} \oplus B_{3g}$ in \mathcal{D}_{2h} . Clearly, the two components T_{1g} and T_{2g} of the $A_{\frac{1}{2}}$ set are so entangled together in \mathcal{O}_h that they cannot split independently from each other when descending in molecular symmetry. Figure 9 shows similar behaviors for the A_1 and A'_1 solutions in $[\text{VF}_6]^{3-}$, where we note in particular that the A_1

Table 8: Splitting of ${}^2T_{2g}$ and ${}^3T_{1g}$ upon descending from \mathcal{O}_h to \mathcal{D}_{4h} and \mathcal{D}_{2h} .

\mathcal{O}_h	\mathcal{D}_{4h}	\mathcal{D}_{2h}
${}^2T_{2g}$	${}^2B_{2g} \oplus {}^2E_g$	${}^2B_{1g} \oplus {}^2B_{2g} \oplus {}^2B_{3g}$
${}^3T_{1g}$	${}^3A_{2g} \oplus {}^3E_g$	${}^3B_{1g} \oplus {}^3B_{2g} \oplus {}^3B_{3g}$

set remains completely symmetry-broken and quadruply degenerate throughout. This seems to suggest that there is some hidden symmetry in the UHF method that persists even when the symmetry of the electronic Hamiltonian is lowered, but it is unfortunately beyond the scope of the current paper and we will have to return to it in a future publication.

In general, symmetry-broken SCF solutions, although better variationally, do not exhibit the correct splitting consistent with the physical distortions required by the Jahn–Teller theorem. This is most easily seen in Figure 9 for $[\text{VF}_6]^{3-}$: along both Q_{e_gu} and Q_{e_gv} , neither A_1 or A'_1 show any appreciable minima that can be attributed to the expected Jahn–Teller stabilization effects. However, when symmetry is restored using NOCI, these effects are recovered. In particular, the ${}^3T_{1g}(\mathcal{O}_h)[A_1 \oplus A'_1]$ NOCI wavefunctions now exhibit the correct splitting in \mathcal{D}_{4h} and \mathcal{D}_{2h} . In addition, the ${}^3A_{2g}[A_1 \oplus A'_1]$ component in \mathcal{D}_{4h} has a deeper minimum than ${}^3E_g[A_1 \oplus A'_1]$ which suggests that axial elongation is preferred along Q_{e_gu} and which is consistent with the fact that A_{2g} has had all of the degeneracy of T_{1g} lifted while E_g still retains a double degeneracy.

Unfortunately, similar observations for the symmetry-broken $A_{\frac{1}{2}}$ solutions in $[\text{TiF}_6]^{3-}$ cannot be made. As seen in Figure 10, along both Q_{e_gu} and Q_{e_gv} , the components arising from $A_{\frac{1}{2}}$ quickly disappear upon coalescence with those from $A'_{\frac{1}{2}}$ that share one or more irreducible representations. In particular, along Q_{e_gu} in \mathcal{D}_{4h} , the $A_{2g} \oplus B_{2g} \oplus E_g$ components of the $A_{\frac{1}{2}}$ solutions coalesce with both B_{2g} and E_g components of $A'_{\frac{1}{2}}$. Similarly, along Q_{e_gv} in \mathcal{D}_{2h} , the $B_{1g} \oplus B_{2g}$ components of $A_{\frac{1}{2}}$ can cross the B_{3g} component of $A'_{\frac{1}{2}}$ easily but disappear upon approaching the B_{1g} and B_{2g} com-

ponents. It is possible that the disappearing wavefunctions have become holomorphic beyond the coalescence points,^{67,68} a behavior we seek to investigate in a future study. However, at the moment, the disappearance of these components causes the set of SCF determinants used for NOCI to have varying dimensionality along Q_{e_gu} and Q_{e_gv} . As a consequence, the NOCI energy curves exhibit discontinuities and are therefore not physically meaningful. We demonstrate this for the Q_{e_gu} distortion in Figure 10. When S_2 lies within the open interval $(-0.5 \times 10^{-3} \text{ \AA}, 0.5 \times 10^{-3} \text{ \AA})$, the $A_{2g} \oplus B_{2g} \oplus E_g$ components of $A_{\frac{1}{2}}$ still exist and are linearly independent of all the other components from $A_{\frac{1}{2}}$ and $A'_{\frac{1}{2}}$. The NOCI space $[A_{\frac{1}{2}} \oplus A'_{\frac{1}{2}}]$ therefore remains nine-dimensional and the lowest 2E_g and ${}^2B_{2g}$ NOCI wavefunctions lie in the vicinity of $-1444.9328 E_h$ (barely visible in Figure 10). However, when S_2 lies outside of $(-0.5 \times 10^{-3} \text{ \AA}, 0.5 \times 10^{-3} \text{ \AA})$, the $A_{2g} \oplus B_{2g} \oplus E_g$ components of $A_{\frac{1}{2}}$ no longer exist and the NOCI space $[A_{\frac{1}{2}} \oplus A'_{\frac{1}{2}}]$ becomes five-dimensional. The surviving E_g components of $A_{\frac{1}{2}}$ can still interact with the E_g components of $A'_{\frac{1}{2}}$ to give the part of the 2E_g NOCI curve outside of $(-0.5 \times 10^{-3} \text{ \AA}, 0.5 \times 10^{-3} \text{ \AA})$, but the B_{2g} component of $A'_{\frac{1}{2}}$ has nothing to interact with and is thus identical to the part of the ${}^2B_{2g}$ NOCI curve on the same domain. The unphysical jumps exhibited by the 2E_g and ${}^2B_{2g}$ NOCI curves as S_2 crosses $\pm 0.5 \times 10^{-3} \text{ \AA}$ are clearly an unphysical artifact of the non-inclusion of the $A_{2g} \oplus B_{2g} \oplus E_g$ wavefunctions from the NOCI space.

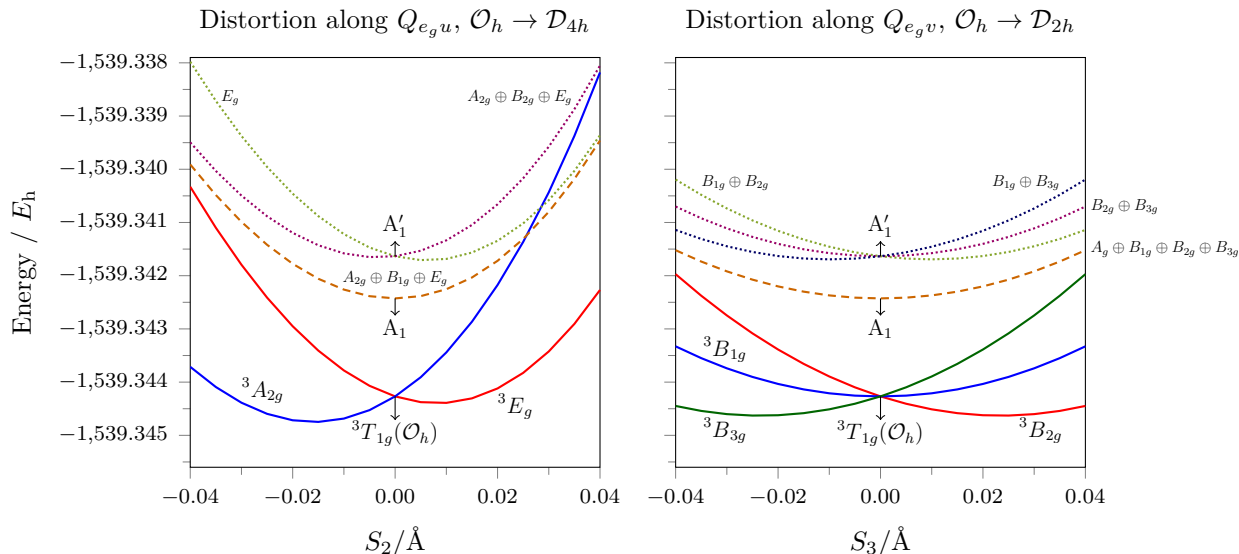


Figure 9: A_1 (dashed) and A'_1 (dotted) solutions and the low-lying NOCI wavefunctions constructed from all of them (solid) along the e_g normal vibrational coordinates of octahedral $[\text{VF}_6]^{3-}$. The zero values of S_2 and S_3 correspond to \mathcal{O}_h while the non-zero values correspond to the lower symmetry groups. All symmetry symbols are irreducible representations of the lower-symmetry group unless indicated otherwise. Spin multiplicities are only shown for NOCI wavefunctions.

7 Conclusion

In this paper, we demonstrate the existence and analyze the properties of multiple low-energy SCF HF solutions in two representative octahedral hexafluorometallate(III) complexes, $[\text{MF}_6]^{3-}$ ($M = \text{Ti}, \text{V}$). The presence of d electrons gives rise to many UHF solutions that are degenerate or nearly degenerate, and that can conserve or break symmetry without any apparent predictable patterns. We therefore focus particularly on the physical meaning of symmetry-broken solutions and investigate how a careful choice of basis for NOCI can yield wavefunctions that restore symmetry, recover a decent amount of static correlation, and give reasonable descriptions of ground and excited electronic states.

In $[\text{TiF}_6]^{3-}$ where there is only a single d electron in the ground configuration, the only correlation involving this electron is the correlation with the $[\text{Ar}]$ core electrons on Ti^{3+} and the ligand electrons on F^- . This gives rise to one set of symmetry-broken UHF solutions that we label $A_{\frac{1}{2}}$, and by restoring the symmetry of these solutions, we obtain NOCI wavefunctions that incorporate this correlation and are thus a vari-

ationally better description of the ${}^2T_{2g}$ ground term.

In $[\text{VF}_6]^{3-}$ where there are two d electrons in the ground configuration, on top of the correlation with the core and ligand electrons which is likely to be weak, there are now strong correlation effects between these two electrons. As a consequence, the number of low-lying UHF solutions that can be found increases significantly and many of them turn out to break spin or spatial symmetry, if not both. All symmetry breaking due to correlation between the two d electrons also causes the core and ligand electrons to relax accordingly due to the self consistency of the SCF method and thereby inadvertently incorporates some correlation to these electrons. More importantly, however, in several cases, symmetry breaking is a direct consequence of the incorporation of inherently multi-determinantal correlation effects due to configuration mixing into single-determinantal wavefunctions, and the restoration of such symmetry allows for configuration mixing to be reasonably described using a single set of degenerate single determinants without having to explicitly construct or obtain determinants belonging to the various interacting configurations.

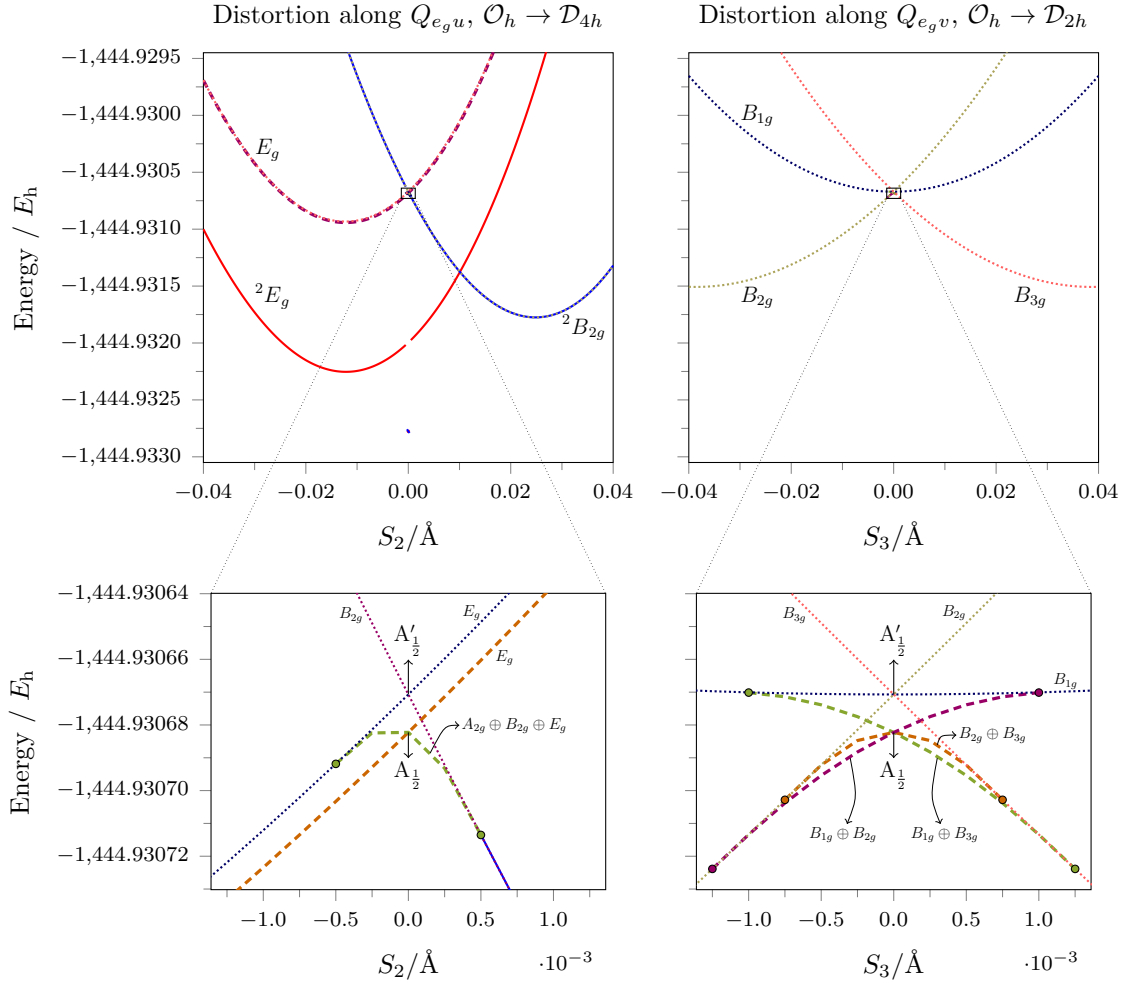


Figure 10: $A_{\frac{1}{2}}$ (dashed) and $A'_{\frac{1}{2}}$ (dotted) solutions and the low-lying NOCI wavefunctions constructed from all of them (solid) along the e_g normal vibrational coordinates of octahedral $[\text{TiF}_6]^{3-}$. The zero values of S_2 and S_3 correspond to \mathcal{O}_h while the non-zero values correspond to the lower symmetry groups. All symmetry symbols are irreducible representations of the lower symmetry group unless indicated otherwise. Spin multiplicities are only shown for NOCI wavefunctions. The 2E_g and ${}^2B_{2g}$ NOCI curves in \mathcal{D}_{4h} lie in the vicinity of $-1444.9328 E_h$ (barely visible in the $Q_{e_g u}$ graph) for $S_2 \in (-0.5 \times 10^{-3} \text{\AA}, 0.5 \times 10^{-3} \text{\AA})$ but exhibit discontinuities at $S_2 = \pm 0.5 \times 10^{-3} \text{\AA}$.

An investigation of the behaviors of the lowest symmetry-broken UHF solutions in $[\text{VF}_6]^{3-}$ upon molecular distortions from the \mathcal{O}_h symmetry to \mathcal{D}_{4h} and \mathcal{D}_{2h} shows that the symmetry of these solutions must be restored using NOCI in order to obtain wavefunctions that can describe stabilization effects dictated by the Jahn–Teller theorem. However, a similar investigation for $[\text{TiF}_6]^{3-}$ runs into difficulties as some of the UHF solutions disappear in \mathcal{D}_{4h} and \mathcal{D}_{2h} , rendering the NOCI energy curves discontinuous and unphysical. It is likely that these solutions have become holomorphic, and if one can locate them beyond the coalescence points as reported elsewhere for various simpler systems,⁶⁸ one can obtain continuous and smooth NOCI energy curves that are physically meaningful.

Even though this paper focuses solely on two simple systems with high molecular symmetry, the insights learned from their results, in particular the use of NOCI to obtain physically meaningful wavefunctions from symmetry-broken SCF solutions and the analysis of correlation using natural orbitals and occupation numbers, are general and can be applied to any system. And even though NOCI wavefunctions are by no means the best approximations to electronic states as they are likely to still miss out dynamic correlation, the fact that they have the right symmetry and exhibit physically proper behaviors bolsters their applicability as references for more involved correlation methods.

Acknowledgment

B.C.H. is grateful for the financial support from the Jardine Foundation, Cambridge Commonwealth, European & International Trust, and Peterhouse during the duration of this work. A.J.W.T. thanks the Royal Society for a University Research Fellowship (UF110161).

A Group-Theoretical Aspects

A.1 Structure of the Time-Reversal Group

Let \mathcal{T} be the group generated by the time-reversal operator $\hat{\Theta}$. The behavior of any spin-pure state with respect to $\hat{\Theta}$ has long been classified by its eigenvalue under $\hat{\Theta}^2$ which is well known^{42,64,69} to take on only two possible values, ± 1 . However, the possibility of $\hat{\Theta}^2$ reversing the sign of certain states means that $\hat{\Theta}^2$ cannot be considered to coincide with the identity \hat{E} but must be treated as a generally distinct operation that satisfies

$$(\hat{\Theta}^2)^2 = \hat{\Theta}^4 = \hat{E}$$

\mathcal{T} is therefore isomorphic to the cyclic group of order 4 which is abelian and has four one-dimensional irreducible representations. The characters of the irreducible representations in \mathcal{T} are shown in Table 9 which is expectedly identical to that of \mathcal{C}_4 .^{3,41} The time-reversal group \mathcal{T} that we identify here is the same as that deduced by Fukutome⁴¹ but we have explicitly written the square of the time-reversal operator as $\hat{\Theta}^2$ instead of $-\hat{E}$ so as to be completely general and also to reveal its cyclic nature.

Table 9: Character table for \mathcal{T} .

\mathcal{T}		\hat{E}	$\hat{\Theta}$	$\hat{\Theta}^2$	$\hat{\Theta}^3$
A	Γ_1	1	1	1	1
B	Γ_2	1	-1	1	-1
E	Γ_3	1	i	-1	$-i$
	Γ_4	1	$-i$	-1	i

A.2 Symmetry Breaking and the Generators of $\mathcal{S} \otimes \mathcal{T}$

The following results are well known in the theories of Lie groups, Lie algebras, and representations. However, we feel that it is in the interest of rigor and completeness to recapitu-

late these results in order to bridge the gap between our definition of symmetry breaking (a group representation concept) and the structure of the generators of $\mathcal{S} \otimes \mathcal{T}$ (an algebra representation concept). We focus first on the full spin-rotation group \mathcal{S} which is isomorphic to the two-dimensional unitary group $\text{SU}(2)$, a matrix Lie group containing all complex 2×2 unitary matrices with determinant 1. Let V_n denote the space of homogeneous polynomials with total degree n ($n \geq 0$) in two complex variables z_1, z_2 that define a column vector $\mathbf{z} \in \mathbb{C}^2$,

$$f(\mathbf{z}) = f(z_1, z_2) = \sum_{k=0}^n a_k z_1^{n-k} z_2^k$$

where the a_k 's are complex coefficients, then V_n is a complex vector space of dimension $n + 1$. There exists a Lie group representation $\Pi_n : \text{SU}(2) \rightarrow \text{GL}(V_n)$ which is a Lie group homomorphism acting on this space and given by

$$[\Pi_n(\mathbf{U})f](\mathbf{z}) = f(\mathbf{U}^{-1}\mathbf{z}) \quad (20)$$

that maps any element \mathbf{U} of $\text{SU}(2)$ to an $(n + 1) \times (n + 1)$ invertible complex matrix in $\text{GL}(V_n)$. Π_n is an irreducible representation of $\text{SU}(2)$.⁷⁰ Thus, from our perspective, the functions $f(z_1, z_2)$ in V_n are symmetry-conserved in $\text{SU}(2)$ as they form a basis for a single irreducible representation Π_n in the group.

We now make the connection to angular momentum operators via the tangent space at the identity of the group. Known as the Lie algebra of the group and denoted by $\mathfrak{su}(2)$, this space contains all real-coefficient linear combinations of the traceless skew-Hermitian matrices $\{\mathbf{X}_1, \mathbf{X}_2, \mathbf{X}_3\}$ satisfying^{71,72}

$$[\mathbf{X}_i, \mathbf{X}_j] \equiv \mathbf{X}_i \mathbf{X}_j - \mathbf{X}_j \mathbf{X}_i = \sum_{k=1}^3 \epsilon_{ijk} \mathbf{X}_k \quad (21)$$

where the Lie bracket $[\cdot, \cdot] : \mathfrak{su}(2) \times \mathfrak{su}(2) \rightarrow \mathfrak{su}(2)$ is a map defined in this space as the commutator of square matrices and obeys the properties of a Lie algebra (see Section 3.1 of Ref. 70) by virtue of the Levi-Civita symbol ϵ_{ijk} . Elements of $\mathfrak{su}(2)$ are infinitesimal generators of $\text{SU}(2)$. By Theorem 3.28 in Ref. 70,

every Lie group representation gives rise to a unique Lie algebra representation. Therefore, for each of the Π_n acting on the space V_n , we can find a corresponding Lie algebra representation $\pi_n : \mathfrak{su}(2) \rightarrow \mathfrak{gl}(V_n)$ acting on the same space. Physically illuminating forms for π_n can be obtained by choosing an appropriate basis for $\mathfrak{su}(2)$. One such basis is given in terms of the Pauli spin matrices as

$$\begin{aligned} \mathbf{X}_1 &= -\frac{i}{2} \begin{pmatrix} 0 & 1 \\ 1 & 0 \end{pmatrix} \\ \mathbf{X}_2 &= -\frac{i}{2} \begin{pmatrix} 0 & -i \\ i & 0 \end{pmatrix} \\ \mathbf{X}_3 &= -\frac{i}{2} \begin{pmatrix} 1 & 0 \\ 0 & -1 \end{pmatrix} \end{aligned}$$

The Lie algebra representations π_n for these elements are easily shown⁷² to be

$$\begin{aligned} \pi_n(\mathbf{X}_1) &= \frac{i}{2} \left(z_2 \frac{\partial}{\partial z_1} + z_1 \frac{\partial}{\partial z_2} \right) \\ \pi_n(\mathbf{X}_2) &= \frac{1}{2} \left(z_2 \frac{\partial}{\partial z_1} - z_1 \frac{\partial}{\partial z_2} \right) \\ \pi_n(\mathbf{X}_3) &= \frac{i}{2} \left(z_1 \frac{\partial}{\partial z_1} - z_2 \frac{\partial}{\partial z_2} \right) \end{aligned}$$

It is trivial to see that any basis element $z_1^{n-k} z_2^k$ of V_n is an eigenfunction of $\pi_n(\mathbf{X}_3)$ with eigenvalue $(i/2)(n - 2k)$. But as $\mathbf{X}_1, \mathbf{X}_2$, and \mathbf{X}_3 do not commute with one another (Equation 21), $\pi_n(\mathbf{X}_1), \pi_n(\mathbf{X}_2)$, and $\pi_n(\mathbf{X}_3)$ do not commute with one another either and therefore $z_1^{n-k} z_2^k$ is not an eigenfunction of either $\pi_n(\mathbf{X}_1)$ or $\pi_n(\mathbf{X}_2)$. However, we can construct the Casimir operator in this representation, $\pi_n(\mathbf{C})$, as⁷⁰

$$\begin{aligned} \pi_n(\mathbf{C}) &= -[\pi_n(\mathbf{X}_1)^2 + \pi_n(\mathbf{X}_2)^2 + \pi_n(\mathbf{X}_3)^2] \\ &= \frac{3}{4} \left(z_1 \frac{\partial}{\partial z_1} + z_2 \frac{\partial}{\partial z_2} \right) + \frac{1}{2} z_1 z_2 \frac{\partial^2}{\partial z_1 \partial z_2} \\ &\quad + \frac{1}{4} \left(z_1^2 \frac{\partial^2}{\partial z_1^2} + z_2^2 \frac{\partial^2}{\partial z_2^2} \right) \end{aligned}$$

which commutes with $\pi_n(\mathbf{X}_1), \pi_n(\mathbf{X}_2)$, and $\pi_n(\mathbf{X}_3)$. Therefore, $z_1^{n-k} z_2^k$ is also an eigenfunction of $\pi_n(\mathbf{C})$ with eigenvalue $(n/2)[(n/2) + 1]$, independent of k .

As $\mathfrak{su}(2)$ contains only skew-Hermitian matrices, any linear combinations of \mathbf{X}_i that in-

volve complex coefficients must lie outside of this space. However, these combinations are needed to arrive at representations that can be identified to the familiar angular momentum operators. It is therefore necessary to consider the complexification of $\mathfrak{su}(2)$, namely $\mathfrak{sl}(2; \mathbb{C})$, the Lie algebra of the two-dimensional special linear group over the complex numbers. Proposition 4.6 in Ref. 70 allows each Lie algebra representation π_n of $\mathfrak{su}(2)$ to be uniquely extended to a Lie algebra representation of $\mathfrak{sl}(2; \mathbb{C})$, also denoted by π_n . By considering the following basis elements in $\mathfrak{sl}(2; \mathbb{C})$:

$$\begin{aligned} \mathbf{J}_+ &= i\mathbf{X}_1 - \mathbf{X}_2 = \begin{pmatrix} 0 & 1 \\ 0 & 0 \end{pmatrix} \\ \mathbf{J}_- &= i\mathbf{X}_1 + \mathbf{X}_2 = \begin{pmatrix} 0 & 0 \\ 1 & 0 \end{pmatrix} \\ \mathbf{J}_3 &= i\mathbf{X}_3 = \frac{1}{2} \begin{pmatrix} 1 & 0 \\ 0 & -1 \end{pmatrix} \end{aligned}$$

we deduce the corresponding π_n :⁷⁰

$$\begin{aligned} \pi_n(\mathbf{J}_+) &= i\pi_n(\mathbf{X}_1) - \pi_n(\mathbf{X}_2) \\ &= -z_2 \frac{\partial}{\partial z_1} \\ \pi_n(\mathbf{J}_-) &= i\pi_n(\mathbf{X}_1) + \pi_n(\mathbf{X}_2) \\ &= -z_1 \frac{\partial}{\partial z_2} \\ \pi_n(\mathbf{J}_3) &= i\pi_n(\mathbf{X}_3) \\ &= -\frac{1}{2} \left(z_1 \frac{\partial}{\partial z_1} - z_2 \frac{\partial}{\partial z_2} \right) \end{aligned}$$

The basis element $z_1^{n-k} z_2^k$ of V_n is now an eigenfunction of $\pi_n(\mathbf{J}_3)$ with eigenvalue $(1/2)(2k-n)$ but is transformed by $\pi_n(\mathbf{J}_+)$ and $\pi_n(\mathbf{J}_-)$ into other basis elements within V_n that are also eigenfunctions of $\pi_n(\mathbf{J}_3)$ but with eigenvalues raised or lowered by 1, respectively.

We are now in a suitable position to make the following comments. First, we identify $\pi_n(\mathbf{C})$ with the \hat{J}^2 operator, $\pi_n(\mathbf{J}_3)$ with the \hat{J}_3 operator, and $\pi_n(\mathbf{J}_\pm)$ with the ladder operators \hat{J}_\pm . The irreducible representation enumerator n can then be equated to $2J$, and within each V_n , the basis element label k can be equated to $J + M_J$. We noted earlier that the functions $f(z_1, z_2)$ in V_n conserve symmetry in $\text{SU}(2)$ as they form a basis for a single irreducible Lie

group representation Π_n . As a consequence, they must also form a basis for the corresponding Lie algebra representation π_n that diagonalize both $\pi_n(\mathbf{C}) \equiv \hat{J}^2$ and $\pi_n(\mathbf{J}_3) \equiv \hat{J}_3$ simultaneously. Since $\text{SU}(2)$ is simply connected, the converse must also be true:⁷⁰ a complete set of simultaneous eigenfunctions of \hat{J}^2 and \hat{J}_3 must conserve symmetry in $\text{SU}(2)$.

The relationship between symmetry breaking and the generator $\hat{\Theta}$ of the time-reversal group \mathcal{T} is much simpler. Since \mathcal{T} is cyclic, the character and also eigenvalue of $\hat{\Theta}$ in each one-dimensional irreducible representation is a distinct fourth root of unity (Table 9). Any state that conserves symmetry in $\hat{\Theta}$ must also be an eigenfunction of $\hat{\Theta}$ that corresponds to one of these eigenvalues, and *vice versa*.

By recognizing that all elements of $\text{SU}(2)$ must take the form⁷⁰

$$U = \begin{pmatrix} U_{11} & U_{12} \\ -U_{12}^* & U_{11}^* \end{pmatrix}$$

where $|U_{11}|^2 + |U_{12}|^2 = 1$ and by using the definition of $\hat{\Theta}$ in (22) together with the property that $\hat{\Theta}$ is antilinear,⁶⁴ we can easily show that $\hat{\Theta}$ commutes with the linear transformation $\Pi_n(U)$ in (20) for all n and U . The group $\mathcal{S} \otimes \mathcal{T}$ is indeed the direct product group of $\text{SU}(2)$ and \mathcal{T} , and since there is a one-to-one correspondence between $\text{SU}(2)$ and $\mathfrak{su}(2)$, the above discussion of symmetry breaking and group generators holds for all Fukutome subgroups of $\mathcal{S} \otimes \mathcal{T}$.

A.3 Commutativity Between $\hat{\Theta}$ and \hat{J}_3 for $M_J = 0$

The effects of $\hat{\Theta}$ and \hat{J}_3 on a state $|J, M_J\rangle$ that conserves symmetry in $\text{SU}(2)$ are given by⁶⁴

$$\hat{\Theta} |J, M_J\rangle = (-1)^{J-M_J} |J, -M_J\rangle \quad (22)$$

$$\hat{J}_3 |J, M_J\rangle = M_J |J, M_J\rangle \quad (23)$$

which are a generalized version of (18) and (19) where J is now used in place of S to denote a general form of angular momentum. The effect of the commutator $[\hat{\Theta}, \hat{J}_3]$ on this state is

therefore

$$\begin{aligned}
[\hat{\Theta}, \hat{J}_3] |J, M_J\rangle &= (\hat{\Theta}\hat{J}_3 - \hat{J}_3\hat{\Theta}) |J, M_J\rangle \\
&= \hat{\Theta}M_J |J, M_J\rangle \\
&\quad - \hat{J}_3(-1)^{J-M_J} |J, -M_J\rangle \\
&= (-1)^{J-M_J} M_J |J, -M_J\rangle \\
&\quad + (-1)^{J-M_J} M_J |J, -M_J\rangle \\
&= 2 \times (-1)^{J-M_J} M_J |J, -M_J\rangle
\end{aligned} \tag{24}$$

Now, consider a non-vanishing wavefunction denoted by Ψ_{M_J} that has a well defined M_J but that is symmetry-broken in $\text{SU}(2)$. Ψ_{M_J} can be written as a sum over the various contributing symmetry-conserved states,

$$\Psi_{M_J} = \sum_J c_J |J, M_J\rangle \quad (c_J \in \mathbb{C})$$

From (24), and noting that $\hat{\Theta}$ is antilinear, the effect of $[\hat{\Theta}, \hat{J}_3]$ on this wavefunction is

$$\begin{aligned}
[\hat{\Theta}, \hat{J}_3]\Psi_{M_J} &= \sum_J [\hat{\Theta}, \hat{J}_3]c_J |J, M_J\rangle \\
&= 2M_J \sum_J c_J^* (-1)^{J-M_J} |J, -M_J\rangle
\end{aligned} \tag{25}$$

which vanishes only when $M_J = 0$. The general non-commutativity between $\hat{\Theta}$ and \hat{J}_3 versus the commutativity between $\hat{\Theta}$ and $\Pi_n(\mathbf{U})$ pointed out in A.2 provides a clear example of how Lie group and Lie algebra representations can take on very different physical meanings and behaviors despite their close mathematical relationship.

B Symmetry Analysis

The matrix \mathbf{X} in (8) that ensures that $\tilde{\mathbf{S}}$ is of full rank is defined as follows. If $N_{\text{indept}} < N_{\text{det}}$, *i.e.*, the N_{det} degenerate Slater determinants are not all linearly independent, then \mathbf{X} is constructed based on Equation (3.172) of Ref. 11. If $N_{\text{indept}} = N_{\text{det}}$, *i.e.*, the N_{det} degenerate Slater determinants are already linearly independent, then we set $\mathbf{X} = \mathbf{I}_{N_{\text{det}}}$ so as to avoid unnecessary mixing of the degenerate Slater deter-

minants in the symmetry analysis that follows. Because of this, $\tilde{\mathbf{S}}$ is only guaranteed to be of full rank but not necessarily equal to $\mathbf{I}_{N_{\text{indept}}}$. This choice of \mathbf{X} does not affect the physics of the problem and still allows us to transform the full NOCI secular equation (12) into an equivalent one in the linearly independent space,

$$\tilde{\mathbf{H}}\tilde{\mathbf{A}} = \tilde{\mathbf{S}}\tilde{\mathbf{A}}\mathbf{E} \tag{26}$$

where $\tilde{\mathbf{H}} = \mathbf{X}^\dagger \mathbf{H} \mathbf{X}$ and $\mathbf{A} = \mathbf{X}\tilde{\mathbf{A}}$. The transformed Slater determinants in the linearly independent space are thus

$$\left\{ {}^m \tilde{\Psi} \mid m = 1, 2, \dots, N_{\text{indept}} \right\} \tag{27}$$

where

$${}^m \tilde{\Psi} = \sum_w^{N_{\text{det}}} {}^w \Psi X_{wm} \tag{28}$$

and

$$\langle {}^m \tilde{\Psi} \mid {}^n \tilde{\Psi} \rangle = \tilde{S}_{mn} \tag{29}$$

For a symmetry operation \hat{R} , we seek the representation matrix $\tilde{\mathbf{D}}(\hat{R})$ in the linearly independent space such that

$$\hat{R} {}^m \tilde{\Psi} = \sum_n^{N_{\text{indept}}} {}^n \tilde{\Psi} \tilde{D}_{nm}(\hat{R}) \tag{30}$$

The non-orthogonal projection operator due to Soriano and Palacios⁴⁷ in this basis takes the form

$$\hat{P}_m = \sum_n^{N_{\text{indept}}} |{}^m \tilde{\Psi}\rangle \tilde{S}_{mn}^{-1} \langle {}^n \tilde{\Psi}| \tag{31}$$

where \tilde{S}_{mn}^{-1} are the matrix elements of $\tilde{\mathbf{S}}^{-1}$ which is guaranteed to exist since $\tilde{\mathbf{S}}$ contains no zero eigenvalues. Noting that the following property always holds,⁴⁷

$$\hat{P}_m |{}^n \tilde{\Psi}\rangle = \delta_{mn} |{}^m \tilde{\Psi}\rangle \tag{32}$$

we apply the projection operator to both sides of (30), relabeling the indices when necessary,

and obtain

$$\begin{aligned}
\hat{P}_m |\hat{R}^{m'} \tilde{\Psi}\rangle &= \sum_{n'}^{N_{\text{indept}}} \hat{P}_m |^{n'} \tilde{\Psi}\rangle \tilde{D}_{n'm'}(\hat{R}) \\
&= \sum_{n'}^{N_{\text{indept}}} \delta_{mn'} |^m \tilde{\Psi}\rangle \tilde{D}_{n'm'}(\hat{R}) \\
&= |^m \tilde{\Psi}\rangle \tilde{D}_{mm'}(\hat{R})
\end{aligned} \tag{33}$$

Multiplying both sides by $\langle^m \tilde{\Psi}|$, we get

$$\langle^m \tilde{\Psi}|\hat{P}_m|\hat{R}^{m'} \tilde{\Psi}\rangle = \tilde{S}_{mm} \tilde{D}_{mm'}(\hat{R}) \tag{34}$$

With the definition of \hat{P}_m in (31), the above equation becomes

$$\begin{aligned}
\tilde{D}_{mm'}(\hat{R}) &= \frac{1}{\tilde{S}_{mm}} \sum_n^{N_{\text{indept}}} \langle^m \tilde{\Psi}|^m \tilde{\Psi}\rangle \tilde{S}_{mn}^{-1} \langle^n \tilde{\Psi}|\hat{R}^{m'} \tilde{\Psi}\rangle \\
&= \sum_n^{N_{\text{indept}}} \tilde{S}_{mn}^{-1} \tilde{T}_{nm'}(\hat{R})
\end{aligned} \tag{35}$$

where we have let $\tilde{T}_{nm'}(\hat{R}) = \langle^n \tilde{\Psi}|\hat{R}^{m'} \tilde{\Psi}\rangle$, which, by (28), can also be written as

$$\begin{aligned}
\tilde{T}_{nm'}(\hat{R}) &= \sum_{wx}^{N_{\text{det}}} \langle^w \Psi X_{wn} | \hat{R}^x \Psi X_{xm'} \rangle \\
&= \sum_{wx}^{N_{\text{det}}} X_{nw}^\dagger T_{wx}(\hat{R}) X_{xm'}
\end{aligned} \tag{36}$$

with $T_{wx}(\hat{R})$ defined in (10). By substituting (36) into (35) and rewriting the result in matrix form, we complete the derivation for (9).

In order to obtain the representation matrix of \hat{R} in the basis of the NOCI wavefunctions given by (11), we first consider the NOCI wavefunctions in the linearly independent space,

$$|^m \tilde{\Phi}\rangle = \sum_n^{N_{\text{indept}}} |^n \tilde{\Psi}\rangle \tilde{A}_{nm} \tag{37}$$

which satisfy

$$\begin{aligned}
\tilde{S}_{mn}^{\text{NOCI}} &= \langle^m \tilde{\Phi} | ^n \tilde{\Phi}\rangle \\
&= \sum_{m'n'}^{N_{\text{indept}}} \tilde{A}_{mm'}^\dagger \langle^{m'} \tilde{\Psi} | ^{n'} \tilde{\Psi}\rangle \tilde{A}_{n'n} \\
&= (\tilde{\mathbf{A}}^\dagger \tilde{\mathbf{S}} \tilde{\mathbf{A}})_{mn}
\end{aligned} \tag{38}$$

We seek $\tilde{\mathbf{D}}^{\text{NOCI}}(\hat{R})$ such that

$$\hat{R} |^m \tilde{\Phi}\rangle = \sum_{m'}^{N_{\text{indept}}} m' \tilde{\Phi} \tilde{D}_{m'm}^{\text{NOCI}}(\hat{R}) \tag{39}$$

To this end, we use the projection operator

$$\hat{P}_n^{\text{NOCI}} = \sum_{n'}^{N_{\text{indept}}} |^n \tilde{\Phi}\rangle (\tilde{S}^{\text{NOCI}})_{nn'}^{-1} \langle^{n'} \tilde{\Phi}| \tag{40}$$

and proceed as above to arrive at

$$\tilde{D}_{nm}^{\text{NOCI}}(\hat{R}) = \sum_{n'}^{N_{\text{indept}}} (\tilde{S}^{\text{NOCI}})_{nn'}^{-1} \langle^{n'} \tilde{\Phi}|\hat{R} |^m \tilde{\Phi}\rangle \tag{41}$$

which is equivalent to

$$\tilde{\mathbf{D}}^{\text{NOCI}}(\hat{R}) = \tilde{\mathbf{A}}^{-1} \tilde{\mathbf{D}}(\hat{R}) \tilde{\mathbf{A}} \tag{42}$$

by virtue of (37) and then (30).

To obtain $\mathbf{D}^{\text{NOCI}}(\hat{R})$ in the basis of the NOCI wavefunctions given by (11), we substitute (37) into (39) to reintroduce the transformed Slater determinants in the linearly independent space and then use (28) to go back to the original space of linearly dependent Slater determinants. This yields

$$\hat{R} |^m \Phi\rangle = \sum_{m'}^{N_{\text{indept}}} m' \Phi \tilde{D}_{m'm}^{\text{NOCI}}(\hat{R}) \tag{43}$$

which has to be equivalent to

$$\hat{R} |^m \Phi\rangle = \sum_{m'}^{N_{\text{indept}}} m' \Phi D_{m'm}^{\text{NOCI}}(\hat{R}) \tag{44}$$

by definition. The linear independence of $|^m \Phi\rangle$ requires that $\tilde{D}_{m'm}^{\text{NOCI}}(\hat{R})$ and $D_{m'm}^{\text{NOCI}}(\hat{R})$ be identical to each other. Thus, by substituting (9) into (42), we arrive at (14) and complete the

derivation.

C Symmetry Transformation

Let \hat{R} be a spatial symmetry operation which must be unitary (see Section 2.7 of Ref. 73). Applying \hat{R} on $\chi_i(\mathbf{x}_i)$ defined in (4) gives

$$\hat{R}\chi_i(\mathbf{x}_i) = \omega_\delta(s_i)\hat{R}[\varphi_\mu(\mathbf{r}_i)]G_i^{\delta\mu}, \quad (45)$$

since \hat{R} can only affect the spatial basis functions. As each spatial basis function is an atomic orbital centred on a particular nucleus in the system, say A , that is clamped fixed, we can write $\varphi_\mu(\mathbf{r}_i)$ as

$$\varphi_\mu(\mathbf{r}_i) = \tilde{\varphi}_\mu(\mathbf{r}_i - \mathbf{R}_A) \quad (46)$$

where \mathbf{R}_A is the position vector of nucleus A in a space-fixed coordinate system and $\tilde{\varphi}$ denotes an atomic orbital. To make matters more illuminating, we rewrite the above as a convolution of an atomic orbital centred at the origin with the three-dimensional Dirac delta function shifted to the position of A :

$$\begin{aligned} \varphi_\mu(\mathbf{r}_i) &= \tilde{\varphi}_\mu(\mathbf{r}_i) * \delta(\mathbf{r}_i - \mathbf{R}_A) \\ &= \int \tilde{\varphi}_\mu(\mathbf{r}')\delta[\mathbf{r}' - (\mathbf{r}_i - \mathbf{R}_A)]d\mathbf{r}' \end{aligned} \quad (47)$$

so that

$$\begin{aligned} \hat{R}[\varphi_\mu(\mathbf{r}_i)] &= \int \hat{R}\tilde{\varphi}_\mu(\mathbf{r}')\hat{R}\delta[\mathbf{r}' - (\mathbf{r}_i - \mathbf{R}_A)]\hat{R}(d\mathbf{r}') \\ &= \int \hat{R}\tilde{\varphi}_\mu(\mathbf{r}')\delta[\mathbf{r}' - \hat{R}(\mathbf{r}_i - \mathbf{R}_A)]|J_{\hat{R}}|d\mathbf{r}' \end{aligned} \quad (48)$$

$$= \hat{R}\varphi_\mu[\hat{R}(\mathbf{r}_i - \mathbf{R}_A)] \quad (49)$$

which is the transformed atomic orbital centered at a possibly different nucleus onto which A is mapped by the action of \hat{R} on the nuclear framework. From (48) to (49), we have used the fact that \hat{R} is a unitary transformation and the modulus of the corresponding Jacobian $J_{\hat{R}}$ must be 1. Substituting this result back into

(45) gives (16) and concludes the derivation.

To determine how each atomic orbital $\tilde{\varphi}$ transforms under \hat{R} , we first need to convert any Cartesian Gaussian functions into pure and real spherical harmonics because the rotation-inversion transformation matrices in these bases can be generated with ease using the recursion method of Ivancic and Ruedenberg.⁷⁴ Let $\tilde{\chi}_{l_c}(\mathbf{x})$ be a fragment of the overall spin-orbital that is constructed from a single complete set of Cartesian Gaussian basis functions of degree l_c located on a single atom, $\{(\tilde{\varphi}_{l_c})_\mu\}$:

$$\tilde{\chi}_{l_c}(\mathbf{x}) = \omega_\delta(s)(\tilde{\varphi}_{l_c})_\mu(\mathbf{r})G_{l_c}^{\delta\mu}, \quad (50)$$

We cannot simply identify l_c with the angular momentum of an equivalent set of spherical harmonics because the set $\{(\tilde{\varphi}_{l_c})_\mu\}$ contains $\frac{1}{2}(l_c + 1)(l_c + 2)$ Cartesian Gaussians and therefore spans a larger space than the set of $2l_c + 1$ spherical harmonics of angular momentum l_c does for all $l_c \geq 2$.⁷⁵ In fact, since

$$\frac{1}{2}(l_c + 1)(l_c + 2) = \sum_{\substack{l \leq l_c \\ l^P = l_c^P}} (2l + 1) \quad (51)$$

where l^P and l_c^P denote the parities of l and l_c , we must allow $(\tilde{\varphi}_{l_c})_\mu$ to be decomposed into all spherical harmonics of the same parity having angular momenta no greater than l_c :

$$(\tilde{\varphi}_{l_c})_\mu = r^{l_c} \sum_{\substack{l \leq l_c \\ l^P = l_c^P}} \sum_m Y_{lm} W_{m\mu}^{(l_c)} \quad (52)$$

where r is the radial distance, Y_{lm} a real spherical harmonic function of degree l and order m , and $\mathbf{W}^{(l_c)}$ the corresponding transformation matrix with $(2l + 1)$ rows and $\frac{1}{2}(l_c + 1)(l_c + 2)$ columns. The elements of $\mathbf{W}^{(l_c)}$ and its inverse for any l and l_c can be easily derived based on earlier work by Schlegel and Frisch for the specific case $l = l_c$.⁷⁵ In real spherical harmonic bases, (50) thus takes the form

$$\tilde{\chi}_{l_c} = \omega_\delta(s) r^{l_c} \sum_{\substack{l \leq l_c \\ l^P = l_c^P}} \sum_m Y_{lm} W_{m\mu}^{(l_c)} G_{l_c}^{\delta\mu}, \quad (53)$$

Since

$$\hat{R}Y_{lm} = \sum_{m'} Y_{lm'} D_{m'm}^{(l)}(\hat{R}) \quad (54)$$

where the representation matrices $\mathbf{D}^{(l)}(\hat{R})$ of any integral l for any rotation-inversion operation \hat{R} can be determined recursively,⁷⁴ applying \hat{R} to both sides of (53) yields

$$\begin{aligned} \hat{R}\tilde{\chi}_{l_c} = \\ \omega_{\cdot\delta}(s) r^{l_c} \sum_{l \leq l_c} \sum_m \sum_{m'} Y_{lm'} D_{m'm}^{(l)}(\hat{R}) W_{m\mu}^{(l_c)} G_{l_c}^{\delta\mu} \end{aligned} \quad (55)$$

A knowledge of $\mathbf{D}^{(l)}(\hat{R})$, $\mathbf{W}^{(l_c)}$ and its inverse allows the coefficients of the transformed spin-orbitals expressed in the original basis to be worked out easily.

D NOCI Natural Orbitals

To determine the one-particle density matrices of the NOCI wavefunctions in (11), we invoke the one-particle density operator

$$\hat{\rho}(\mathbf{x}) = \sum_{i=1}^{N_e} \delta(\mathbf{x}_i - \mathbf{x}) \quad (56)$$

where $\delta(\mathbf{x}_i - \mathbf{x})$ is the Dirac delta function. The one-particle density of the NOCI wavefunction ${}^m\Phi$ is therefore

$$\begin{aligned} {}^m\rho(\mathbf{x}) &= \sum_{i=1}^{N_e} \langle {}^m\Phi | \delta(\mathbf{x}_i - \mathbf{x}) | {}^m\Phi \rangle \\ &= \sum_{wx}^{N_{\det}} A_{xm} A_{wm}^* {}^{wx}\rho(\mathbf{x}) \end{aligned} \quad (57)$$

where ${}^{wx}\rho(\mathbf{x})$ is the transition density given by

$${}^{wx}\rho(\mathbf{x}) = \sum_{i=1}^{N_e} \langle {}^w\Psi | \delta(\mathbf{x}_i - \mathbf{x}) | {}^x\Psi \rangle \quad (58)$$

Noting that ${}^w\Psi$ and ${}^x\Psi$ are single Slater determinants, we can write

$${}^{wx}\rho(\mathbf{x}) = \sum_{i=1}^{N_e} \left\langle {}^w\Omega \left| \delta(\mathbf{x}_i - \mathbf{x}) \right| \sum_{\sigma} (-1)^{\sigma} \hat{\mathcal{P}}_{\sigma}({}^x\Omega) \right\rangle \quad (59)$$

using the trick in Appendix M of Ref. 14, where

$${}^w\Omega = \prod_j^{N_e} {}^w\chi_j(\mathbf{x}_j), \quad {}^x\Omega = \prod_k^{N_e} {}^x\chi_k(\mathbf{x}_k)$$

are the corresponding Hartree products of the two Slater determinants. Assuming that the two sets of spin-orbitals have been Löwdin paired^{30,76,77} to become bi-orthogonal, *i.e.*,

$$\langle {}^w\chi_j | {}^x\chi_k \rangle = {}^{wx}s_j \delta_{jk} \quad (\text{no sum over } j) \quad (60)$$

which allows (59) to be reduced to a simple form,

$${}^{wx}\rho(\mathbf{x}) = \sum_{i=1}^{N_e} \left(\prod_{j \neq i}^{N_e} {}^{wx}s_j \right) {}^x\chi_i(\mathbf{x}) {}^w\chi_i^*(\mathbf{x}) \quad (61)$$

(57) thus becomes

$$\begin{aligned} {}^m\rho(\mathbf{x}) = \\ \sum_{wx}^{N_{\det}} \sum_{i=1}^{N_e} A_{xm} A_{wm}^* \left(\prod_{j \neq i}^{N_e} {}^{wx}s_j \right) {}^x\chi_i(\mathbf{x}) {}^w\chi_i^*(\mathbf{x}) \end{aligned} \quad (62)$$

which upon expansion of the spin-orbitals in terms of the basis functions by (4) yields the following expression for the one-particle density in the *covariant* basis:

$${}^m\rho(\mathbf{x}) = {}^m P^{\delta\mu, \varepsilon\nu} \omega_{\cdot\delta}(s) \varphi_{\cdot\mu}(\mathbf{r}) \omega_{\varepsilon}^*(s) \varphi_{\nu}^*(\mathbf{r})$$

where ${}^m P^{\delta\mu, \varepsilon\nu}$ is an element of the one-particle density matrix in the *contravariant* representa-

tion for the NOCI wavefunction ${}^m\Phi$:

$${}^m P^{\delta\mu, \varepsilon\nu} = \sum_{wx}^{N_{\text{det}}} \sum_{i=1}^{N_e} A_{xm} A_{wm}^* \left(\prod_{j \neq i}^{N_e} s_j^{wx} \right) x G_i^{\delta\mu, \cdot} \left(w G_i^\dagger \right)^{\cdot, \varepsilon\nu} \quad (63)$$

To obtain natural spin-orbital coefficients in the representation consistent with that in (4), the density matrix must first be converted to the mixed representation before being diagonalized,

$${}^m P^{\delta\mu}_{\cdot, \varepsilon\nu} = {}^m P^{\delta\mu, \zeta\xi} S_{\zeta\xi, \varepsilon\nu}^{\text{AO}} \quad (64)$$

where $S_{\zeta\xi, \varepsilon\nu}^{\text{AO}}$ denotes the overlap of the underlying basis functions,

$$S_{\zeta\xi, \varepsilon\nu}^{\text{AO}} = \langle \omega_{\zeta \cdot}(s) | \omega_{\varepsilon \cdot}(s) \rangle \langle \varphi_{\xi \cdot}(\mathbf{r}) | \varphi_{\nu \cdot}(\mathbf{r}) \rangle \quad (65)$$

The coefficients for the i^{th} natural spin-orbital of ${}^m\Phi$ then satisfy

$${}^m P^{\delta\mu}_{\cdot, \varepsilon\nu} {}^m G_i^{\varepsilon\nu} = {}^m \lambda_i {}^m G_i^{\delta\mu} \quad (66)$$

where ${}^m \lambda_i$ is the corresponding occupation number.

By applying appropriate constraints, we can simplify (63) and obtain expressions for the one-particle density matrix in RHF and UHF. Specifically, in UHF, we can write

$${}^m \rho(\mathbf{x}) = ({}^m P_{\alpha}^{\mu\nu} + {}^m P_{\beta}^{\mu\nu}) \varphi_{\mu}(\mathbf{r}) \varphi_{\nu}^*(\mathbf{r})$$

where

$${}^m P_{\alpha}^{\mu\nu} = \sum_{wx}^{N_{\text{det}}} \sum_{i=1}^{N_{\alpha}} A_{xm} A_{wm}^* \left(\prod_{j \neq i}^{N_e} s_j^{wx} \right) x G_i^{1\mu, \cdot} \left(w G_i^\dagger \right)^{\cdot, 1\nu}$$

and

$${}^m P_{\beta}^{\mu\nu} = \sum_{wx}^{N_{\text{det}}} \sum_{i=N_{\alpha}+1}^{N_{\beta}} A_{xm} A_{wm}^* \left(\prod_{j \neq i}^{N_e} s_j^{wx} \right) x G_i^{2\mu, \cdot} \left(w G_i^\dagger \right)^{\cdot, 2\nu}$$

which can be diagonalized in a similar manner to obtain the natural orbital coefficients and the

corresponding occupation numbers.

Supporting Information

Supporting Information. Detailed Q-CHEM inputs for searches of SCF solutions in $[\text{TiF}_6]^{3-}$ and $[\text{VF}_6]^{3-}$ using metadynamics. Spin-orbital isosurfaces of SCF solutions in $(\text{B}^{3+})(\text{q}^-)_6$. Detailed SCF and NOCI results of $[\text{TiF}_6]^{3-}$ and $[\text{VF}_6]^{3-}$ listing overlap matrices, energy and $\langle \hat{S}^2 \rangle$ values.

This information is available free of charge via the Internet at <http://pubs.acs.org>.

References

- (1) Griffith, J. S. *The Theory of Transition-Metal Ions*; Cambridge University Press: Cambridge, United Kingdom, 2009.
- (2) Mabbs, F. E.; Machin, D. J. *Magnetism and Transition Metal Complexes*; Dover Publications, Inc.: Mineola, New York, 2008.
- (3) Sugano, S.; Tanabe, Y.; Kamimura, H. *Multiplets of Transition-Metal Ions in Crystals*; Academic Press, 1970.
- (4) (a) Tanabe, Y.; Sugano, S. On the Absorption Spectra of Complex Ions. I. *J. Phys. Soc. Japan* **1954**, *9*, 753–766; (b) Tanabe, Y.; Sugano, S. On the Absorption Spectra of Complex Ions II. *J. Phys. Soc. Japan* **1954**, *9*, 766–779; (c) Tanabe, Y.; Sugano, S. On the Absorption Spectra of Complex Ions, III The Calculation of the Crystalline Field Strength. *J. Phys. Soc. Japan* **1956**, *11*, 864–877.
- (5) Condon, E. U.; Shortley, G. *The Theory of Atomic Spectra*; Cambridge University Press: Cambridge, United Kingdom, 1935.
- (6) Dreuw, A.; Head-Gordon, M. Single-Reference *Ab Initio* Methods for the Calculation of Excited States of Large Molecules. *Chem. Rev.* **2005**, *105*, 4009–4037.

- (7) Hartree, D. R. The Wave Mechanics of an Atom with a Non-Coulomb Central Field. Part I. Theory and Methods. *Math. Proc. Cambridge Philos. Soc.* **1928**, *24*, 89–110.
- (8) Fock, V. Näherungsmethode zur Lösung des quantenmechanischen Mehrkörperproblems. *Zeitschrift für Phys.* **1930**, *61*, 126–148.
- (9) Hartree, D. R.; Hartree, W. Self-Consistent Field, with Exchange, for Beryllium. *Proc. R. Soc. London. Ser. A - Math. Phys. Sci.* **1935**, *150*, 9–33.
- (10) Roothaan, C. C. J. New Developments in Molecular Orbital Theory. *Rev. Mod. Phys.* **1951**, *23*, 69–89.
- (11) Attila, S.; Neil, S. O. *Modern Quantum Chemistry: Introduction to Advanced Electronic Structure Theory*; Dover Publications, Inc.: Mineola, New York, 1996.
- (12) Hohenberg, P.; Kohn, W. Inhomogeneous Electron Gas. *Phys. Rev.* **1964**, *136*, B864–B871.
- (13) Bransden, B. H.; Joachain, C. J. *Quantum Mechanics*, 2nd ed.; Pearson Education Limited: Harlow, United Kingdom, 2000; p 404.
- (14) Piela, L. *Ideas of Quantum Chemistry*, 2nd ed.; Elsevier, 2013.
- (15) Bene, J. E. D.; Ditchfield, R.; Pople, J. A. Self-Consistent Molecular Orbital Methods. X. Molecular Orbital Studies of Excited States with Minimal and Extended Basis Sets. *J. Chem. Phys.* **1971**, *55*, 2236–2241.
- (16) Stanton, J. F.; Gauss, J.; Ishikawa, N.; Head-Gordon, M. A Comparison of Single Reference Methods for Characterizing Stationary Points of Excited State Potential Energy Surfaces. *J. Chem. Phys.* **1995**, *103*, 4160–4174.
- (17) McLachlan, A. D.; Ball, M. A. Time-Dependent Hartree–Fock Theory for Molecules. *Rev. Mod. Phys.* **1964**, *36*, 844–855.
- (18) Casida, M. E. In *Recent Development and Applications of Modern Density Functional Theory*; Seminario, J. M., Ed.; 1996; Vol. 4; pp 391–439.
- (19) Burke, K.; Werschnik, J.; Gross, E. K. U. Time-Dependent Density Functional Theory: Past, present, and future. *J. Chem. Phys.* **2005**, *123*, 062206.
- (20) Elliott, P.; Furche, F.; Burke, K. In *Reviews in Computational Chemistry*; Lipkowitz, K. B., Cundari, T. R., Eds.; John Wiley & Sons, Inc., 2009.
- (21) Maier, T. M.; Bahmann, H.; Arbuznikov, A. V.; Kaupp, M. Validation of Local Hybrid Functionals for TDDFT Calculations of Electronic Excitation Energies. *J. Chem. Phys.* **2016**, *144*, 074106.
- (22) Thom, A. J. W.; Head-Gordon, M. Locating Multiple Self-Consistent Field Solutions: An Approach Inspired by Metadynamics. *Phys. Rev. Lett.* **2008**, *101*, 193001.
- (23) Sherrill, C.; Lee, M. S.; Head-Gordon, M. On the Performance of Density Functional Theory for Symmetry-Breaking Problems. *Chem. Phys. Lett.* **1999**, *302*, 425–430.
- (24) Cohen, R. D.; Sherrill, C. D. The Performance of Density Functional Theory for Equilibrium Molecular Properties of Symmetry Breaking Molecules. *J. Chem. Phys.* **2001**, *114*, 8257–8269.
- (25) Cook, D. B. Broken Symmetry in the Electronic Structure of the Ferrocene Molecule. *Int. J. Quantum Chem.* **1992**, *43*, 197–207.
- (26) Jaworska, M.; Lodowski, P.; Nowakowski, J. Broken-Symmetry Hartree–Fock Solutions in the RHF Wavefunction of Dicyclobutadienenickel. *Chem. Phys. Lett.* **1995**, *232*, 328–334.

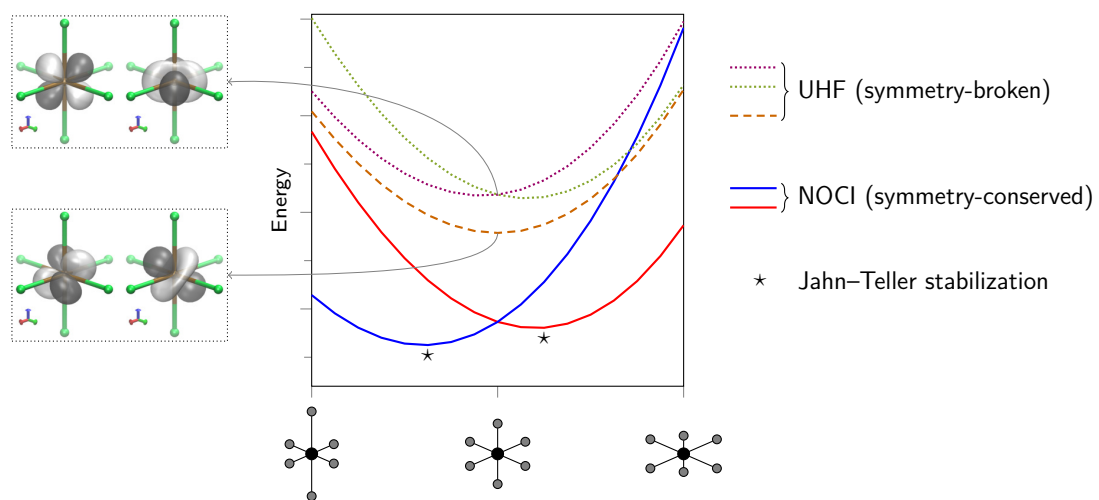
- (27) Jaworska, M.; Lodowski, P. Symmetry Breaking in HF Wave Functions of Fe(CH)₂. *J. Math. Chem.* **1999**, *25*, 7–21.
- (28) Pantazis, D. A. Meeting the Challenge of Magnetic Coupling in a Triply-Bridged Chromium Dimer: Complementary Broken-Symmetry Density Functional Theory and Multireference Density Matrix Renormalization Group Perspectives. *J. Chem. Theory Comput.* **2019**, *15*, 938–948.
- (29) (a) Noodleman, L. Valence Bond Description of Antiferromagnetic Coupling in Transition Metal Dimers. *J. Chem. Phys.* **1981**, *74*, 5737–5743; (b) Noodleman, L.; Case, D. A.; Aizman, A. Broken Symmetry Analysis of Spin Coupling in Iron-Sulfur Clusters. *J. Am. Chem. Soc.* **1988**, *110*, 1001–1005.
- (30) Thom, A. J. W.; Head-Gordon, M. Hartree–Fock Solutions as a Quasidiabatic Basis for Non-Orthogonal Configuration Interaction. *J. Chem. Phys.* **2009**, *131*, 124113.
- (31) Benavides-Riveros, C. L.; Lathiotakis, N. N.; Marques, M. A. L. Towards a Formal Definition of Static and Dynamic Electronic Correlations. *Phys. Chem. Chem. Phys.* **2017**, *19*, 12655–12664.
- (32) Jiménez-Hoyos, C. A.; Henderson, T. M.; Tsuchimochi, T.; Scuseria, G. E. Projected Hartree–Fock Theory. *J. Chem. Phys.* **2012**, *136*, 164109.
- (33) Jiménez-Hoyos, C. A.; Rodríguez-Guzmán, R.; Scuseria, G. E. Multi-Component Symmetry-Projected Approach for Molecular Ground State Correlations. *J. Chem. Phys.* **2013**, *139*, 204102.
- (34) Jiménez-Hoyos, C. A.; Rodríguez-Guzmán, R.; Scuseria, G. E. Excited Electronic States from a Variational Approach Based on Symmetry-Projected Hartree–Fock Configurations. *J. Chem. Phys.* **2013**, *139*, 224110.
- (35) Slater, J. C. The Theory of Complex Spectra. *Phys. Rev.* **1929**, *34*, 1293–1322.
- (36) Head-Gordon, M.; Maslen, P. E.; White, C. A. A Tensor Formulation of Many-Electron Theory in a Nonorthogonal Single-Particle Basis. *J. Chem. Phys.* **1998**, *108*, 616–625.
- (37) Landau, L. D.; Lifshitz, E. M. *Quantum Mechanics - Non-Relativistic Theory*, 3rd ed.; Pergamon Press Ltd, 1977.
- (38) Heine, V. *Group Theory in Quantum Mechanics. An Introduction to its Present Usage*; Pergamon Press Ltd, 1960.
- (39) Tsukerblat, B. S. *Group Theory in Chemistry and Spectroscopy: A Simple Guide to Advanced Usage*; Dover Publications, Inc.: Mineola, New York, 2006.
- (40) Cook, D. B. *Handbook of Computational Quantum Chemistry*; Dover Publications, Inc.: Mineola, New York, 2005.
- (41) Fukutome, H. Unrestricted Hartree–Fock Theory and Its Applications to Molecules and Chemical Reactions. *Int. J. Quantum Chem.* **1981**, *20*, 955–1065.
- (42) Wigner, E. *Group Theory and Its Application to the Quantum Mechanics of Atomic Spectra*; Academic Press: London, 1959; p 386.
- (43) James, G.; Liebeck, M. *Representations and Characters of Groups*; Cambridge University Press: Cambridge, United Kingdom, 2001.
- (44) Stuber, J. L.; Paldus, J. In *Fundamental World of Quantum Chemistry: A Tribute to the Memory of Per-Olov Löwdin, Volume 1*; Brändas, E., Kryachko, E. S., Eds.; Kluwer Academic Publishers, 2003; pp 67–139.
- (45) Jiménez-Hoyos, C. A.; Henderson, T. M.; Scuseria, G. E. Generalized Hartree–Fock Description of Molecular Dissociation. *J. Chem. Theory Comput.* **2011**, *7*, 2667–2674.

- (46) Henderson, T. M.; Jiménez-Hoyos, C. A.; Scuseria, G. E. Magnetic Structure of Density Matrices. *J. Chem. Theory Comput.* **2018**, *14*, 649–659.
- (47) Soriano, M.; Palacios, J. J. Theory of Projections with Nonorthogonal Basis Sets: Partitioning Techniques and Effective Hamiltonians. *Phys. Rev. B* **2014**, *90*, 075128.
- (48) Amos, A. T.; Hall, G. G. Single Determinant Wave Functions. *Proc. R. Soc. London. Ser. A. Math. Phys. Sci.* **1961**, *263*, 483–493.
- (49) Mayhall, N. J.; Horn, P. R.; Sundstrom, E. J.; Head-Gordon, M. Spin-Flip Non-Orthogonal Configuration Interaction: a Variational and Almost Black-Box Method for Describing Strongly Correlated Molecules. *Phys. Chem. Chem. Phys.* **2014**, *16*.
- (50) Sundstrom, E. J.; Head-Gordon, M. Non-Orthogonal Configuration Interaction for the Calculation of Multielectron Excited States. *J. Chem. Phys.* **2014**, *140*.
- (51) Repeated representations are not a problem. For example, if both $\{^m\Phi\}$ and $\{^n\Phi\}$ form two bases for the same irreducible representation Γ , NOCI must already take into account their symmetry-allowed mutual interaction and lift their degeneracy with respect to each other so that the $\{^m\Phi\}$ wavefunctions only transform amongst themselves under any symmetry operation of the group, as do the $\{^n\Phi\}$ wavefunctions.
- (52) Humphrey, W.; Dalke, A.; Schulten, K. VMD – Visual Molecular Dynamics. *Journal of Molecular Graphics* **1996**, *14*, 33–38.
- (53) Pulay, P. Convergence Acceleration of Iterative Sequences. The Case of SCF Iteration. *Chem. Phys. Lett.* **1980**, *73*, 393–398.
- (54) Shao, Y.; Gan, Z.; Epifanovsky, E.; Gilbert, A. T.; Wormit, M.; Kussmann, J.; Lange, A. W.; Behn, A.; Deng, J.; Feng, X.; Ghosh, D.; Goldey, M.; Horn, P. R.; Jacobson, L. D.; Kaliman, I.; Khaliullin, R. Z.; Kuś, T.; Landau, A.; Liu, J.; Proynov, E. I.; Rhee, Y. M.; Richard, R. M.; Rohrdanz, M. A.; Steele, R. P.; Sundstrom, E. J.; Woodcock, H. L.; Zimmerman, P. M.; Zuev, D.; Albrecht, B.; Alguire, E.; Austin, B.; Beran, G. J. O.; Bernard, Y. A.; Berquist, E.; Brandhorst, K.; Bravaya, K. B.; Brown, S. T.; Casanova, D.; Chang, C.-M.; Chen, Y.; Chien, S. H.; Closser, K. D.; Crittenden, D. L.; Diedenhofen, M.; DiStasio, R. A.; Do, H.; Dutoi, A. D.; Edgar, R. G.; Fatehi, S.; Fusti-Molnar, L.; Ghysels, A.; Golubeva-Zadorozhnaya, A.; Gomes, J.; Hanson-Heine, M. W.; Harbach, P. H.; Hauser, A. W.; Hohenstein, E. G.; Holden, Z. C.; Jagau, T.-C.; Ji, H.; Kaduk, B.; Khistyayev, K.; Kim, J.; Kim, J.; King, R. A.; Klunzinger, P.; Kosenkov, D.; Kowalczyk, T.; Krauter, C. M.; Lao, K. U.; Laurent, A. D.; Lawler, K. V.; Levchenko, S. V.; Lin, C. Y.; Liu, F.; Livshits, E.; Lochan, R. C.; Luenser, A.; Manohar, P.; Manzer, S. F.; Mao, S.-P.; Mardirossian, N.; Marenich, A. V.; Maurer, S. A.; Mayhall, N. J.; Neuscamman, E.; Oana, C. M.; Olivares-Amaya, R.; O’Neill, D. P.; Parkhill, J. A.; Perrine, T. M.; Peverati, R.; Prociuk, A.; Rehn, D. R.; Rosta, E.; Russ, N. J.; Sharada, S. M.; Sharma, S.; Small, D. W.; Sodt, A.; Stein, T.; Stück, D.; Su, Y.-C.; Thom, A. J.; Tsuchimochi, T.; Vanovschi, V.; Vogt, L.; Vydrov, O.; Wang, T.; Watson, M. A.; Wenzel, J.; White, A.; Williams, C. F.; Yang, J.; Yeganeh, S.; Yost, S. R.; You, Z.-Q.; Zhang, I. Y.; Zhang, X.; Zhao, Y.; Brooks, B. R.; Chan, G. K.; Chipman, D. M.; Cramer, C. J.; Goddard, W. A.; Gordon, M. S.; Hehre, W. J.; Klamt, A.; Schaefer, H. F.; Schmidt, M. W.; Sher-

- rill, C. D.; Truhlar, D. G.; Warshel, A.; Xu, X.; Aspuru-Guzik, A.; Baer, R.; Bell, A. T.; Besley, N. A.; Chai, J.-D.; Dreuw, A.; Dunietz, B. D.; Furlani, T. R.; Gwaltney, S. R.; Hsu, C.-P.; Jung, Y.; Kong, J.; Lambrecht, D. S.; Liang, W.; Ochsenfeld, C.; Rassolov, V. A.; Slipchenko, L. V.; Subotnik, J. E.; Van Voorhis, T.; Herbert, J. M.; Krylov, A. I.; Gill, P. M.; Head-Gordon, M. *Advances in Molecular Quantum Chemistry Contained in the Q-Chem 4 Program Package. Mol. Phys.* **2015**, *113*, 184–215.
- (55) van der Walt, S.; Colbert, S. C.; Varoquaux, G. The NumPy Array: A Structure for Efficient Numerical Computation. *Comput. Sci. Eng.* **2011**, *13*, 22–30.
- (56) Stone, J. *An Efficient Library for Parallel Ray Tracing and Animation*. M.Sc. thesis, Computer Science Department, University of Missouri-Rolla, 1998.
- (57) Housecroft, C. E.; Sharpe, A. G. *Inorganic Chemistry*, 4th ed.; Pearson, 2012.
- (58) A Fast Intrinsic Localization Procedure Applicable for *Ab Initio* and Semiempirical Linear Combination of Atomic Orbital Wave Functions. *J. Chem. Phys.* **1989**, *90*, 4916–4926.
- (59) Thom, A. J. W.; Sundstrom, E. J.; Head-Gordon, M. LOBA: a Localized Orbital Bonding Analysis to Calculate Oxidation States, with Application to a Model Water Oxidation Catalyst. *Phys. Chem. Chem. Phys.* **2009**, *11*, 11297.
- (60) Hatfield, W. E.; Nassiff, P. J.; Couch, T. W.; Villa, J. F. Magnetism and Spectroscopy of a Series of Hexafluorotitanates(III). *Inorg. Chem.* **1971**, *10*, 368–373.
- (61) Strictly speaking, one cannot be sure that such a T_{2g} wavefunction is indeed the exact ground eigenfunction of the electronic Hamiltonian for $[\text{TiF}_6]^{3-}$ without solving the electronic Schrödinger equation exactly, and so one cannot claim with certainty that the UHF solutions reported provide approximations to the ground electronic state of $[\text{TiF}_6]^{3-}$. Group theory only requires that the exact eigenfunctions of the electronic Hamiltonian for $[\text{TiF}_6]^{3-}$ transform as single irreducible representations of \mathcal{O}_h but is completely silent to their ordering. Nevertheless, if $[\text{TiF}_6]^{3-}$ is assumed to behave qualitatively similar to a true d^1 system by virtue of the approximately totally symmetric singlet Ar core and F^- ligands (see Chapter 7 of Ref. 1), then its true ground and first excited wavefunctions are expected to be described by the ${}^2T_{2g}$ and 2E_g terms, respectively.
- (62) Lykos, P.; Pratt, G. W. Discussion on The Hartree–Fock Approximation. *Rev. Mod. Phys.* **1963**, *35*, 496–501.
- (63) The D shell in vanadium’s 6-31G* is commonly constructed with six Cartesian functions of degree 2 for the angular part. There is, however, an s component contained in this (see Appendix C) which is of no interest to the model system where the two electrons are constrained to occupy only the five d orbitals. We thus use the pure (and real) d form instead for the angular part of the basis functions in the D shell to eliminate the unnecessary totally symmetric s component.
- (64) Stedman, G. E.; Butler, P. H. Time Reversal Symmetry in Applications of Point Group Theory. *J. Phys. A. Math. Gen.* **1980**, *13*, 3125–3140.
- (65) The irreducible representations spanned by a_0^* are shown in Table 5b and those spanned by A_0 are shown in Figure 5b. The attentive reader will notice that the ${}^1T_{1g}$ component in a_0^* is apparently missing from A_0 . This, however, can be attributed to the incomplete spin purification using time reversal, because, as shown in Table S5b in the Supporting Informa-

tion, A_0 does contain a T_{1g} component denoted by ${}^{\circ}T_{1g}[A_0]$ with $\langle \hat{S}^2 \rangle \approx 0.1003$. This unfortunately results in it being assigned to an undefined spin multiplicity based on our 1×10^{-2} threshold (signified by “ \circ ”). However, ${}^{\circ}T_{1g}[A_0]$ still contains a ${}^1T_{1g}$ component among other even- S contaminations.

- (66) Jahn, H. A.; Teller, E. Stability of Polyatomic Molecules in Degenerate Electronic States - I—Orbital Degeneracy. *Proc. R. Soc. London. Ser. A - Math. Phys. Sci.* **1937**, *161*, 220–235.
- (67) Hiscock, H. G.; Thom, A. J. W. Holomorphic Hartree–Fock Theory and Configuration Interaction. *J. Chem. Theory Comput.* **2014**, *10*, 4795–4800.
- (68) Burton, H. G. A.; Thom, A. J. W. Holomorphic Hartree–Fock Theory: An Inherently Multireference Approach. *J. Chem. Theory Comput.* **2016**, *12*, 167–173.
- (69) Mead, C. A. The “Noncrossing” Rule for Electronic Potential Energy Surfaces: The Role of Time-Reversal Invariance. *J. Chem. Phys.* **1979**, *70*, 2276–2283.
- (70) Hall, B. C. *Lie Groups, Lie Algebras, and Representations*, 2nd ed.; Graduate Texts in Mathematics; Springer International Publishing, 2015; Vol. 222.
- (71) Pfeifer, W. *The Lie Algebras $su(N)$* ; Birkhäuser, Basel: Basel, Switzerland, 2003.
- (72) Woit, P. *Quantum Theory, Groups and Representations*; Springer International Publishing, 2017.
- (73) Altmann, S. L. *Rotations, Quaternions, and Double Groups*; Dover Publications, Inc.: New York, 2005.
- (74) (a) Ivanic, J.; Ruedenberg, K. Rotation Matrices for Real Spherical Harmonics. Direct Determination by Recursion. *J. Phys. Chem.* **1996**, *100*, 6342–6347; (b) Ivanic, J.; Ruedenberg, K. Rotation Matrices for Real Spherical Harmonics. Direct Determination by Recursion. ADDITIONS AND CORRECTIONS. *J. Phys. Chem.* **1998**, *102*, 9099–9100.
- (75) Schlegel, H. B.; Frisch, M. J. Transformation Between Cartesian and Pure Spherical Harmonic Gaussians. *Int. J. Quantum Chem.* **1995**, *54*, 83–87.
- (76) Löwdin, P.-O. Band Theory, Valence Bond, and Tight-Binding Calculations. *J. Appl. Phys.* **1962**, *33*, 251–280.
- (77) Mayer, I. Löwdin’s Pairing Theorem and Some of Its Applications. *Mol. Phys.* **2010**, *108*, 3273–3278.



For Table of Contents Only.

Supporting information for:
Symmetry in Multiple Self-Consistent-Field
Solutions of Transition-Metal Complexes

Bang C. Huynh* and Alex J. W. Thom

University Chemical Laboratory, Lensfield Road, Cambridge CB2 1EW, United Kingdom

E-mail: cbh31@cam.ac.uk

Contents

1	Converging into Multiple Solutions	S2
2	$[\text{TiF}_6]^{3-}$: Detailed Results	S6
3	$[(\text{B}^{3+})(\text{q}^-)_6]$: Spin-Orbitals	S8
4	$[\text{VF}_6]^{3-}$: Detailed Results	S9

1 Converging into Multiple Solutions

Listings 1–3 show the Q-CHEM input files for preliminary low-convergence metadynamics search of UHF solutions in $[\text{TiF}_6]^{3-}$ and $[\text{VF}_6]^{3-}$. Each of the located solutions is then reconverged into with `SCF_CONVERGENCE` set to 13 to ensure that its DIIS error is smaller than 1×10^{-13} .

Listing 1: Q-CHEM input for preliminary low-convergence metadynamics search of $M_S = \frac{1}{2}$ UHF solutions in $[\text{TiF}_6]^{3-}$.

```

1 $molecule
2   -3 2
3   --
4   3 2
5   Ti   0.0000000   0.0000000   0.0000000
6   --
7   -1 1
8   F   0.0000000   0.0000000   2.0274000
9   --
10  -1 1
11  F   0.0000000   0.0000000  -2.0274000
12  --
13  -1 1
14  F   0.0000000   2.0274000   0.0000000
15  --
16  -1 1
17  F   0.0000000  -2.0274000   0.0000000
18  --
19  -1 1
20  F   2.0274000   0.0000000   0.0000000
21  --
22  -1 1
23  F  -2.0274000   0.0000000   0.0000000
24 $end
25 $rem
26 BASIS 6-31G*
27 EXCHANGE hf
28 UNRESTRICTED true
29 SCF_ALGORITHM diis
30 SCF_GUESS fragmo
31 SCF_CONVERGENCE 7
32 MAX_SCF_CYCLES 1000
33 SYMMETRY off
34 DIIS_SEPARATE_ERRVEC true
35 SYM_IGNORE true
36 MOM_START 1
37 $end
38 $rem_frgm
39 SCF_CONVERGENCE 5
40 THRESH 8
41 $end
42 @@@
43 $molecule
44 read
45 $end
46 $rem
47 BASIS 6-31G*
48 EXCHANGE hf
49 UNRESTRICTED true
50 SCF_GUESS read
51 SCF_ALGORITHM diis
52 SCF_CONVERGENCE 7
53 SCF_SAVEMINIMA 100
54 SCF_MAX_CYCLES 1000000
55 MOM_START 1
56 PRINT_ORBITALS true
57 SCF_MINFIND_INITNORM 00010
58 SCF_MINFIND_INCREASEFACTOR 10800
59 SCF_MINFIND_WELLTHRESH 6
60 SCF_MINFIND_RANDOMMIXING -15708
61 SCF_MINFIND_NRANDOMMIXES 2
62 SCF_MINFIND_MIXMETHOD 1
63 SCF_MINFIND_MIXENERGY 00200
64 SCF_MINFIND_RESTARTSTEPS 1000
65 SYMMETRY off
66 DIIS_SEPARATE_ERRVEC true
67 SYM_IGNORE true
68 $end

```

Listing 2: Q-CHEM input for preliminary low-convergence metadynamics search of $M_S = 1$ UHF solutions in $[\text{VF}_6]^{3-}$.

```

1 $molecule
2   -3 3
3   --
4   3 3
5   V   0.0000000    0.0000000    0.0000000
6   --
7   -1 1
8   F   0.0000000    0.0000000    1.9896000
9   --
10  -1 1
11  F   0.0000000    0.0000000   -1.9896000
12  --
13  -1 1
14  F   0.0000000    1.9896000    0.0000000
15  --
16  -1 1
17  F   0.0000000   -1.9896000    0.0000000
18  --
19  -1 1
20  F   1.9896000    0.0000000    0.0000000
21  --
22  -1 1
23  F  -1.9896000    0.0000000    0.0000000
24 $end
25 $rem
26   BASIS 6-31G*
27   EXCHANGE hf
28   UNRESTRICTED true
29   SCF_ALGORITHM diis
30   SCF_GUESS fragmo
31   SCF_CONVERGENCE 7
32   MAX_SCF_CYCLES 1000
33   SYMMETRY off
34   DIIS_SEPARATE_ERRVEC true
35   SYM_IGNORE true
36   MOM_START 1
37 $end
38 $rem_frgm
39   SCF_CONVERGENCE 3
40   THRESH 6
41 $end
42 @@@
43 $molecule
44   read
45 $end
46 $rem
47   BASIS 6-31G*
48   EXCHANGE hf
49   UNRESTRICTED true
50   SCF_GUESS read
51   SCF_ALGORITHM diis
52   SCF_CONVERGENCE 7
53   SCF_SAVEMINIMA 700
54   SCF_MAX_CYCLES 10000000
55   MOM_START 1
56   PRINT_ORBITALS true
57   SCF_MINFIND_INITNORM 00010
58   SCF_MINFIND_INCREASEFACTOR 10800
59   SCF_MINFIND_WELLTHRESH 6
60   SCF_MINFIND_RANDOMMIXING -15708
61   SCF_MINFIND_NRANDOMMIXES 2
62   SCF_MINFIND_MIXMETHOD 1
63   SCF_MINFIND_MIXENERGY 00200
64   SCF_MINFIND_RESTARTSTEPS 1000
65   SYMMETRY off
66   DIIS_SEPARATE_ERRVEC true
67   SYM_IGNORE true
68 $end

```

Listing 3: Q-CHEM input for preliminary low-convergence metadynamics search of $M_S = 0$ UHF solutions in $[\text{VF}_6]^{3-}$.

```

1 $molecule
2   -3 1
3   --
4   3 1
5   V   0.0000000    0.0000000    0.0000000
6   --
7   -1 1
8   F   0.0000000    0.0000000    1.9896000
9   --
10  -1 1
11  F   0.0000000    0.0000000   -1.9896000
12  --
13  -1 1
14  F   0.0000000    1.9896000    0.0000000
15  --
16  -1 1
17  F   0.0000000   -1.9896000    0.0000000
18  --
19  -1 1
20  F   1.9896000    0.0000000    0.0000000
21  --
22  -1 1
23  F  -1.9896000    0.0000000    0.0000000
24 $end
25 $rem
26   BASIS 6-31G*
27   EXCHANGE hf
28   UNRESTRICTED true
29   SCF_ALGORITHM diis
30   SCF_GUESS fragmo
31   SCF_CONVERGENCE 7
32   MAX_SCF_CYCLES 100000
33   SCF_MINFIND_RESTARTSTEPS 10000
34   SYMMETRY off
35   DIIS_SEPARATE_ERRVEC true
36   SYM_IGNORE true
37   MOM_START 1
38 $end
39 $rem_frgm
40   SCF_CONVERGENCE 6
41   THRESH 9
42 $end
43 @@@
44 $molecule
45   read
46 $end
47 $rem
48   BASIS 6-31G*
49   EXCHANGE hf
50   UNRESTRICTED true
51   SCF_GUESS read
52   SCF_ALGORITHM diis
53   SCF_CONVERGENCE 7
54   SCF_SAVEMINIMA 500
55   SCF_MAX_CYCLES 100000000
56   MOM_START 1
57   PRINT_ORBITALS true
58   SCF_MINFIND_INITNORM 00010
59   SCF_MINFIND_INCREASEFACTOR 10800
60   SCF_MINFIND_WELLTHRESH 6
61   SCF_MINFIND_RANDOMMIXING -15708
62   SCF_MINFIND_NRANDOMMIXES 2
63   SCF_MINFIND_MIXMETHOD 1
64   SCF_MINFIND_MIXENERGY 00180
65   SCF_MINFIND_RESTARTSTEPS 3000
66   SYMMETRY off
67   DIIS_SEPARATE_ERRVEC true
68   SYM_IGNORE true
69 $end

```

2 $[\text{TiF}_6]^{3-}$: Detailed Results

Table S1: Overlap matrices for degenerate, linearly independent UHF solutions in $[\text{TiF}_6]^{3-}$.

(a) $A_{\frac{1}{2}}$ solutions in $[\text{TiF}_6]^{3-}$.

	$A_{\frac{1}{2},1}$	$A_{\frac{1}{2},2}$	$A_{\frac{1}{2},3}$	$A_{\frac{1}{2},4}$	$A_{\frac{1}{2},5}$	$A_{\frac{1}{2},6}$
$A_{\frac{1}{2},1}$	1.0000	-0.4991	0.4991	-0.4991	-0.4991	0.0000
$A_{\frac{1}{2},2}$	-0.4991	1.0000	0.0000	-0.4991	0.4991	0.4991
$A_{\frac{1}{2},3}$	0.4991	0.0000	1.0000	-0.4991	0.0000	-0.4991
$A_{\frac{1}{2},4}$	-0.4991	-0.4991	-0.4991	1.0000	0.0000	-0.4991
$A_{\frac{1}{2},5}$	-0.4991	0.4991	0.4991	0.0000	1.0000	-0.4991
$A_{\frac{1}{2},6}$	0.0000	0.4991	-0.4991	-0.4991	-0.4991	1.0000

(b) $A'_{\frac{1}{2}}$ solutions in $[\text{TiF}_6]^{3-}$.

	$A'_{\frac{1}{2},1}$	$A'_{\frac{1}{2},2}$	$A'_{\frac{1}{2},3}$
$A'_{\frac{1}{2},1}$	1.0000	0.0000	0.0000
$A'_{\frac{1}{2},2}$	0.0000	1.0000	0.0000
$A'_{\frac{1}{2},3}$	0.0000	0.0000	1.0000

(c) $B_{\frac{1}{2}}$ solutions in $[\text{TiF}_6]^{3-}$.

	$B_{\frac{1}{2},1}$	$B_{\frac{1}{2},2}$	$B_{\frac{1}{2},3}$
$B_{\frac{1}{2},1}$	1.0000	0.4988	-0.4988
$B_{\frac{1}{2},2}$	0.4988	1.0000	0.4988
$B_{\frac{1}{2},3}$	-0.4988	0.4988	1.0000

Table S2: Energies and $\langle \hat{S}^2 \rangle$ values of $M_S = \frac{1}{2}$ UHF solutions in $[\text{TiF}_6]^{3-}$.

Ψ_{UHF}	Energy/ E_h	$\langle \hat{S}^2 \rangle$
$A_{\frac{1}{2}}$	-1444.930 682 2	0.7522
$A'_{\frac{1}{2}}$	-1444.930 670 6	0.7522
$B_{\frac{1}{2}}$	-1444.866 682 6	0.7527

Table S3: Energies and $\langle \hat{S}^2 \rangle$ values of $M_S = \frac{1}{2}$ NOCI wavefunctions in $[\text{TiF}_6]^{3-}$.

Φ	Energy/ E_h	$\langle \hat{S}^2 \rangle$
${}^2T_{2g}[A_{\frac{1}{2}}]$	-1444.932 637 2	0.7512
${}^\infty T_{1g}[A_{\frac{1}{2}}]$	-1442.625 283 3	1.8403
${}^2T_{2g}[A_{\frac{1}{2}} \oplus A'_{\frac{1}{2}}]$	-1444.932 776 5	0.7512
${}^\infty T_{2g}[A_{\frac{1}{2}} \oplus A'_{\frac{1}{2}}]$	-1442.693 102 2	1.5549
${}^\infty T_{1g}[A_{\frac{1}{2}} \oplus A'_{\frac{1}{2}}]$	-1442.625 283 3	1.8403
${}^2E_g[B_{\frac{1}{2}}]$	-1444.868 243 3	0.7517
${}^\infty A_{2g}[B_{\frac{1}{2}}]$	-1442.930 806 7	2.0321

3 $[(B^{3+})(q^-)_6]$: Spin-Orbitals

Table S4: Representative isosurface plots for the Pipek–Mezey-localized spatial parts of the occupied spin-orbitals of the UHF solutions in the toy system $[(B^{3+})(q^-)_6]$. The point charges (not shown here) are located octahedrally on the Cartesian axes. In (a), both spin-orbitals χ_1 and χ_2 have $m_s = \frac{1}{2}$. In (b), χ_1 has $m_s = \frac{1}{2}$ whereas $\bar{\chi}_2$ has $m_s = -\frac{1}{2}$ as indicated by the bar. The spin-orbitals of all solutions within one set have similar forms and are related by the symmetry operations of \mathcal{O}_h . Axis triad: red- x ; green- y ; blue- z .

(a) $M_S = 1$			(b) $M_S = 0$		
Ψ_{UHF}	χ_1	χ_2	Ψ_{UHF}	χ_1	$\bar{\chi}_2$
a_1			a_0^*		
a'_1			a'_0		
b_1			a''_0		
c_1			b_0		
d_1			c_0		
e_1			d_0		
f_1			e_0		

4 $[\text{VF}_6]^{3-}$: Detailed Results

Table S5: Overlap matrices for degenerate, linearly independent UHF solutions in $[\text{VF}_6]^{3-}$.

(a) A_1 solutions in $[\text{VF}_6]^{3-}$.

	$A_{1,1}$	$A_{1,2}$	$A_{1,3}$	$A_{1,4}$
$A_{1,1}$	1.0000	-0.3318	-0.3318	0.3318
$A_{1,2}$	-0.3318	1.0000	-0.3318	0.3318
$A_{1,3}$	-0.3318	-0.3318	1.0000	0.3318
$A_{1,4}$	0.3318	0.3318	0.3318	1.0000

(b) A'_1 solutions in $[\text{VF}_6]^{3-}$.

	$A'_{1,1}$	$A'_{1,2}$	$A'_{1,3}$	$A'_{1,4}$	$A'_{1,5}$	$A'_{1,6}$
$A'_{1,1}$	1.0000	-0.4851	-0.4851	-0.4851	-0.4851	0.0000
$A'_{1,2}$	-0.4851	1.0000	0.0000	0.4851	-0.4851	-0.4851
$A'_{1,3}$	-0.4851	0.0000	1.0000	-0.4851	0.4851	-0.4851
$A'_{1,4}$	-0.4851	0.4851	-0.4851	1.0000	0.0000	0.4851
$A'_{1,5}$	-0.4851	-0.4851	0.4851	0.0000	1.0000	0.4851
$A'_{1,6}$	0.0000	-0.4851	-0.4851	0.4851	0.4851	1.0000

(c) B_1 solutions in $[\text{VF}_6]^{3-}$.

	$B_{1,1}$	$B_{1,2}$	$B_{1,3}$
$B_{1,1}$	1.0000	0.0000	0.0000
$B_{1,2}$	0.0000	1.0000	0.0000
$B_{1,3}$	0.0000	0.0000	1.0000

(d) C_1 solutions in $[\text{VF}_6]^{3-}$.

	$C_{1,1}$	$C_{1,2}$	$C_{1,3}$
$C_{1,1}$	1.0000	0.0000	0.0000
$C_{1,2}$	0.0000	1.0000	0.0000
$C_{1,3}$	0.0000	0.0000	1.0000

(e) D_1 solutions in $[\text{VF}_6]^{3-}$.

	$D_{1,1}$	$D_{1,2}$	$D_{1,3}$	$D_{1,4}$	$D_{1,5}$	$D_{1,6}$
$D_{1,1}$	1.0000	0.0000	0.2492	-0.2492	-0.2492	0.2492
$D_{1,2}$	0.0000	1.0000	0.2492	-0.2492	0.2492	-0.2492
$D_{1,3}$	0.2492	0.2492	1.0000	0.0000	-0.2492	-0.2492
$D_{1,4}$	-0.2492	-0.2492	0.0000	1.0000	-0.2492	-0.2492
$D_{1,5}$	-0.2492	0.2492	0.2492	-0.2492	1.0000	0.0000
$D_{1,6}$	0.2492	-0.2492	-0.2492	-0.2492	0.0000	1.0000

(f) E_1 solutions in $[\text{VF}_6]^{3-}$.

	$E_{1,1}$	$E_{1,2}$	$E_{1,3}$
$E_{1,1}$	1.0000	0.0000	0.0000
$E_{1,2}$	0.0000	1.0000	0.0000
$E_{1,3}$	0.0000	0.0000	1.0000

(g) F_1 solutions in $[\text{VF}_6]^{3-}$.

	$F_{1,1}$
$F_{1,1}$	1.0000

(h) A_0 solutions in $[\text{VF}_6]^3$.

	$A_{0,1}$	$A_{0,2}$	$A_{0,3}$	$A_{0,4}$	$A_{0,5}$	$A_{0,6}$	$A_{0,7}$	$A_{0,8}$	$A_{0,9}$	$A_{0,10}$	$A_{0,11}$	$A_{0,12}$	$A_{0,13}$	$A_{0,14}$	$A_{0,15}$	$A_{0,16}$	$A_{0,17}$	$A_{0,18}$	$A_{0,19}$	$A_{0,20}$	$A_{0,21}$	$A_{0,22}$	$A_{0,23}$	$A_{0,24}$
$A_{0,1}$	1.0000	-0.1601	0.0000	-0.5036	-0.7469	0.2936	-0.1601	0.2936	-0.7469	-0.0709	0.3182	0.3182	0.0156	-0.2471	-0.3182	0.3182	-0.0156	-0.2471	0.1221	-0.0390	-0.0390	-0.1221	0.0390	0.0390
$A_{0,2}$	-0.1601	1.0000	-0.1221	-0.1221	0.0390	0.0390	0.0709	-0.7469	0.2936	0.1601	-0.0156	-0.2471	-0.3182	0.3182	-0.3182	0.3182	-0.2471	-0.0156	0.5036	-0.2936	-0.0390	0.0000	-0.7469	0.0390
$A_{0,3}$	0.0000	-0.1221	1.0000	0.0709	-0.2471	-0.0156	-0.1221	-0.0156	-0.2471	0.5036	0.0390	0.0390	-0.2936	-0.7469	-0.0390	0.0390	0.2936	-0.7469	0.1601	-0.3182	-0.3182	-0.1601	0.3182	0.3182
$A_{0,4}$	-0.5036	-0.1221	0.0709	1.0000	0.3182	0.3182	-0.1221	0.3182	0.3182	0.0000	-0.7469	0.2936	-0.0390	0.0390	-0.2936	-0.7469	0.0390	0.0390	0.1601	0.2471	0.0156	-0.1601	-0.0156	-0.2471
$A_{0,5}$	-0.7469	0.0390	-0.2471	0.3182	1.0000	-0.1601	0.2936	-0.3182	0.2471	-0.0390	-0.1221	-0.5036	0.1221	0.0000	0.0390	-0.2936	-0.0390	0.7469	0.0156	0.1601	0.3182	0.3182	0.0709	0.0156
$A_{0,6}$	0.2936	0.0390	-0.0156	0.3182	-0.1601	1.0000	-0.7469	0.0156	-0.3182	-0.0390	-0.5036	-0.1221	0.0000	-0.1221	-0.7469	-0.0390	-0.2936	-0.0390	0.2471	-0.0709	-0.2471	0.3182	-0.1601	-0.3182
$A_{0,7}$	-0.1601	0.0709	-0.1221	-0.1221	0.2936	-0.7469	1.0000	0.0390	0.0390	0.1601	0.3182	0.3182	0.2471	-0.0156	0.2471	-0.0156	0.3182	0.3182	0.0000	0.7469	-0.5036	0.0390	0.2936	0.2936
$A_{0,8}$	0.2936	-0.7469	-0.0156	0.3182	-0.3182	0.0156	0.0390	1.0000	-0.1601	-0.0390	-0.0390	0.7469	0.2936	-0.0390	0.1221	-0.5036	0.0000	-0.1221	-0.3182	0.3182	0.1601	-0.2471	0.2471	0.0709
$A_{0,9}$	-0.7469	0.2936	-0.2471	0.3182	0.2471	-0.3182	0.0390	-0.1601	1.0000	-0.0390	-0.2936	-0.0390	0.0390	0.7469	0.5036	-0.1221	-0.1221	0.0000	-0.3182	-0.0156	-0.0709	-0.0156	-0.3182	-0.1601
$A_{0,10}$	-0.0709	0.1601	0.5036	0.0000	-0.0390	-0.0390	0.1601	-0.0390	-0.0390	1.0000	0.2471	0.0156	0.3182	-0.3182	-0.0156	0.2471	-0.3182	-0.3182	-0.1221	-0.7469	0.2936	0.1221	-0.2936	0.7469
$A_{0,11}$	0.3182	-0.0156	0.0390	-0.7469	-0.1221	-0.5036	0.3182	-0.0390	-0.2936	0.2471	1.0000	-0.1601	-0.0709	-0.1601	0.3182	0.2471	-0.3182	0.0156	-0.0390	0.0000	0.0390	0.2936	-0.1221	0.7469
$A_{0,12}$	0.3182	-0.2471	0.0390	0.2936	-0.5036	-0.1221	0.3182	0.7469	-0.0390	0.0156	-0.1601	1.0000	0.1601	0.0000	-0.0156	-0.3182	0.2471	-0.3182	-0.0390	0.1221	0.2936	-0.7469	0.0000	-0.0390
$A_{0,13}$	0.0156	-0.3182	-0.2936	-0.0390	0.1221	0.0000	0.2471	0.2936	0.0390	0.3182	-0.0709	0.1601	1.0000	0.1601	0.2471	0.3182	-0.0156	0.3182	-0.7469	-0.5036	0.7469	-0.0390	0.1221	0.0390
$A_{0,14}$	-0.2471	0.3182	-0.7469	0.0390	0.0000	-0.1221	-0.0156	-0.0390	0.7469	-0.3182	-0.1601	0.0709	0.1601	1.0000	0.3182	0.0156	-0.3182	0.2471	-0.2936	0.1221	0.0390	0.0390	-0.5036	-0.2936
$A_{0,15}$	-0.3182	-0.3182	-0.0390	-0.2936	0.0390	-0.7469	0.2471	0.1221	0.5036	-0.0156	0.3182	-0.0156	0.2471	0.3182	1.0000	0.1601	0.1601	-0.0709	-0.7469	-0.0390	0.0000	-0.0390	0.2936	0.1221
$A_{0,16}$	0.3182	0.3182	0.0390	-0.7469	-0.2936	-0.0390	-0.0156	-0.5036	-0.1221	0.2471	0.2471	-0.3182	0.3182	0.0156	0.1601	1.0000	0.0709	-0.1601	-0.2936	-0.7469	0.1221	0.0390	-0.0390	0.0000
$A_{0,17}$	-0.0156	-0.2471	0.2936	0.0390	-0.0390	-0.2936	0.3182	0.0000	-0.1221	-0.3182	-0.3182	0.2471	-0.0156	-0.3182	0.1601	0.0709	-0.1601	-0.0390	0.0390	0.1221	-0.7469	0.7469	-0.5036	-0.0390
$A_{0,18}$	-0.2471	-0.0156	-0.7469	0.0390	0.7469	-0.0390	0.3182	-0.1221	0.0000	-0.3182	0.0156	-0.3182	0.3182	0.2471	-0.0709	-0.1601	-0.1601	1.0000	-0.0390	0.2936	0.5036	0.2936	-0.0390	-0.1221
$A_{0,19}$	0.1221	0.5036	0.1601	0.1601	0.0156	0.2471	0.0000	-0.3182	-0.3182	-0.1221	-0.0390	-0.0390	-0.7469	-0.2936	-0.7469	-0.2936	-0.0390	-0.0390	1.0000	0.3182	-0.2471	-0.0709	-0.3182	0.0156
$A_{0,20}$	-0.0390	-0.2936	-0.3182	0.2471	0.1601	-0.0709	-0.0390	0.3182	-0.0156	-0.7469	0.0000	0.1221	-0.5036	0.1221	-0.0390	-0.7469	0.0390	0.2936	0.3182	1.0000	-0.3182	0.0156	0.1601	-0.2471
$A_{0,21}$	-0.0390	-0.0390	-0.3182	0.0156	0.3182	-0.2471	0.7469	0.1601	-0.0709	0.2936	0.0390	0.2936	0.7469	0.0390	0.0000	0.1221	0.1221	0.5036	-0.2471	-0.3182	1.0000	-0.3182	-0.0156	0.1601
$A_{0,22}$	-0.1221	0.0000	-0.1601	-0.1601	0.3182	0.3182	-0.5036	-0.2471	-0.0156	0.1221	0.2936	-0.7469	-0.0390	0.0390	-0.0390	0.0390	-0.7469	0.2936	-0.0709	0.0156	-0.3182	1.0000	-0.2471	0.3182
$A_{0,23}$	0.0390	-0.7469	0.3182	-0.0156	0.0709	-0.1601	0.0390	0.2471	-0.3182	-0.2936	-0.1221	0.0000	0.1221	-0.5036	0.2936	-0.0390	0.7469	-0.0390	-0.3182	0.1601	-0.0156	-0.2471	1.0000	-0.3182
$A_{0,24}$	0.0390	0.0390	0.3182	-0.2471	0.0156	-0.3182	0.2936	0.0709	-0.1601	0.7469	0.7469	-0.0390	0.0390	-0.2936	0.1221	0.0000	-0.5036	-0.1221	0.0156	-0.2471	0.1601	0.3182	-0.3182	1.0000

(i) A'_0 solutions in $[\text{VF}_6]^3$.

	$A'_{0,1}$	$A'_{0,2}$	$A'_{0,3}$	$A'_{0,4}$	$A'_{0,5}$	$A'_{0,6}$	$A'_{0,7}$	$A'_{0,8}$	$A'_{0,9}$	$A'_{0,10}$	$A'_{0,11}$	$A'_{0,12}$
$A'_{0,1}$	1.0000	-0.0074	-0.0074	0.0074	-0.0074	0.0000	0.0000	-0.4844	0.4844	0.4844	-0.4844	0.0000
$A'_{0,2}$	-0.0074	1.0000	0.0000	-0.0074	-0.0074	0.0074	-0.4844	0.0000	0.0000	-0.4844	-0.4844	0.4844
$A'_{0,3}$	-0.0074	0.0000	1.0000	0.0074	0.0074	0.0074	-0.4844	0.0000	0.0000	0.4844	0.4844	0.4844
$A'_{0,4}$	0.0074	-0.0074	0.0074	1.0000	0.0000	0.0074	0.4844	-0.4844	-0.4844	0.0000	0.0000	0.4844
$A'_{0,5}$	-0.0074	-0.0074	0.0074	0.0000	1.0000	-0.0074	-0.4844	-0.4844	-0.4844	0.0000	0.0000	-0.4844
$A'_{0,6}$	0.0000	0.0074	0.0074	0.0074	-0.0074	1.0000	0.0000	0.4844	-0.4844	0.4844	-0.4844	0.0000
$A'_{0,7}$	0.0000	-0.4844	-0.4844	0.4844	-0.4844	0.0000	1.0000	-0.0074	0.0074	0.0074	-0.0074	0.0000
$A'_{0,8}$	-0.4844	0.0000	0.0000	-0.4844	-0.4844	0.4844	-0.0074	1.0000	0.0000	-0.0074	-0.0074	0.0074
$A'_{0,9}$	0.4844	0.0000	0.0000	-0.4844	-0.4844	-0.4844	0.0074	0.0000	1.0000	-0.0074	-0.0074	-0.0074
$A'_{0,10}$	0.4844	-0.4844	0.4844	0.0000	0.0000	0.4844	0.0074	-0.0074	-0.0074	1.0000	0.0000	0.0074
$A'_{0,11}$	-0.4844	-0.4844	0.4844	0.0000	0.0000	-0.4844	-0.0074	-0.0074	-0.0074	0.0000	1.0000	-0.0074
$A'_{0,12}$	0.0000	0.4844	0.4844	0.4844	-0.4844	0.0000	0.0000	0.0074	-0.0074	0.0074	-0.0074	1.0000

(j) A''_0 solutions in $[\text{VF}_6]^{3-}$.

	$A''_{0,1}$	$A''_{0,2}$	$A''_{0,3}$	$A''_{0,4}$	$A''_{0,5}$	$A''_{0,6}$
$A''_{0,1}$	1.0000	0.0000	0.0000	0.0000	0.0000	0.0000
$A''_{0,2}$	0.0000	1.0000	0.0000	0.0000	0.0000	0.0000
$A''_{0,3}$	0.0000	0.0000	1.0000	0.0000	0.0000	0.0000
$A''_{0,4}$	0.0000	0.0000	0.0000	1.0000	0.0000	0.0000
$A''_{0,5}$	0.0000	0.0000	0.0000	0.0000	1.0000	0.0000
$A''_{0,6}$	0.0000	0.0000	0.0000	0.0000	0.0000	1.0000

(k) B_1 solutions in $[\text{VF}_6]^{3-}$.

	$B_{0,1}$	$B_{0,2}$	$B_{0,3}$	$B_{0,4}$	$B_{0,5}$	$B_{0,6}$
$B_{0,1}$	1.0000	0.0196	-0.0196	0.0196	-0.0196	0.1927
$B_{0,2}$	0.0196	1.0000	-0.1927	0.0196	-0.0196	0.0196
$B_{0,3}$	-0.0196	-0.1927	1.0000	-0.0196	0.0196	-0.0196
$B_{0,4}$	0.0196	0.0196	-0.0196	1.0000	-0.1927	0.0196
$B_{0,5}$	-0.0196	-0.0196	0.0196	-0.1927	1.0000	-0.0196
$B_{0,6}$	0.1927	0.0196	-0.0196	0.0196	-0.0196	1.0000

(l) C_0 solutions in $[\text{VF}_6]^{3-}$.

	$C_{0,1}$	$C_{0,2}$	$C_{0,3}$	$C_{0,4}$	$C_{0,5}$	$C_{0,6}$
$C_{0,1}$	1.0000	0.0000	0.0000	0.0000	0.0000	0.0000
$C_{0,2}$	0.0000	1.0000	0.0000	0.0000	0.0000	0.0000
$C_{0,3}$	0.0000	0.0000	1.0000	0.0000	0.0000	0.0000
$C_{0,4}$	0.0000	0.0000	0.0000	1.0000	0.0000	0.0000
$C_{0,5}$	0.0000	0.0000	0.0000	0.0000	1.0000	0.0000
$C_{0,6}$	0.0000	0.0000	0.0000	0.0000	0.0000	1.0000

(m) D_0 solutions in $[\text{VF}_6]^{3-}$.

	$D_{0,1}$	$D_{0,2}$	$D_{0,3}$
$D_{0,1}$	1.0000	0.0000	0.0000
$D_{0,2}$	0.0000	1.0000	0.0000
$D_{0,3}$	0.0000	0.0000	1.0000

(n) E_0 solutions in $[\text{VF}_6]^{3-}$.

	$E_{0,1}$	$E_{0,2}$	$E_{0,3}$	$E_{0,4}$	$E_{0,5}$	$E_{0,6}$
$E_{0,1}$	1.0000	0.0000	0.0000	0.0000	0.0000	0.0000
$E_{0,2}$	0.0000	1.0000	0.0000	0.0000	0.0000	0.0000
$E_{0,3}$	0.0000	0.0000	1.0000	0.0000	0.0000	0.0000
$E_{0,4}$	0.0000	0.0000	0.0000	1.0000	0.0000	0.0000
$E_{0,5}$	0.0000	0.0000	0.0000	0.0000	1.0000	0.0000
$E_{0,6}$	0.0000	0.0000	0.0000	0.0000	0.0000	1.0000

Table S6: Energies and $\langle \hat{S}^2 \rangle$ values of UHF solutions in $[\text{VF}_6]^{3-}$.

(a) $M_S = 1$			(b) $M_S = 0$		
Ψ_{UHF}	Energy/ E_h	$\langle \hat{S}^2 \rangle$	Ψ_{UHF}	Energy/ E_h	$\langle \hat{S}^2 \rangle$
A_1	-1539.342 426 8	2.0040	A_0	-1539.308 615 5	1.0025
A'_1	-1539.341 634 5	2.0040	A'_0	-1539.308 046 9	1.0029
B_1	-1539.336 034 6	2.0045	A''_0	-1539.306 202 6	1.0037
C_1	-1539.288 311 1	2.0035	B_0	-1539.265 997 4	0.8090
D_1	-1539.275 057 2	2.0039	C_0	-1539.252 886 8	1.0034
E_1	-1539.235 493 9	2.0049	D_0	-1539.244 025 8	0.0000
F_1	-1539.227 738 3	2.0044	E_0	-1539.220 447 3	1.0046

Table S7: Energies and $\langle \hat{S}^2 \rangle$ values of NOCI wavefunctions constructed from single sets of degenerate UHF solutions in $[\text{VF}_6]^{3-}$.

(a) $M_S = 1$

Φ	Energy/ E_h	$\langle \hat{S}^2 \rangle$
${}^3T_{1g}[\text{A}_1]$	-1539.343 588 1	2.0035
${}^\infty A_{2g}[\text{A}_1]$	-1538.325 139 2	2.4185
${}^3T_{1g}[\text{A}'_1]$	-1539.344 221 4	2.0033
${}^\infty T_{2g}[\text{A}'_1]$	-1539.170 472 0	2.0483
${}^3T_{2g}[\text{D}_1]$	-1539.291 289 5	2.0025
${}^3T_{1g}[\text{D}_1]$	-1539.226 578 2	2.0079

(b) $M_S = 0$

Φ	Energy/ E_h	$\langle \hat{S}^2 \rangle$	Φ	Energy/ E_h	$\langle \hat{S}^2 \rangle$
${}^3T_{1g}[\text{A}_0]$	-1539.344 562 8	2.0000	${}^1T_{2g}[\text{A}_0]$	-1539.280 372 3	0.0038
${}^3A_{2g}[\text{A}_0]$	-1537.822 202 5	2.0006	${}^1E_g[\text{A}_0]$	-1539.277 092 3	0.0032
${}^3T_{1g}[\text{A}_0]$	-1536.959 663 1	2.0016	${}^\infty T_{1g}[\text{A}_0]$	-1539.083 650 4	0.1003
${}^3T_{2g}[\text{A}_0]$	-1536.940 633 2	2.0008	${}^\infty A_{1g}[\text{A}_0]$	-1539.054 571 1	0.0455
${}^3E_g[\text{A}_0]$	-1536.338 308 7	2.0011	${}^\infty T_{2g}[\text{A}_0]$	-1539.001 417 3	0.1574
${}^3T_{1g}[\text{A}'_0]$	-1539.343 374 0	2.0000	${}^1T_{2g}[\text{A}'_0]$	-1539.279 171 5	0.0042
${}^3T_{2g}[\text{A}'_0]$	-1539.018 782 0	2.0002	${}^\infty T_{1g}[\text{A}'_0]$	-1539.114 279 7	0.0750
${}^3T_{1g}[\text{A}''_0]$	-1539.337 207 1	2.0000	${}^1T_{2g}[\text{A}''_0]$	-1539.275 198 0	0.0073
${}^3T_{2g}[\text{B}_0]$	-1539.284 759 3	2.0000	${}^1E_g[\text{B}_0]$	-1539.273 565 6	0.0029
			${}^1A_{1g}[\text{B}_0]$	-1539.216 510 2	0.0027
${}^3T_{2g}[\text{C}_0]$	-1539.286 871 7	2.0000	${}^1T_{2g}[\text{C}_0]$	-1539.218 901 9	0.0067
			${}^1E_g[\text{D}_0]$	-1539.274 205 4	0.0000
			${}^1A_{1g}[\text{D}_0]$	-1539.183 666 9	0.0000
${}^3T_{1g}[\text{E}_0]$	-1539.237 428 1	2.0000	${}^1T_{1g}[\text{E}_0]$	-1539.203 466 5	0.0092

Table S8: Energies and $\langle \hat{S}^2 \rangle$ values of $M_S = 1$ NOCI wavefunctions constructed from all interacting low-lying UHF solutions in $[\text{VF}_6]^{3-}$.

(a) ${}^3T_{1g}[\text{A}_1, \text{A}'_1, \text{B}_1 (\text{D}_1, \text{E}_1)]$			(b) ${}^3T_{1g}[\text{D}_1, \text{E}_1 (\text{A}_1, \text{A}'_1, \text{B}_1)]$		
Φ	Energy/ E_h	$\langle \hat{S}^2 \rangle$	Φ	Energy/ E_h	$\langle \hat{S}^2 \rangle$
${}^3T_{1g}[\text{A}_1]$	-1539.343 588 1	2.0035	${}^3T_{1g}[\text{D}_1]$	-1539.226 578 2	2.0079
${}^3T_{1g}[\text{A}_1 \oplus \text{D}_1]$	-1539.343 637 3	2.0035	${}^3T_{1g}[\text{A}_1 \oplus \text{D}_1]$	-1539.218 700 2	2.0086
${}^3T_{1g}[\text{A}_1 \oplus \text{D}_1 \oplus \text{E}_1]$	-1539.343 645 4	2.0035	${}^3T_{1g}[\text{A}_1 \oplus \text{A}'_1 \oplus \text{D}_1]$	-1539.220 884 6	2.0077
${}^3T_{1g}[\text{A}_1 \oplus \text{E}_1]$	-1539.343 645 1	2.0035	${}^3T_{1g}[\text{A}_1 \oplus \text{A}'_1 \oplus \text{B}_1 \oplus \text{D}_1]$	-1539.220 993 0	2.0076
${}^3T_{1g}[\text{A}_1 \oplus \text{A}'_1]$	-1539.344 268 5	2.0033	${}^3T_{1g}[\text{A}_1 \oplus \text{B}_1 \oplus \text{D}_1]$	-1539.220 955 1	2.0076
${}^3T_{1g}[\text{A}_1 \oplus \text{A}'_1 \oplus \text{D}_1]$	-1539.344 550 5	2.0033	${}^3T_{1g}[\text{A}'_1 \oplus \text{D}_1]$	-1539.219 102 0	2.0085
${}^3T_{1g}[\text{A}_1 \oplus \text{A}'_1 \oplus \text{D}_1 \oplus \text{E}_1]$	-1539.344 707 9	2.0033	${}^3T_{1g}[\text{A}'_1 \oplus \text{B}_1 \oplus \text{D}_1]$	-1539.220 914 2	2.0076
${}^3T_{1g}[\text{A}_1 \oplus \text{A}'_1 \oplus \text{E}_1]$	-1539.344 697 1	2.0033	${}^3T_{1g}[\text{B}_1 \oplus \text{D}_1]$	-1539.220 154 2	2.0080
${}^3T_{1g}[\text{A}_1 \oplus \text{A}'_1 \oplus \text{B}_1]$	-1539.344 320 0	2.0033	${}^3T_{1g}[\text{D}_1 \oplus \text{E}_1]$	-1539.237 524 5	2.0033
${}^3T_{1g}[\text{A}_1 \oplus \text{A}'_1 \oplus \text{B}_1 \oplus \text{D}_1]$	-1539.344 691 3	2.0034	${}^3T_{1g}[\text{A}_1 \oplus \text{D}_1 \oplus \text{E}_1]$	-1539.230 200 7	2.0036
${}^3T_{1g}[\text{A}_1 \oplus \text{A}'_1 \oplus \text{B}_1 \oplus \text{D}_1 \oplus \text{E}_1]$	-1539.344 826 6	2.0034	${}^3T_{1g}[\text{A}_1 \oplus \text{A}'_1 \oplus \text{D}_1 \oplus \text{E}_1]$	-1539.230 358 1	2.0035
${}^3T_{1g}[\text{A}_1 \oplus \text{A}'_1 \oplus \text{B}_1 \oplus \text{E}_1]$	-1539.344 811 0	2.0034	${}^3T_{1g}[\text{A}_1 \oplus \text{A}'_1 \oplus \text{B}_1 \oplus \text{D}_1 \oplus \text{E}_1]$	-1539.230 661 9	2.0035
${}^3T_{1g}[\text{A}_1 \oplus \text{B}_1]$	-1539.343 981 5	2.0034	${}^3T_{1g}[\text{A}_1 \oplus \text{B}_1 \oplus \text{D}_1 \oplus \text{E}_1]$	-1539.230 521 5	2.0034
${}^3T_{1g}[\text{A}_1 \oplus \text{B}_1 \oplus \text{D}_1]$	-1539.344 690 8	2.0034	${}^3T_{1g}[\text{A}'_1 \oplus \text{D}_1 \oplus \text{E}_1]$	-1539.230 291 3	2.0035
${}^3T_{1g}[\text{A}_1 \oplus \text{B}_1 \oplus \text{D}_1 \oplus \text{E}_1]$	-1539.344 824 4	2.0034	${}^3T_{1g}[\text{A}'_1 \oplus \text{B}_1 \oplus \text{D}_1 \oplus \text{E}_1]$	-1539.230 519 6	2.0034
${}^3T_{1g}[\text{A}_1 \oplus \text{B}_1 \oplus \text{E}_1]$	-1539.344 788 5	2.0034	${}^3T_{1g}[\text{B}_1 \oplus \text{D}_1 \oplus \text{E}_1]$	-1539.230 519 5	2.0034
${}^3T_{1g}[\text{A}'_1]$	-1539.344 221 4	2.0033	${}^3T_{1g}[\text{A}_1 \oplus \text{E}_1]$	-1539.228 054 8	2.0053
${}^3T_{1g}[\text{A}'_1 \oplus \text{D}_1]$	-1539.344 399 4	2.0033	${}^3T_{1g}[\text{A}_1 \oplus \text{A}'_1 \oplus \text{E}_1]$	-1539.228 104 4	2.0052
${}^3T_{1g}[\text{A}'_1 \oplus \text{D}_1 \oplus \text{E}_1]$	-1539.344 466 4	2.0033	${}^3T_{1g}[\text{A}_1 \oplus \text{A}'_1 \oplus \text{B}_1 \oplus \text{E}_1]$	-1539.229 932 3	2.0043
${}^3T_{1g}[\text{A}'_1 \oplus \text{E}_1]$	-1539.344 464 2	2.0033	${}^3T_{1g}[\text{A}_1 \oplus \text{B}_1 \oplus \text{E}_1]$	-1539.228 689 2	2.0048
${}^3T_{1g}[\text{A}'_1 \oplus \text{B}_1]$	-1539.344 224 9	2.0033	${}^3T_{1g}[\text{A}'_1 \oplus \text{E}_1]$	-1539.228 097 4	2.0052
${}^3T_{1g}[\text{A}'_1 \oplus \text{B}_1 \oplus \text{D}_1]$	-1539.344 663 1	2.0033	${}^3T_{1g}[\text{A}'_1 \oplus \text{B}_1 \oplus \text{E}_1]$	-1539.228 756 2	2.0048
${}^3T_{1g}[\text{A}'_1 \oplus \text{B}_1 \oplus \text{D}_1 \oplus \text{E}_1]$	-1539.344 818 9	2.0033	${}^3T_{1g}[\text{B}_1 \oplus \text{E}_1]$	-1539.228 655 4	2.0049
${}^3T_{1g}[\text{A}'_1 \oplus \text{B}_1 \oplus \text{E}_1]$	-1539.344 810 7	2.0034			
${}^3T_{1g}[\text{B}_1 \oplus \text{D}_1]$	-1539.342 471 5	2.0044			
${}^3T_{1g}[\text{B}_1 \oplus \text{D}_1 \oplus \text{E}_1]$	-1539.343 046 7	2.0044			
${}^3T_{1g}[\text{B}_1 \oplus \text{E}_1]$	-1539.342 873 0	2.0046			

(c) ${}^3T_{2g}[\text{D}_1 (\text{C}_1)]$

Φ	Energy/ E_h	$\langle \hat{S}^2 \rangle$
${}^3T_{1g}[\text{C}_1 \oplus \text{D}_1]$	-1539.291 471 1	2.0024
${}^3T_{2g}[\text{D}_1]$	-1539.291 289 5	2.0025

Table S9: Energies and $\langle \hat{S}^2 \rangle$ values of $M_S = 0$ NOCI wavefunctions constructed from all interacting low-lying UHF solutions in $[\text{VF}_6]^{3-}$.

(a) ${}^3T_{1g}[\text{A}_0, \text{A}'_0, \text{A}''_0 (\text{E}_0)]$			(b) ${}^3T_{1g}[\text{E}_0 (\text{A}_0, \text{A}'_0, \text{A}''_0)]$		
Φ	Energy/ E_h	$\langle \hat{S}^2 \rangle$	Φ	Energy/ E_h	$\langle \hat{S}^2 \rangle$
${}^3T_{1g}[\text{A}_0]$	-1539.344 562 8	2.0000	${}^3T_{1g}[\text{E}_0]$	-1539.237 428 1	2.0000
${}^3T_{1g}[\text{A}_0 \oplus \text{E}_0]$	-1539.345 147 7	2.0000	${}^3T_{1g}[\text{A}_0 \oplus \text{E}_0]$	-1539.230 715 1	2.0000
${}^3T_{1g}[\text{A}_0 \oplus \text{A}'_0]$	-1539.344 869 5	2.0000	${}^3T_{1g}[\text{A}_0 \oplus \text{A}'_0 \oplus \text{E}_0]$	-1539.231 370 6	2.0000
${}^3T_{1g}[\text{A}_0 \oplus \text{A}'_0 \oplus \text{E}_0]$	-1539.346 010 2	2.0000	${}^3T_{1g}[\text{A}_0 \oplus \text{A}'_0 \oplus \text{A}''_0 \oplus \text{E}_0]$	-1539.231 557 6	2.0000
${}^3T_{1g}[\text{A}_0 \oplus \text{A}'_0 \oplus \text{A}''_0]$	-1539.344 880 8	2.0000	${}^3T_{1g}[\text{A}_0 \oplus \text{A}''_0 \oplus \text{E}_0]$	-1539.231 556 7	2.0000
${}^3T_{1g}[\text{A}_0 \oplus \text{A}'_0 \oplus \text{A}''_0 \oplus \text{E}_0]$	-1539.346 638 2	2.0000	${}^3T_{1g}[\text{A}'_0 \oplus \text{E}_0]$	-1539.230 735 2	2.0000
${}^3T_{1g}[\text{A}_0 \oplus \text{A}''_0]$	-1539.344 758 9	2.0000	${}^3T_{1g}[\text{A}'_0 \oplus \text{A}''_0 \oplus \text{E}_0]$	-1539.231 229 3	2.0000
${}^3T_{1g}[\text{A}_0 \oplus \text{A}''_0 \oplus \text{E}_0]$	-1539.346 550 1	2.0000	${}^3T_{1g}[\text{A}''_0 \oplus \text{E}_0]$	-1539.231 120 1	2.0000
${}^3T_{1g}[\text{A}'_0]$	-1539.343 374 0	2.0000			
${}^3T_{1g}[\text{A}'_0 \oplus \text{E}_0]$	-1539.344 405 3	2.0000			
${}^3T_{1g}[\text{A}'_0 \oplus \text{A}''_0]$	-1539.343 485 6	2.0000			
${}^3T_{1g}[\text{A}'_0 \oplus \text{A}''_0 \oplus \text{E}_0]$	-1539.344 643 7	2.0000			
${}^3T_{1g}[\text{A}''_0]$	-1539.337 207 1	2.0000			
${}^3T_{1g}[\text{A}''_0 \oplus \text{E}_0]$	-1539.343 515 1	2.0000			

(c) ${}^3T_{2g}[\text{B}_0, \text{C}_0]$

Φ	Energy/ E_h	$\langle \hat{S}^2 \rangle$
${}^3T_{1g}[\text{B}_0]$	-1539.284 759 3	2.0000
${}^3T_{2g}[\text{B}_0 \oplus \text{C}_0]$	-1539.289 062 9	2.0000
${}^3T_{1g}[\text{C}_0]$	-1539.286 871 7	2.0000

(d) ${}^1T_{2g}[A_0, A'_0, A''_0 (C_0)]$

Φ	Energy/ E_h	$\langle \hat{S}^2 \rangle$
${}^1T_{2g}[A_0]$	-1539.280 372 3	0.0038
${}^1T_{2g}[A_0 \oplus C_0]$	-1539.281 663 9	0.0040
${}^1T_{2g}[A_0 \oplus A'_0]$	-1539.280 372 4	0.0038
${}^1T_{2g}[A_0 \oplus A'_0 \oplus C_0]$	-1539.281 664 3	0.0040
${}^1T_{2g}[A_0 \oplus A'_0 \oplus A''_0]$	-1539.280 461 8	0.0038
${}^1T_{2g}[A_0 \oplus A'_0 \oplus A''_0 \oplus C_0]$	-1539.281 851 9	0.0041
${}^1T_{2g}[A_0 \oplus A''_0]$	-1539.280 434 5	0.0038
${}^1T_{2g}[A_0 \oplus A''_0 \oplus C_0]$	-1539.281 795 8	0.0040
${}^1T_{2g}[A'_0]$	-1539.279 171 5	0.0042
${}^1T_{2g}[A'_0 \oplus C_0]$	-1539.281 014 8	0.0042
${}^1T_{2g}[A'_0 \oplus A''_0]$	-1539.279 288 9	0.0039
${}^1T_{2g}[A'_0 \oplus A''_0 \oplus C_0]$	-1539.281 082 4	0.0045
${}^1T_{2g}[A''_0]$	-1539.275 198 0	0.0073
${}^1T_{2g}[A''_0 \oplus C_0]$	-1539.279 609 9	0.0072

(e) ${}^1T_{2g}[C_0 (A_0, A'_0, A''_0)]$

Φ	Energy/ E_h	$\langle \hat{S}^2 \rangle$
${}^1T_{2g}[C_0]$	-1539.218 901 9	0.0067
${}^1T_{2g}[A_0 \oplus C_0]$	-1539.214 604 1	0.0069
${}^1T_{2g}[A_0 \oplus A'_0 \oplus C_0]$	-1539.214 723 9	0.0067
${}^1T_{2g}[A_0 \oplus A'_0 \oplus A''_0 \oplus C_0]$	-1539.214 769 9	0.0068
${}^1T_{2g}[A_0 \oplus A''_0 \oplus C_0]$	-1539.214 604 9	0.0069
${}^1T_{2g}[A'_0 \oplus C_0]$	-1539.214 697 7	0.0068
${}^1T_{2g}[A'_0 \oplus A''_0 \oplus C_0]$	-1539.214 703 9	0.0068
${}^1T_{2g}[A''_0 \oplus C_0]$	-1539.214 490 0	0.0067

(f) ${}^1E_g[A_0, B_0, D_0]$

Φ	Energy/ E_h	$\langle \hat{S}^2 \rangle$
${}^1E_g[A_0]$	-1539.277 092 3	0.0032
${}^1E_g[A_0 \oplus B_0]$	-1539.281 683 7	0.0016
${}^1E_g[A_0 \oplus B_0 \oplus D_0]$	-1539.281 683 7	0.0016
${}^1E_g[A_0 \oplus D_0]$	-1539.278 520 2	0.0013
${}^1E_g[B_0]$	-1539.273 565 6	0.0029
${}^1E_g[B_0 \oplus D_0]$	-1539.278 131 7	0.0070
${}^1E_g[D_0]$	-1539.274 205 4	0.0000

(g) ${}^1A_{1g}[B_0 (D_0)]$

Φ	Energy/ E_h	$\langle \hat{S}^2 \rangle$
${}^1A_{1g}[B_0]$	-1539.216 510 2	0.0027
${}^1A_{1g}[B_0 \oplus D_0]$	-1539.216 510 9	0.0027